A Tale of Chaos and Colour

Influencing the photophysical properties and glass forming abilities of BODIPY dyes *via* structural modification

CLARA SCHÄFER

UNIVERSITY OF GOTHENBURG

Department of Chemistry and Molecular Biology

University of Gothenburg

2023

DOCTORAL THESIS

Submitted for fulfilment of the requirements for the degree of

Doctor of Philosophy in Chemistry

A Tale of Chaos and Colour: Influencing the photophysical properties and glass forming abilities of BODIPY dyes *via* structural modification

Cover illustration: BODIPY chemistry and colour by Hannah Schäfer-Eger

clara.schafer@chem.gu.se

ISBN 978-91-8069-237-3 (PRINT)
ISBN 978-91-8069-238-0 (PDF)

Department of Chemistry and Molecular Biology

SE-412 96 Göteborg

Sweden

Printed in Borås, Sweden 2023

Printed by Stema Specialtryck AB

Abstract

Organic dyes are everyday contributors in chemistry, physics and biology. BODIPY dyes were used as model dye class in this thesis. They are well-known for their versatility, which mainly originates from the tuneability of their photophysical properties upon changes in their molecular structure. This thesis strives to deepen the knowledge of the structure-to-photophysical properties relationship of those fluorophores. Furthermore, it demonstrates how the intrinsic properties of the dye can be influenced by modifying the molecular structure.

Structural homologues of the BODIPY and the aza-BODIPY class were synthesised. The homologues differ only in the bridging atom. Moreover, they are decorated with electron withdrawing and donating groups. The effects of those groups were analysed for each class individually and additionally compared within the two classes. This revealed different behaviours of the two dye classes that were previously unexplored.

To strategically decrease the singlet-triplet energy gap, a BODIPY-anthracene dyad, which populates a charge separated state, and can then undergo charge recombination into the triplet state, was oligomerised. Oligomerisation in a non-conjugated fashion mimics a fixed J-aggregate thus facilitating strong exciton coupling. This lowers the singlet state of the oligomers, without having a large effect on the triplet energy. Therefore, the energy gap, which can be described as the energy loss of the system, can be decreased.

Furthermore, a new dye material, a room temperature dye glass, was fabricated. BODIPY derivatives equipped with different alkyl chains were synthesised and subsequently mixed. Upon mixing the entropy of the system is increased, leading to a decrease in the materials ability to crystallise and aggregate. The material now forms an amorphous solid state, a glass, which inherits the monomeric optical properties of the dye components.

The results presented in this thesis highlight that by modifying the molecular structure of a dye molecule, its intrinsic properties can be governed according to ones needs. This is of great importance for the *in vivo* design of dyes as well as the fabrication of new materials.

Keywords: BODIPYs, structure-to-optical properties relationship, entropy, amorphous materials, exciton coupling

Sammanfattning på Svenska

Organiska färgämnen har en central roll inom kemi, fysik och biologi. BODIPY är en klass färgämnen som användes som modell i denna avhandling. De är välkända för sin mångsidighet, som huvudsakligen beror på möjligheten att skräddarsy deras fotofysiska egenskaper genom förändringar i deras molekylära struktur. Denna avhandling strävar efter att fördjupa kunskapen om förhållandet mellan struktur och fotofysiska egenskaper hos dessa fluoroforer. Dessutom visas hur färgämnets egenskaper kan påverkas genom att modifiera den molekylära strukturen.

Strukturella homologer av BODIPY- och aza-BODIPY-klassen syntetiserades. Homologerna skiljer sig åt endast i den överbryggande atomen, och de är båda dekorerade med elektrondragande och donerande grupper. Effekterna av dessa grupper analyserades för varje klass individuellt och jämfördes dessutom inom de två klasserna. Detta resulterade i upptäckten av olika beteenden hos de två färgämnesklasserna som tidigare var outforskade.

För att strategiskt minska singlett-triplettenergigapet oligomeriserades en BODIPY-antracendyad, som *via* ett laddningsseparerat tillstånd kan genomgå laddningsrekombination till tripletttillståndet. Oligomerisering på ett okonjugerat sätt efterliknar ett fixerat J-aggregat underlättar således stark exciton-excitonkoppling. Detta sänker singletttillståndet för oligomererna, utan att ha någon stor effekt på triplettenergin. Därför kan energigapet, som kan beskrivas som systemets energiförlust, minskas.

Vidare tillverkades ett nytt färgmaterial, ett rumstempererat färgglas. BODIPY-derivat utrustade med olika alkylkedjor syntetiserades och blandades. Vid blandning ökar systemets entropi, vilket leder till en minskning av materialens förmåga att kristallisera och aggregera. Materialet bildar då ett amorft fast tillstånd, ett glas, som har de monomera optiska egenskaperna hos färgämneskomponenterna.

Resultaten som presenteras i denna avhandling visar att genom att modifiera molekylstrukturen hos en färgämnesmolekyl kan dess inneboende egenskaper styras enligt behov. Detta är av stor betydelse för *in vivo* design av färgämnen samt tillverkning av nya material.

Nyckelord: BODIPYs, relation mellan struktur och optiska egenskaper, entropi, amorfa material, excitonkoppling

List of Publications

The research results that are presented in this thesis are based on the findings reported in the following papers. The author's contribution is mentioned for each paper, below.

Paper I

Entropic Mixing Allows Monomeric-Like Absorption in Neat BODIPY Films

Clara Schäfer, Jürgen Mony, Thomas Olsson, and Karl Börjesson, *Chem. Eur. J.* **2020**, *26*, 14295–14299.

Synthesised and characterised all the molecules, performed steady-state and time-resolved spectroscopy in liquid as well as in solid state together with J.M.. Prepared the films and performed optical microscopy on the films. Wrote the paper together with the other authors.

Paper II

The effect of the aza-N-bridge and push-pull moieties, a comparative study between BODIPYs and aza-BODIPYs

Clara Schäfer, Jürgen Mony, Thomas Olsson, and Karl Börjesson, *J. Org. Chem.* **2022**, *87*, 2569−2579.

Involved in the design of the project. Designed the synthesis route. Synthesised and characterised all the molecules, performed steady-state and time-resolved measurements, except the transient absorption measurements which were performed by J.M.. Wrote the paper together with the other authors.

Paper III

Room Temperature Dye Glasses - A Guideline towards the Fabrication of Amorphous Dye Films with Monomeric Absorption and Emission

Clara Schäfer, Sandra Hultmark, Yizhou Yang, Christian Müller, and Karl Börjesson, *Chem. Mater.* **2022**, *34, 20,* 9294–9302.

Involved in the design of the project. Designed, synthesised, and characterised all the molecules, and performed all steady-state and time-resolved spectroscopy in solution and solid state. Prepared solid samples and performed mixing experiments. Assisted in sample preparation for DSC and FSC measurements, which were performed and analysed by S.H.. Wrote the paper together with the other authors.

Paper IV

Selective reduction of the singlet excited state to decrease the singlet-triplet energy gap *via* intramolecular exciton-exciton coupling

Clara Schäfer, Rasmus Ringström, Jörg Hanrieder, Bo Albinsson, and Karl Börjesson, *Manuscript.*

Involved in the design of the molecules. Synthesised and characterised the molecules. Performed steady-state and time resolved optical spectroscopy, including transient absorption

measurements. Analysed the results together with the other authors. Wrote the paper together with the other authors. MALDI measurements were performed by J.H. and diffusion NMR was performed and analysed by Z.T. (The Swedish NMR-centre). Electrochemical analysis was performed by R.R..

Further research articles of the author, which are not included in the thesis.

Paper i **Interplay between polaritonic and molecular trap states**

Jürgen Mony, Yi Yu, Clara Schäfer, Suman Mallik, Kushbu Kushwaha, and Karl Börjesson, *J. Phys. Chem. C* **2022**, *126* (18), 7965-7972.

Paper ii **Detachable all-carbon-linked 3D covalent organic framework films for semiconductor/COF heterojunctions by continuous flow synthesis**

Yizhou Yang, Clara Schäfer and Karl Börjesson, *Chem* **2022**, *8* (8), 2217-2227.

Paper iii **A Highly Conductive All-Carbon Linked 3D Covalent Organic Framework Film**

Yizhou Yang, Suman Mallick, Fernando Izquierdo-Ruiz, Clara Schäfer, Xing Xing, Martin Rahm, Karl Börjesson, *Small* **2021**, *17* (40), 2103152.

Paper iv **Electroactive Covalent Organic Framework Enabling Photo-stimulus-responsive Devices**

Yizhou Yang, Amritha P Sandra, Alexander Idström, Clara Schäfer, Martin Andersson, Lars Evenäs, Karl Börjesson, *J. Am. Chem. Soc.* **2022**, 144, 35, 16093–16100.

Paper v **A self-standing three-dimensional covalent organic framework film**

Yizhou Yang, Yanyan Chen, Fernando Izquierdo-Ruiz, Clara Schäfer, Martin Rahm, Karl Börjesson, *Nat. Commun.* **2023**, *14*, 220.

Acknowledgements

One does not just do a PhD isolated or all by themselves. There are people helping out with experiments and analysis. Other people make your day better, and some just simply make your day. This section is here to thank all those people, so I hope you are prepared to read the word 'thanks' in several forms. Although, I will try to keep this short.

First, I want to thank my supervisor Prof. Karl Börjesson for giving me the opportunity of pursuing my PhD. The freedom you gave me during my PhD pushed me to go beyond my limits. You introduced me to a research field I have never thought I would enter and can now handle without constant doubt in myself. Therefore, I am most grateful for explanatory discussions whenever I needed them. I hope you never lose your optimism and passion; they make you a very good supervisor.

Another big thank you to Thomas Olsson. You have been a great help with all synthetic problems during my PhD time. Thank you for making the problems sound less problematic, like calling my purifications 'side product search' or trying to understand the magical mechanism with me. I really appreciate the time you took out of your days as professor emeritus to take the position as my co-supervisor.

I also want to thank Morten Grøtli for much appreciated advice and discussions. I am even grateful that you insisted that I write my ISP properly. It was actually a great help (and I hate to admit that). But mostly I want to thank you and for always having an open ear (and office door) to discuss problems or even just talk.

What would research be without collaborators. It was truly a pleasure to work with all of you. Thank you! Christian Müller and Sandra Hultmark for introducing me into the world of thermal analysis and entropic mixing. Jürgen Mony for all the help with optical analysis and making cavities out of very misbehaving molecules. Yizhou Yang for the help with AFM and GIWAXS. Rasmus Ringström and Bo Albinsson for helping out with the oligomer project, last minute.

NMRs. Well, that's a thing an organic chemist is slightly dependent on. Bijan! You deserve a major callout just for keeping the 400 alive and filled as long as you could. But you know that's not all you do. Thank you for everything! But the 400 died and the people from the NMR centre had to step in and save the day. Thanks to all of you, especially Ulrika and Zoltan, for helping to find a solution so quickly! Zoltan thanks for helping with diffusion NMRs, and for the kindness and enthusiasm you greet people with, even on your bad days.

Administration is a necessary evil that Linn, Johanna, Catarina and Ingrid somehow just manage (as if it would all make sense). If we only had more of you! Thanks to you, for always finding the administrative answer to the many administrative questions that come along during the PhD journey.

Floor 8 has been the place I probably spend most of my time in the last couple of years. I want to express my gratitude to all past and present members. My group members, office mates, lab mates, climbing and gym companions, lunch buddies and afterwork friends. This also needs to be extended to the people from floor 9. There have been a lot of epic, memorable moments that will stay with me forever. Thank you for all of this!

I have met some amazing people during my time here. People, I don't want to miss in my life anymore. Those people I mean here, are although well aware of what I want to tell them, and how grateful I am to them!

And now, if you feel like you have been dismissed or forgotten and should have definitely been personally mentioned here fill your name on the dotted line.

Thank you ……., you are great!

Contents

Abbreviations

A	Acceptor
ACN	Acetonitrile
Ac_2O	Acetic anhydride
AcOH	Acetic acid
AOs	Atomic orbitals
BODIPY	Boron-dipyrrin/ boron dipyrromethene
CR	Charge recombination
CSS	Charge separated state
CT	Charge transfer
CTS	Charge transfer state
D	Donor
DCE	1,2-Dichloroethane
DCM	Dichloromethane
DDQ	2,3-dichloro-5,6-dicyano-*p*-benzoquinone
DMF	Dimethylformamide
DSC	Differential scanning calorimetry
EA	Electron affinity
EDG	Electron donating group
eT	Electron transfer
EWG	Electron withdrawing group
FSC	Fast scanning calorimetry
GIWAXS	Grazing-incidence wide-angle x-ray scattering

HOMO	Highest occupied molecular orbital
IC	Internal conversion
IP	Ionisation potential
IPA	Isopropyl alcohol
IR	Infrared
IRF	Instrument response function
ISC	Intersystem crossing
LUMO	Lowest unoccupied molecular orbital
MeOH	Methanol
MOs	Molecular orbitals
NIR	Near infrared
NMR	Nuclear magnetic resonance
PeT	Photoinduced electron transfer
PIFA	Phenyliodine(III)-bis(trifluoroacetate)
RP-ISC	Radical pair intersystem crossing
S_EAr	Electrophilic aromatic substitution
S_NAr	Nucleophilic aromatic substitution
SOCT-ISC	Spin orbit charge transfer intersystem crossing
T_b	Boiling temperature
T_g	Glass transition temperature
T_m	Melting temperature
TCSPC	Time-correlated single photon counting
THF	Tetrahydrofuran
Tos	Tosylate
TosMIC	Tosylmethyl isocyanide

TTA-UC	Triplet-triplet annihilation upconversion
UV	Ultraviolet
Vis	Visible
VR	Vibrational relaxation

Introduction

Dyes have been a fundamental part of our society for thousands of years. Mankind has used colours to express themselves since its very beginning. The first dyes were taken from nature. Minerals, plants, and animals surrounding us offer a large palette of colours. Until now some cultures use those resources to paint their faces or dye their fabrics. The first paintings date back around 30 000 – 40 000 years and can be found on the walls of caves. Here black was mainly obtained from charcoal, which allows us to perform carbon dating techniques to determine the age. Red, brown, and yellow pigments were accessed using soil. The used earths contain impure forms of iron oxides (Fe_2O_3), and manganese oxides. White pigments were obtained from chalk or bones, so calcium carbonate ($CaCO_3$) or calcium phosphate ($Ca_3(PO_4)_2$).[1] This colour palette was based on minerals and offered a rather limited range. Nonetheless, in rare occasions dull green tones, from mineral clay containing aluminium, iron, magnesium, and potassium, accompany the earthy colours.

Around 2500 BC the ancient Egyptian culture contributed largely to the identification of new sources of colours using pigments obtained from minerals, plants, and animals. Art and therefore colours, especially blue, had a high significance in the ancient Egyptian culture. New natural pigments based on copper containing minerals like malachite ($Cu_2(CO_3)(OH)_2$), which has deep green colours and azurite ($Cu_3(CO_3)_2(OH)_2$) with a deep blue colour, were added to the colour palette. Lapis lazuli, a gemstone known for its deep blue colour, contains of a mixture of different minerals with variable amounts of sodium or calcium ($(Na,Ca)_{7-8}(AlSiO_{12})(S,SO_4,Cl)$). It was highly valued as both a pigment source and for jewellery. Aside from blue and green also yellow Orpiment, obtained from a mineral containing toxic arsenic sulfide (As_2S_3), and red Cinnabar, from an also toxic mercury sulfide (HgS) containing mineral, were added to the available colours. Apart from minerals, the Egyptians also pioneered the use of plants and animals as sources of pigments. They extracted dye molecules and transformed them into pigments by precipitating the dye onto particles of colourless binders like chalk. Here dyes from plants were used, like Indigo, a blue dye, extracted from the leaves of *Indigofera* plant family, and Alizarin, a red-purple dye, extracted out of the roots of *Rubia tinctorum* (Madder). Carmine red was obtained by crushing dried cochineal insects.[1-2] Egyptians also manufactured pigments to extend their resources. One of these pigments has the chemical formula $CaCuSi_4O_{10}$ and is known as Egyptian blue. Most likely it was made by heating sand (SiO_2), some calcium source like lime ($CaCO_3$), a copper containing mineral like azurite to 800-900 °C under oxygen with a mixture of sodium sulphate (Na_2SO_4), soda (Na_2CO_3) and sodium chloride (NaCl).[3]

Inheriting this colour palette, now highly enriched in versatility, the Greeks and Romans also added plenty of options. Ink from octopi for example afforded a brown pigment after

purification.[1] Another pigment, Tyrian purple, obtained from Murex shellfish, became one of the most expensive pigments for the next centuries.[2] In addition to natural pigments also artificial pigments were added to the palette. Red (Pb_3O_4) and yellow (PbO) lead, also referred to as Minimum and Massicot respectively, are examples of such artificial pigments.[1] Over time the colour palette grew richer with plenty of contributions by different cultures, that grew technically more advanced. However, since this thesis has a focus on organic chemistry a jump over some centuries is in order.

In London of 1856, Perkin attempted to synthesise Quinine, used in the treatment of malaria, from coal tar. His attempted synthesis resulted in a red powder, not Quinine. Aniline, as a starting material, was supposed to shed light on the reaction. But the oxidation of aniline with potassium dichromate was also unsuccessful and resulted in a black solid. This solid upon extraction with alcohol resulted in a purple-coloured solution. Perkin had discovered the aniline dye Mauveine, which he initially called Mauve.[4] Only much later in 2008, Mauve was shown to be a complex mixture of several derivatives.[5] Perkin commercialised production of the dye, for staining clothes. This discovery of the first synthetically obtained organic dye changed, not only Perkins's life, but also the world of colorants permanently. Shortly after Perkin's development, and the industrial success of Mauveine, the second synthetic aniline dye entered the market. In Lyon in 1859, Verguin obtained Fuchsine, or Magenta, displaying a crimson red colour, by reacting aniline with tin tetrachloride ($SnCl_4$), and commercialised the process.[6] The industrial success of synthetic aniline dyes in England and France also had an impact on the German chemical industry. Here, within only a couple of years companies like 'Meister, Lucius and Brüning' -later known as Hoechst- were founded. They manufactured dyes like Magenta, and later also aldehyde green, a derivative of Magenta, found by Brüning.[2]

The knowledge obtained from the development of synthetic routes towards aniline dyes was used by chemists to develop new dyes or synthesise already known dyes. Greabe and Lieberman worked on synthesising Alizarin, and published a synthetic protocol in 1869.[7] The structure was later discovered by Caro and von Bayer. Graebe together with Caro, who worked at the 1865 founded 'Badische anilin und Sodafabrik' (BASF), improved the synthesis of Alizarin. Soon the synthetic dye replaced the natural dye almost completely. Other natural dyes were replaced by synthetic dyes soon after. Von Bayer discovered the chemical structure of Indigo in 1883 and postulated a synthetic route.[8] However, the commercialisation of Indigo was first achieved by BASF and Hoechst in 1897. Indigo remains an important dye until today, as it is used to dye denim.

In their eagerness to find more aniline-based structures and improving the ways of making dyes in general, chemists developed different dye classes, and along with them new synthetic strategies. In 1858 for example, Griess discovered diazotisation. This laid the groundwork for azo dyes. Soon after, the first azo dye Bismarck brown was developed by Martius and Lightfood, and entered the market. Other azo dyes followed, like Chrysoidine developed by Caro and Witt in 1875.[2] Many azo dyes, covering the whole spectrum, but mainly red, orange, and yellow, are still used today. In 1876, Caro who still worked for BASF found another dye class, when trying to develop more aniline dyes. He synthesised Methylene blue, a thiazine dye, which was used as a cotton stain. The

structure was elucidated nine years later by Bernthsen, another chemist working on aniline dyes, who synthesised phenothiazine.[9]

The development of new synthetic organic dyes was flourishing, and more and more dyes entered the market. Although mainly developed for staining fabrics, dyes were soon started to be utilised in different fields. In 1887, Methylene blue was found to selectively stain malaria organisms in blood smears, and, in 1891, Gutman and Ehrlich used it as an antimalarial agent.[9-10] After some modifications of the structure, at the company Bayer, it became a widely used drug. Later in the 1940s, due to their earlier results, other thiazine dyes, like phenothiazine, were used as lead structures in medicinal chemistry, which in 1950 led to the development of chlorpromazine.[11]

In the 20th century, dyes received an increased amount of attention in the scientific community. Their properties were investigated more. The potential of interacting with light was obvious but needed to be studied further. Egyptian blue, for example, was found to have exceptionally high near-infrared (NIR) luminescence with an emission maximum at 910 nm, emission quantum yields of about 10 %. and an excited state lifetime of 107 μs.[12] Some dyes were found to have promising conducting properties. Indigoid dyes like indigo and Tyrian purple showed good energy transfer properties in their solid state, and their use in organic electronics was explored.[8] Due to previous success with Methylene blue and other thiazine dyes, further utilisation in medicine and biology was investigated. With more knowledge about their properties, new avenues were opened for dyes. By now synthetic organic dyes reach us in every part of our life. In areas like colorants, organic electronics and medical treatment stretching to research in biology, medicine, chemistry, and physics.

Undoubtedly, dye chemistry has experienced an astonishing growth of newly designed structures and materials. Now the design of dye compounds, which are in their photophysical properties specialised for a certain application, has become more important. Newly developed avenues in organic chemistry allow for either, targeted, sophisticated modifications of already existing, organic dye backbones, or entirely new molecular structures. The applications for dyes are now various and universal. As a result of this, the requirements any application has towards a dye, regarding both optical and molecular properties, are highly divergent. Fundamental understanding of the photophysical processes of a dye and the structure-to-optical properties relationship are crucial for targeted molecular design, regarding the optical properties. To maximise the applicability of a dye another aspect, the intrinsic physical properties, must be likewise considered. New dye materials need to be developed, for dyes to live up to their full potential.

Research aim

The research presented in this thesis grew out of a requirement. A dye material, with an as high dye concentration as possible in solid state should be developed. The optical properties of the material should simultaneously be of monomeric nature. Thus, not be disturbed by aggregation or crystallisation of the dye molecules. In other words, a glass like material of a dye was desired. For this a relatively new avenue of preparing glassy

materials was approached, entropic mixing. A refined and generally applicable method based on entropic mixing should be developed and utilised to form a room temperature chromophore glass.

Boron dipyrromethene dyes, also referred to as BODIPY dyes, were used as a model chromophore in this thesis. In project I and project III (leading to paper I and paper III), BODIPY series were designed and synthesised, where the derivatives carry different alkyl chains. In project I, it was realised that the molecular design was insufficient, and more effort needed to be devoted towards it. The design of the BODIPY series synthesised for project III, was targeting the weak points of the previous derivatives. Subsequently, two or more of those derivatives were blended. The obtained blends were then investigated in solid state, using optical microscopy and optical spectroscopy to evaluate the new dye material. The material, if the desired optical properties were observed, was further investigated regarding its ability to form a glass. Therefore, differential, and fast scanning calorimetry were used to obtain information on the thermal behaviour of the new material.

Working with BODIPY dyes, some fundamental interest regarding the structure-to-optical properties relationship arose, especially towards a subclass of BODIPYs, the aza-BODIPY dyes. The BODIPY class has a carbon as the bridging atom, whereas a nitrogen atom in this position defines the aza-BODIPYs. To gather more insight on how the optical properties of these two dye classes can be influenced, by attaching different electron withdrawing/donating groups, two sets of dyes were designed and synthesised in project II (leading to paper II). Each set contains different combinations of electron withdrawing/donating groups. The only difference in between the two sets is the bridging atom in between the pyrrolic units. Each set was evaluated spectroscopically to gather insight on their structure-to-optical properties relationship, individually. Furthermore, the two sets of dyes were compared to one another to shed light on the differences in between the two dyes classes, which are structurally only different in one atom.

A major energy loss factor in organic photosensitisers is a large singlet-triplet energy gap. To target this issue, molecular architecture was used methodically in project IV (leading to paper IV). The singlet state energy should be decreased without changing the energy of the triplet state, thus, lowering the singlet-triplet energy gap, *via* exciton coupling. A BODIPY-anthracene dyad, which could efficiently populate the triplet state of the BODIPY was selected as a model compound. Tethered oligomers of the dyad, mimicking fixed J-aggregates with strong exciton coupling, were synthesised, and subsequently spectroscopically evaluated.

Overall, the research discussed in this thesis seeks to deepen and utilise the knowledge of the fundamental correlation of the molecular architecture to the intrinsic molecular properties. Understanding this relationship, enables fabrication of tailor-made molecules and new materials. Both of which can improve already established applications, as well as open new avenues for organic dyes in the future.

Background and Methods

Dyes have been used for centuries and they will most certainly be used as long as humans walk the earth. The development of organic dyes and materials thereof is thriving and often targets specific applications. To develop new organic dyes or dye materials it is of fundamental importance to understand how dyes interact with light. The research presented in this thesis focuses on organic dyes, their interactions with each other, and with light. Within this chapter, the fundamental theoretical background, necessary to follow the research conducted in this thesis, will be briefly discussed. The first section starts with the nature of light and molecules. This is followed by the processes that occur after a molecule has interacted with a photon. In the next section, the interactions between molecules will be discussed. Here also the states of matter will be presented, and transitions in between them. In the end of each section, the methods used primarily in the conducted projects, whose results are presented in this thesis, will be introduced.

The nature of light

The term light is defined as an electromagnetic radiation which shows both properties of a wave and a particle. In 1865, Maxwell described light as a propagating wave of synchronised oscillating fields, one of which is magnetic and the other one electric.[13] These waves can be characterised by their frequency (ν) of oscillation, its wavelength (λ), and its velocity (the speed of light $c = 2.998 \cdot 10^8$ ms^{-1} in vacuum). These stand in the relationship $\lambda\nu = c$. The wavelength of the light is inversely proportional to its frequency. To understand black-body radiation Planck constructed a complementary theory about the nature of light. He quantised the energy of light, where each frequency provides a specific amount of energy, a quantum.[14] Here lower frequencies would provide a smaller amount of energy and higher frequencies a larger amount of energy. Inspired by Planck's theory, Einstein shortly after described light not as a continuous stream, but as a stream of quantum packets of energy, in order to describe the photoelectric effect.[15] They were later given the name photons. The energy (E) of a photon is described by Planck's constant ($h = 6.6261 \cdot 10^{-34}$ J s) and its frequency, according to **Equation 1**.

$$E = h\nu = \frac{hc}{\lambda} \quad (1)$$

The fraction of light that can be detected by the human eye is called visible light (Vis). In the electromagnetic spectrum, visible light is typically in the wavelength range of 400-700 nm. This translates to frequencies of 420-750 terahertz and is located between the infrared (IR) region, which describes wavelengths of 700 nm and above, and the ultraviolet (UV) region, wavelengths of 400 nm and below.

The nature of molecules

Molecules are assemblies of atoms, connected by covalent bonds. Each atom comprises of a dense positively charged nucleus in the centre which is surrounded by one or more negatively charged electrons.

Electrons and Atoms: Just like light, electrons have properties of both waves and particles. The sum of the kinetic and potential energy of a particle can be described quantum-mechanically by the Schrödinger equation. It describes the states or in other words the behaviour of an electron in an atom as wave functions. These wave functions -squared- are probability distributions, called atomic orbitals (AOs) and describe the region of space an electron can be found in around the nucleus. The probability distributions occupy a three-dimensional space and require therefore three coordinates to be described. These coordinates are called quantum numbers. The principal quantum number (n) describes the energy, so the size of the orbital. Where n is a natural number. Orbitals having the same principal quantum number are referred to as being one shell, whereas those shells are referred to by letters. n = 1 is called K, then, L, M, N, and so on follow successively. The angular quantum number (l) describes the shape of the orbital and can take values of $0 \leq l \leq (n-1)$. The value of l describes the number of nodal planes through the origin. Orbitals with l = 0 are therefore spherical, having zero nodal planes, they are known as s-orbitals. p-Orbitals have l = 1, and have therefore one nodal plane, d-orbitals have two nodal planes (l = 2), and so on. Orbitals with the same n yet a different l value are referred to as one subshell. Within one subshell, all orbitals have the same energy. The third quantum number is the magnetic quantum number (m_l) and describes the orientation of an orbital in space. Its value is dependent on l as follows, $-l \leq m_l \leq l$. s-Orbitals are spherically symmetric and therefore have $m_l = 0$. Nonetheless the other orbitals have specific angular orientations, or directions, in space. For p-orbitals m_l can take the values -1, 0 and 1. Translated into cartesian coordinates the p-orbital then has three orientations: p_x, p_y and p_z.[16]

Each orbital can hold a maximum of two electrons. Therefore, to describe one electron in an atom its intrinsic angular momentum, its spin, needs to be considered. The spin is described by two quantum numbers s and m_s. The spin quantum number s has a fixed value of s = ½ for an electron. This value denotes the magnitude of the spin angular momentum and is therefore never negative. The spin magnetic quantum number m_s, on the other hand, describes the orientation of the spin angular momentum of the electron. An electron spin is thus assigned either $m_s = -1/2$ or $m_s = +1/2$, often referred to as 'up/↑' and 'down/↓' spin. Every electron in the atom has, therefore, a unique set of four quantum numbers. The first three quantum numbers n, l and m_l specify the atomic orbital in question, and the fourth, m_s, the orientation of the electron spin.[16]

In atoms with more than one electron, the energy of electronic repulsion has to be considered. This makes an exact solution of the Schrödinger equation difficult. Instead, approximate solutions are used to determine the energy of multielectron systems considering both, functions describing each single electron independently, as well as inter-electronic repulsion. To get the ground electronic configuration of an atom the electrons are filled into the orbitals from low to higher energies according to the Aufbau

principle. Before occupying any orbital with two electrons following the Pauli principle, all orbitals of the same subshell have to be filled with single electrons first as far as possible, having the same spin, according to Hund's rule.[16]

In multi-electron systems, the total spin angular momentum ($\mathcal{S}$) of the system has to be considered. $\mathcal{S}$ is a non-negative integer or half-integer, obtained by coupling the individual spin angular momenta according to the Glebsch-Gordan series ($\mathcal{S} = s_1+s_2, s_1+s_2-1, \ldots, |s_1-s_2|$).[16] Thus, for two electrons $\mathcal{S} = 1, 0$, depending on their relative orientation. To consider here is that, according to the Pauli principle, an electron pair (two electrons in the same orbital) must have paired spins. Electrons with paired spins have a net spin of zero, because the antiparallel spin magnetic angular momenta of the two electrons cancel each other out. This is the case for the inner, fully occupied shells. Therefore, these do not need to be considered in the total spin angular momentum. The total angular momentum of two parallel spins, however, fulfils the condition $\mathcal{S} = 1$ which can be achieved by a number of possible orientations. The number of possible orientations is called the spin multiplicity ($M = 2\mathcal{S} + 1$). If the electronic state of an atom has $S = 0$ it is referred to as singlet state and an electronic state of $\mathcal{S} = 1$ is referred to as triplet state.[16]

For orbitals filled with only one electron another effect is observed. Here, the spin angular momentum and the magnetic angular momentum of the orbital can mix. This magnetic interaction is called spin-orbit coupling and causes the electronic configuration to split into different energy levels. The strength, and thus, the effect the coupling has on the energy levels, depends on the relative orientation of the angular momenta, and on the nuclear charge. Therefore, heavier atoms show a stronger spin-orbit coupling. This is known as the heavy-atom effect.[16]

Molecules: To describe electronic configurations of molecules, molecular orbitals (MOs) are used, just like AOs for atoms. They are determined by a linear combination of atomic orbitals, to describe the electron distribution over the whole molecule. The electrons occupying the inner atomic orbitals are assumed to be unperturbed. Whereas the outer electrons, called the valence electrons, of all bonded atoms are contributing to the MOs. Electrons are filled in the MOs according to the Aufbau principle, the Pauli principle and following Hund's rule to get the ground electronic configuration of the molecule. Due to the Pauli principle most (organic) molecules are in a singlet ground state -Whereas O_2, which is the most famous exception, has a triplet ground state.- The MOs of particular interest considering a molecules reactivity, or their interaction with light, are the highest occupied molecular orbital (HOMO) and the lowest unoccupied molecular orbital (LUMO), the so-called frontier orbitals.[17] As molecules are assemblies of atoms the quantum mechanical description gets even more difficult. Now, the energies of both electrons and nuclei have to be considered. Due to the huge mass difference of those two the Born-Oppenheimer approximation is used. It states, that nuclear and electronic motions can be separated.[18] Here the nuclei are treated as fixed in space - so fixed in one conformation - while the electrons move rapidly around them. This is then repeated for different conformations of the nuclei, to get an idea about the energy of the molecule in respect to different geometries. The result of such calculations is a potential energy

curve of the electronic state. Within every electronic state there are several vibrational levels. These vibrational levels are wavefunctions, describing the movement of the nucleus, caused by vibrations of the nucleus around its equilibrium position.

Interaction of light and molecules

Light in its nature is both an oscillating electric and magnetic field and can interact with the negatively charged electron clouds surrounding the nuclei. The nuclei and thus the electrons can take different configurations, and the rearrangement from one to another induces a transition dipole moment. An electric wave of light, or one photon, interacts with the electron cloud of the molecule through columbic forces, causing an oscillation between the ground and final electronic configuration. An oscillating electric field is hence induced in the molecule. The probability of a transition to occur is higher the larger the transition dipole moment is, thus the larger the interaction between the two electric fields is. The orientation of the transition dipole moment is also crucial for an electronic transition to occur. It has to align with the incident oscillating field of the photon. A photon can also only be absorbed by a molecule if the energy of the incoming photon is equal to the energy difference in between the final and initial state of the electron. This satisfies the Bohr frequency condition ($\Delta E = h\nu$). Upon absorption of one photon, one electron is elevated to an orbital with a higher energy. In molecules this is often associated with a transition of an electron from the HOMO to the LUMO. The energy difference in between the two orbitals is referred to as the HOMO-LUMO gap. The electronic state of a molecule having one electron in the LUMO, leaving an electron-hole in the HOMO can also be referred to as exciton. However, the frontier orbital energy diagram shown in **Figure 1** does not take the rest of the electrons into account and is therefore less precise than a diagram visualising energy as states. The energy states diagram, like the typically used Perrin-Jablonski diagram shown in **Figure 2**, takes the total energy of the molecule into account, including the electron-electron interactions. Therefore, they are more often used when discussing photophysics. Here, upon an absorption event the molecule goes from the lowest energetic state, the ground state (S_0/T_0) to a higher energetic state, the excited state (S_n/T_n).

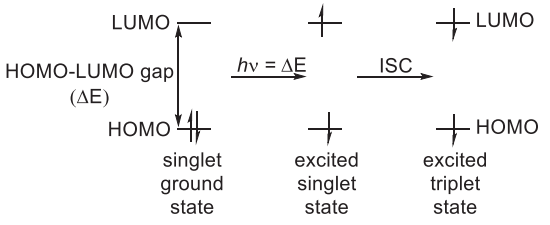

Figure 1. Absorption and intersystem crossing represented in the frontier orbital energy diagram.

For light to induce a transition not only the energy must be conserved but also the angular momentum, the spin. This means that only transitions in between the same spin states, singlet to singlet ($S_0 \rightarrow S_n$ / $S_n \rightarrow S_0$) or triplet to triplet ($T_0 \rightarrow T_n$ / $T_n \rightarrow T_0$), are 'spin allowed'. Transitions between singlet and triplet states would require a momentum change of the electron spin. These transitions are hence 'spin forbidden'.[19]

Photoinduced processes

Absorption: As previously mentioned, most molecules are in a singlet ground state and thus, the photoinduced processes introduced here, and shown in **Figure 2** in a Perrin-Jablonski-diagram, will assume S_0 as the ground state. Nonetheless, the processes can happen in the same fashion from a triplet ground state T_0. A transition from S_0 to S_n usually happens from the lowest vibrational level of the ground state to any vibrational level of an excited state. It depends on the overlap of the wavefunctions describing the nuclei movement (thus vibrational levels) on the initial and final electronic states. The larger the overlap the higher is the probability of a transition, resulting in a higher intensity absorption band. This is often referred to as the Franck-Condon principle.[19] The combined intensity of all absorption bands depends on the transition dipole moment.

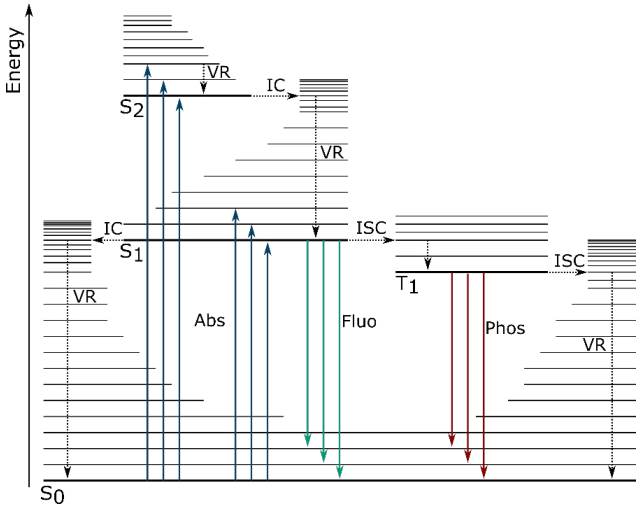

Figure 2. A typical Perrin-Jablonski diagram illustrating possible radiative (solid lines) and non-radiative (dotted lines) processes. Electronic levels are shown in thick black lines (S_0, S_1, S_2 and T_1) and vibrational levels are shown with thin black lines. Radiative processes are depicted with solid, coloured lines, blue for absorption (Abs), green for fluorescence (Fluo) and red for phosphorescence (Phos). Non-radiative processes are depicted with dotted lines and labelled accordingly, vibrational relaxation (VR), internal conversion (IC) and intersystem crossing (ISC).

Non-radiative processes: From the different vibrational levels from the first excited state or higher excited states -electronic level n>1- the molecule relaxes rapidly into its lowest vibrational level of S_1, which is a relatively long-lived state. This happens *via* vibrational relaxation (VR), which is relaxation within the same electronic level, or *via* internal conversion (IC), which describes a change of state within the same multiplicity. IC is usually followed by vibrational relaxation and is therefore seen as an irreversible process, although IC itself is formally an adiabatic process. After reaching the lowest vibrational level of S_1 the molecule can continue a non-radiative decay either *via* IC followed by VR back to the ground state or *via* intersystem crossing (ISC) into an isoenergetic vibrational level of the triplet excited state. This process (see **Figure 1**) is spin forbidden due to the change in multiplicity, and thus usually slower than competing processes. However, the rate of ISC can be increased using different approaches. One way to enhance ISC is by

spin-orbit coupling. Here, the change in the spin angular momentum is compensated by the change in orbital angular momentum. Practically, this can for example be achieved by using the heavy-atom effect, thus adding e.g., iodine, to the molecular structure. Another effect of spin-orbit coupling is that a change in orbital type can also increase the rate of ISC, according to the El-Sayed rules.[20] Several donor-acceptor dyads have also shown to enhance ISC *via* charge-transfer/separation followed by charge recombination. This will be further discussed in a later section of this thesis. Once the molecule has undergone ISC, it relaxes to the lowest vibrational level of the triplet state T_1 *via* VR. From T_1 the molecule can now continue with a non-radiative decay *via* another ISC followed by VR back to the singlet ground state.

Radiative processes: Instead of non-radiative decay, molecules in both the S_1 and the T_1 state can undergo a radiative decay. This process is called fluorescence in case of the molecule being in the singlet state and phosphorescence for a molecule in the triplet state. Most molecules obey Kasha's rule, stating that emission/radiative decay happens from the lowest excited state level in each multiplicity.[21] This rule derives from the energy gap law, which predicts the IC rate between two electronic levels to be inversely proportional to their energy difference.[22] This in combination with the Franck-Condon principle leads to the emission envelope commonly being a mirror image of the absorption envelope, where the difference in absorption and emission maxima is called the Stokes-shift.[18]

Different transitions occur at different timescales, or in other words they have different rate constants (k_x), where x describes the transition in question. Transitions that occur within the same state multiplicity are usually happening on a faster timescale, whereas transitions between different multiplicities are commonly slower. Absorption happens in a matter of femtoseconds (10^{-15} s). IC and VR are the next fastest transitions given that they are happening within the same multiplicity, and that they are usually covering smaller energy gaps, yet the rate constant is depending on the energy gap. For typical energy gaps between S_2 and S_1 they occur in the picosecond range (10^{-12} s). ISC, as this transition involves a spin flip, is slower than the other non-radiative decays about 10^{-8} s, however it can approach the picosecond range if the ISC efficiency is increased by e.g., spin-orbit coupling. The two described radiative decays, fluorescence and phosphorescence, are considerably slower than the non-radiative processes, when considering going in between the multiplicities. Fluorescence, a transition within the same multiplicity, happens normally in a few nanoseconds (10^{-9} s). Whereas phosphorescence is slower, due to the required spin flip during the transition, and can happen over a few microseconds to seconds (10^{-6}-10^{0} s).[17]

To anticipate the efficiency of a transition within the molecule, the quantum yield of the process (Φ_x) is determined. It is the ratio of the number of transition events per number of absorbed photons, and is determined for a specific wavelength. The quantum yields of fluorescence (Φ_F) is described by the ratio of emitted photons per absorbed photons. This value can also be expressed using rate constants. Fluorescence is a process following first-order kinetics, and its quantum yield can hence be described by the radiative rate (k_R) divided by the sum of all deactivating processes, k_R and all non-radiative rates (k_{NR}).

For the S_1 state this rate can be referred to as rate of fluorescence (k_F) and relates to Φ_F as shown in **Equation 2.**

$$\Phi_F = \frac{N_{\text{emitted photons}}}{N_{\text{absorbed photons}}} = \frac{k_F}{k_F + k_{NR}} \quad (2)$$

The average time a molecule spends in the excited state is described by the excited state lifetime (τ). The lifetime is determined for specific states and therefore depends on the transitions that depopulate that state. For example, the lifetime of the S_1 state can be expressed by the fluorescence lifetime (τ_F). It is inversely proportional to the sum of the rates for all deactivation processes from this state. τ_F can therefore be expressed according to **Equation 3**.

$$\tau_F = \frac{1}{k_F + k_{NR}} \quad (3)$$

The radiative rate and the non-radiative rate can therefore be expressed as the ratio of fluorescence quantum yield and the fluorescence lifetime as in **Equation 4a** and **4b**.

$$k_F = \frac{\Phi_F}{\tau_F} \quad (4a)$$

$$k_{NR} = \frac{1 - \Phi_F}{\tau_F} \quad (4b)$$

Photoinduced electron transfer: Photoinduced processes do not only involve transitions in between the energy levels of a single molecule. Energy-transfer processes or electron-transfer processes can also happen in between two molecules, or two different molecular units of supermolecules e.g., dyads. Energy transfer can occur through either electron exchange interactions which require orbital overlap, or *via* dipole-dipole interactions that originate from an oscillating electric field in space. Electron transfer can only occur *via* electron exchange interactions and thus requires orbital overlap.[19]

Electron-transfer reactions are fundamental chemical reactions where an electron is transferred from a donor (D) to an acceptor (A). The donor is thus oxidised while the acceptor is reduced, as seen in **Equation 5**.

$$D + A \rightarrow D^+ + A^- \quad (5)$$

This process can happen in the ground state as well as in the exited state. According to **Equations 6a** and **6b**, in a photoinduced electron transfer process (PeT), an electron from the excited state (D*/A*) is transferred to form the two separated, charged radical species $D^{+\cdot}$ and $A^{-\cdot}$.[19] The PeT process can also be called charge transfer (CT) and results is a new energetic state called charge transfer state (CTS). The process is also often referred to as charge separation where the final state is called the charge separated state (CSS).

$$D^* + A \rightarrow D^{+\cdot} + A^{-\cdot} \quad (6a)$$

$$D + A^* \rightarrow D^{+\cdot} + A^{-\cdot} \quad (6b)$$

The driving force for electron transfer is the overall change in the Gibbs free energy (ΔG). Considering the ground state electron-transfer (eT) in the gas phase ΔG_{et} can be calculated using the ionisation potential (IP) of the ground state of D (IP_D), and the

electron affinity (EA) of the ground state of A (EA_A), according to **Equation 7**. Where (IP_D) and (EA_A) can also be represented by the electrochemical potentials for oxidation $E^0_{(D^+/D)}$ and reduction $E^0_{(A/A^-)}$, respectively.

$$\Delta G_{eT} = IP_D - EA_A = E^0_{(D^+/D)} - E^0_{(A/A^-)} \quad (7)$$

Considering PeT, i.e., electron-transfer from a molecule in its excited state, the change in Gibbs free energy (ΔG_{PeT}) now also depends on the electronic excitation energy of the excited species (E_{exc}). The excitation energy is available to do work and can assist in moving electrons within an electron-transfer process. The final species obtained in this process are separate species of opposite charges. Thus, a gain in coulombic energy as a result of bringing two opposite charges closer together, has to be considered as well. This gain in energy depends on several factors and is represented by the Coulombic term. These variables are the approach distance of the two charged species (r), which can be approximated by the sum of the radii of the two ions, and the dielectric constant of the solvent (ε) since, depending on the polarity of the solvent, the charged species can be shielded, and thus stabilised more or less. Including the excitation energy and the Coulombic term into the equation for the change in free energy for excited state electron transfer we get **Equation 8.**

$$\Delta G_{PeT} = E^0_{(D^+/D)} - E^0_{(A/A^-)} - E_{exc} - N_A \frac{e^2}{4\pi\varepsilon_0\varepsilon r} \quad (8)$$

Where N_A is Avogadro's number ($N_A = 6.022 \cdot 10^{23}$ mol^{-1}), e is the charge of the electron ($e = 1.60 \cdot 10^{-19}$ C), and ε_0 is the permittivity of vacuum ($\varepsilon_0 = 8.85 \cdot 10^{-12}$ C^2 N^{-1} m^{-1}). The increased driving force for electron transfer, as a result of the excitation energy, clarifies why the excited state species oxidises and reduces more readily than the ground state species.[19]

Regenerating the initial excited states from this CSS, after VR already occurred, is an endergonic process. The back electron transfer process would therefore result in the ground states of D and A.[19] However, it has been observed that in D-A type molecules the CSS can recombine to form the locally excited triplet state of either the Donor or the Acceptor. This has been attributed to two different mechanisms, depending on the distance between the two units. For the so called radical pair ISC (RP-ISC) a long linker unit between D and A is required.[23] Opposite to this, for compact D-A type molecules another process the so called spin-orbit charge transfer ISC (SOCT-ISC) has been observed.[23-24] In this kind of molecules, the donor and acceptor are directly linked together leading to a rapid PeT, and therefore a rapid CSS formation. The geometry of the donor and acceptor must be orthogonal. Due to this geometry, the change in spin-angular momentum is accompanied by a change in orbital-angular momentum, in an event of ISC. This results in a conservation of the total angular momentum of the system.[25] SOCT-ISC is further addressed in a later section, using a directly linked BODIPY-anthracene molecule.

Excimer and Exciplex formation: Excited state molecules can form exited state complexes, upon collision with a ground state molecule. This collision can happen in

between two different molecular species or the same molecular species, according to **Equation 9a** and **9b** respectively.

$$B^* + C = (BC)^* \quad (9a)$$

$$B^* + B = (BB)^* \quad (9b)$$

In the case of the two colliding molecules being different, the excited state species is called an exciplex. When two identical molecules form such a complex it is referred to as an excimer. These complexes are stabilised by CT interactions between the two molecules. Since they are formed in the excited state, after absorption, no change is observed in the absorption spectrum, but in the emission spectrum. Signature of this phenomenon is a concentration-dependent, vibrationally unstructured, and red shifted emission, which is no longer a mirror image of the monomeric absorption. Excimer and exciplex formation can be probed using time resolved emission. It shows first mainly monomeric emission. After a short while excimer/exciplex emission arises and increases over time, while the monomeric emission decreases.[19]

Experimental analysis of photoinduced processes in molecules

Steady state measurements

Steady state absorption: Absorption of light by a molecule is studied by an ultraviolet-visible (UV-Vis) spectrophotometer. Most common UV-Vis spectrophotometers rely on the dual beam design shown in **Figure 3a**. One beam, the reference beam, is lead through air, the solution used to dissolve the sample, or the substrate the sample is deposited on, and then to the detector. The second beam is lead through the sample before it gets to the detector as well. The sample can be a solution of the molecule in a solvent (**Figure 3b**) or a solid sample. In **Figure 3c** a solid sample is demonstrated as a thin film on a substrate, as this is the solid samples used in projects I and III. By comparing the intensities of the reference beam (I_0) and the beam that has passed through the sample (I) the transmittance (T) of the sample is detected according to **Equation 10**.

$$T = \frac{I}{I_0} \quad (10)$$

This detected transmittance is then expressed in the form of absorbance (A), according to **Equation 11.**

$$A = \log\left(\frac{I_0}{I}\right) \quad (11)$$

The absorbance of a molecule gives information about the molecules ability to absorb light. This is quantified by the molar absorptivity (ε). ε can be determined, when the concentration of the sample (c) and the pathlength of the sample (l) -for liquid samples- is known. Their relationship is expressed by the Beer-Lambert-Bouguer law, shown in **Equation 12.**

$$A(\lambda) = \varepsilon(\lambda)cl \quad (12)$$

For solid samples the ability of the material to absorb light is often referred to as absorptivity. This value expresses the absorbance per thickness unit of the material.

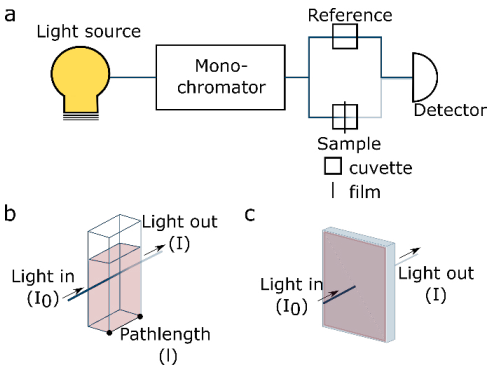

Figure 3. a: Schematic representation of a dual beam UV-Vis spectrophotometer. b: An imaginary liquid sample in a cuvette which absorbs light. c: An imaginary thin film of a sample, deposited on a glass plate, which absorbs light.

How the molecule absorbs light over a certain spectral range can be determined by varying the wavelength of the incident light beam. The transmittance is then detected for several points within the range of interest. To be able to cover a large spectral range, a UV-Vis spectrophotometer is equipped with different lamps. A deuterium arc lamp to cover the UV spectral range (190nm-320nm) and a tungsten filament lamp for the Vis and infrared range (320nm-2500nm). From the light source the light enters the monochromator, where it is dispersed in its constitutional waves by a diffraction grating. The wavelength is chosen by rotation of the diffraction grating, and then focusing the light of wanted wavelength on the exit slit. By scanning through a range of wavelengths the typical absorption spectrum is obtained.

Steady state emission: To get information about the emission properties of a molecule a spectrofluorometer is used. A typical setup of a spectrofluorometer is shown in **Figure 4**. Here light, typically originating from a Xenon lamp is sent through a monochromator to choose a specific excitation wavelength for the molecule. After the sample is excited, the emission is detected after a second monochromator unit, placed in an 90° angle to the excitation unit. This emission monochromator unit scans over the set wavelength range. The following detector is detecting the incoming photons, depending on their wavelength. The result of this measurement is an emission spectrum.

If instead the excitation monochromator is scanning over a certain spectral range, and the emission monochromator unit is fixed, the result of the measurement is called an excitation spectrum. This spectrum shows, which light is used to populate the excited state from which the emission is originating. The excitation spectrum for an ideal system -where Kasha's rule applies- should overlap with the absorption spectrum after normalising both of them.

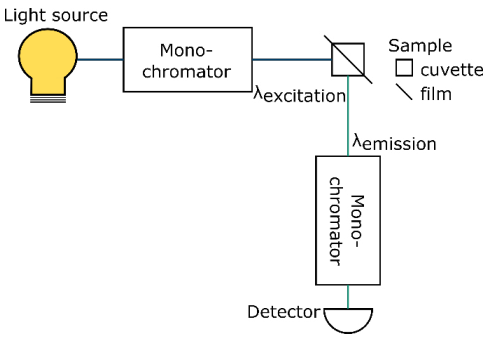

Figure 4. Schematic representation of a spectrofluorometer.

Using different accessories for the spectrofluorometer different information about the molecule's emission behaviour can be obtained. Using a cryostat or peltier element the temperature dependence of emission can be determined. An integrating sphere can be used to determine the quantum yield of fluorescence, by the absolute method. This is especially valuable to investigate the quantum yields of a solid sample. However, if both the absorption and the emission are known, Φ_F can be obtained using the relative method instead. Another requirement for this method to be feasible is, that a low absorbing sample is used in a 90° configuration. Using the relative method, a reference compound, with known Φ_F and absorption and emission in a similar range as the unknown compound is required. First the absorption of the compounds is measured, and the intensity of the absorption at the excitation wavelength is noted. Afterwards the emission of the compounds is measured using identical instrument settings. The area of the emission envelope is then integrated and the Φ_F can be determined according to **Equation 13.**

$$\Phi_{F_s} = \frac{n_s^2 A_{ref} F_s I_{ref}}{n_{ref}^2 A_s F_{ref} I_s} \Phi_{F_{ref}} \qquad (13)$$

Where (s) denotes the sample with unknown Φ_F and (ref) the reference compound. *n* is the refractive index of the solvent, A the absorbance at the excitation wavelength, F the integrated emission intensity and I the excitation intensity. The latter should be identical for the sample and the reference, if identical instrument settings were employed, and the intensity of the excitation light source is identical.

Time resolved measurements

Time resolved emission: To measure an average population timespan of an emissive excited state before it decays, a technique called time-correlated single photon counting (TCSPC) can be used. TCSPC is a digital counting technique. The sample is excited using a short-pulsed laser diode, where the wavelength of the laser-light needs to overlap with the excitation spectrum of the sample. At the time of excitation, the laser pulse, a timer starts. The first emitted photon hitting the detector stops the timer. This is repeated several times. The multiple timespans recorded are then plotted in a histogram, where the x-axis shows the recorded timespan from excitation to emission and the y-axis shows the number of photons detected. The obtained data can subsequently be fitted to obtain τ_F. For the fit to be more accurate the instrument response function (IRF) is

measured using the same method and settings. To obtain the IRF a highly scattering sample is used. The IRF is then deconvoluted from the measured histogram. A lifetime measurement including the IRF and an according fit is shown in **Figure 5**.

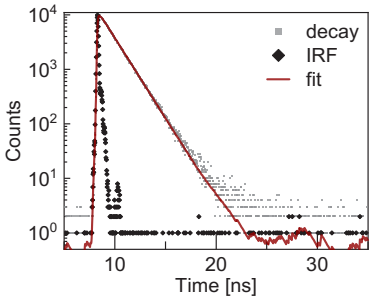

Figure 5. Lifetime measurement (grey) of ***s*P-BDP** (project III). Emission was recorded at 558 nm using a 510 nm laser diode for excitation. The IRF of the 510 nm laser diode is shown in black, and the fit in red. The fit gave a lifetime of τ_F = 1.52 ns.

Transient absorption: Some excited states decay non-radiatively and can therefore not be measured using TCSPC. To get information about the behaviour of non-radiative excited states, transient absorption spectroscopy can be used. Here the absorption of the excited state is followed over time. In this thesis, transient absorption at relatively long timescales using laser flash photolysis was performed. A schematic representation of the setup of the transient absorption spectrometer used is shown in **Figure 6a**.

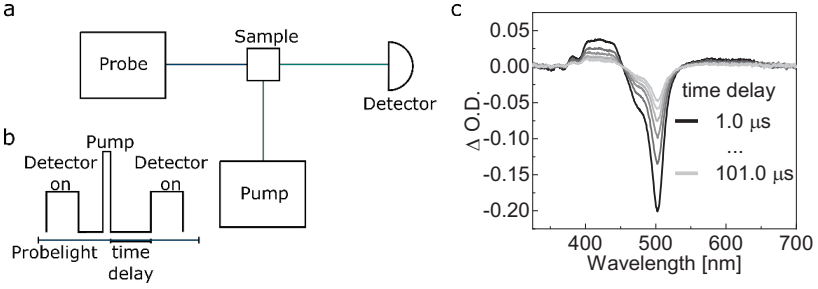

Figure 6. a: Simplified schematic representation of the transient absorption setup used in the scope of this thesis. b: Schematic pump-probe sequence used, with representative time delay. c: Transient absorption spectrum of the **Ph-Antra-BDP** monomer (project IV), as exemplary transient absorption scan with different time delays.

It consists of a continuous probe light which in this case is white light. Perpendicular to that is the pump beam. The pump unit generates a laser pulse of a specific wavelength, and the last part is the detector. The probe light shines through the sample and hits the detector, which records a spectrum. Within the measurement, the pump unit pulses a laser pulse to excite the sample, and after a certain time delay the probe light is detected again, as shown schematically in **Figure 6b**. The probe light, which is constantly shining is hence detected without/before the pulse and with/after the pulse. The difference in between those two scenarios of the detected probe light is the signal obtained, which is given as ΔO.D., shown in **Figure 6c**. The signal obtained can be positive representing

absorption from an excited state. A negative signal is corresponding to either depopulation of the ground state, called the ground state bleach, or stimulated emission from the sample. Depending on the detector used one wavelength can be observed over time or a wavelength range.

Interactions between molecules

How an organic molecule interacts with light is usually described on a single molecule, for the sake of simplicity. However, molecules are not available as isolated systems. Dilute solutions are the most common systems used to observe dye molecules, and how they interact with light. In this situation we can sometimes already observe that, for example the nature of the solvent influences some of the processes that occur after a molecule absorbs a photon. More concentrated systems also present altered properties compared to less concentrated systems. These observations are the result of interactions in between molecules, which are referred to as intermolecular interactions.

Intermolecular interactions: As opposed to the covalent, intramolecular interactions in between the atoms of a single molecule, intermolecular interactions are non-covalent. These interactions occur either in between different molecules or in between parts of the molecule. Intermolecular interactions determine the structural features as well as the physical properties, like the state/phase, of a large molecule or several molecules. Their basis are attractive or repulsive forces in between different molecules or parts of the molecule. Here we must distinguish between different kinds of molecules, ions, and neutral molecules. If the distribution of electrons within a neutral molecule is asymmetric an electric dipole-moment is induced. This dipole-moment can be either permanent, where two atoms of different electronegativities are bonded together, or temporary, where the dipole moment is induced when the molecule is affected by an external electric field. These temporary dipoles, also referred to as induced dipoles, can be induced by either ions or molecules with a permanent dipole moment in close proximity.

Interactions between different molecules are featured in several different facets and are usually categorised into ion-ion, ion-dipole, ion-induced dipole, dipole-dipole, dipole-induced dipole, and induced dipole-induced dipole interactions. Ion-ion interactions are the strongest intermolecular interactions. The resulting ionic bonds are formed by attractive forces in between differently charged ions. Ionic-dipole interactions as well as ionic-induced dipole interactions can be observed when a charged molecule interacts with an uncharged molecule. An example for this would be a solvent forming an ordered shell around a charged molecule.

In general interactions which do not include an ionic partner can be collected under the term van-der-Waals interactions.[26] Presumably the most know dipole-dipole interaction is the hydrogen bond. This is usually a bond connecting a hydrogen atom which is covalently bound to a more electronegative atom, the hydrogen bond donor, and an electronegative atom, commonly bearing a lone pair, the hydrogen bond acceptor.[27]

Interactions between induced dipole moments are also known as London dispersion forces. They are the weakest interactions between two molecules, yet they are

omnipresent. Nonetheless, one interaction should be highlighted here. Molecules having a π-system, an aromatic ring, exhibit a specific charge separation over the aromatic system. Looking at benzene, for example the six C-H bond dipoles give rise to a molecular quadrupole, where the sites above and below the benzene ring are negatively charged and the plane in the middle is positively charged, as shown in **Figure 7a**. Interactions between π-systems, the so called π-π-interaction, can occur in different geometries (**Figure 7b**). The T-shape or edge-to-phase geometry would be the preferred geometry although not accessible in larger aromatic systems. Thus, larger aromatic systems interact in the so-called slip stacked or displaced fashion.[28]

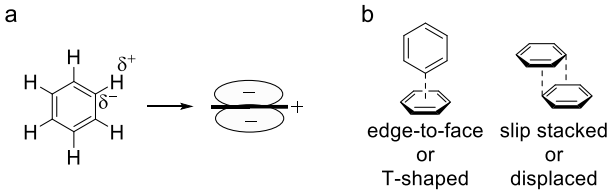

Figure 7. a: Schematic representation of the charge distribution in a π-system, taking benzene as example. b: The different geometries of π-π-interactions.

Matter: Bulk matter consists of a large number of molecules, atoms or ions. It can be present in three physical states or phases, solid, liquid, and gas. The gas state represents a state where molecules are spatially separated, and only interact with each other to a significant extent upon collision. The states liquid and solid, however, are described as condensed states of matter, where the molecules interact more with each other. According to the nature of a molecule, hence the strength and kind of intermolecular interactions, it presents itself in one of the three states at room temperature.

From the initial state at room temperature, when energy in form of heat, pressure, or both is added or removed, matter will undergo a transition into another phase. At a given pressure, this phase transition, which in other words is the spontaneous change from one phase into another phase, occurs at a characteristic temperature, referred to as transition temperature. Upon heating, a liquid will undergo a phase transition into the gas phase (vaporisation) at the boiling temperature (T_b), and a solid will undergo a transition into the liquid phase at the melting temperature (T_m). The reverse processes condensation (gas→liquid) and freezing (liquid→solid) for the same compound upon cooling happen at the same temperatures.

Phase transitions are processes, which can be explained by a change in the internal energy of the state upon a change in external conditions, like pressure and temperature. Where, at the transition temperature between two states itself, the free energy of the two states is equal. Enthalpy (H) represents the internal energy (U) of a system plus the product of pressure (*p*) and volume (V). Looking at systems with a constant pressure, the change in enthalpy is equal to the energy added to, or removed from the system, in the form of heat. Upon a phase transition, the enthalpy of the system increases or decreases, while the total energy is conserved in a closed system. Thus. the change in enthalpy is constant whatever direction the phase transition regards. For a phase transition to

happen spontaneously and directed, another factor must be taken into account, i.e. the entropy (S) of the system. Entropy can be described as the degree of disorder or randomness in a system. Considering a system with constant pressure, the change of entropy is either positive or negative for a system upon a phase transition. The sign of the value is dependent on the direction of the phase transition. If the system gains a more ordered structure after the transition, the entropy of the system decreases. Upon heating of the system, the entropy increases. The entropy is zero for all perfectly crystalline substances at T=0 K.[16]

Phase transitions can be expressed using the Gibbs free energy of a system (G=H-TS). Upon a phase transition all the three descriptive values of G change. Using the exclamation of dH=dU+pdV+Vdp and considering a closed system, not undergoing expansion, where we can use dU=TdS-pdV, we obtain **Equation 14**.

$$\mathrm{dG} = \mathrm{TdS} - p\mathrm{dV} + p\mathrm{dV} + \mathrm{V}dp - \mathrm{TdS} - \mathrm{SdT} = \mathrm{V}dp - \mathrm{SdT} \qquad (14)$$

Now considering constant pressure and having stated that S>0 for all substances, apart from perfect crystalline substances at T=0 K, this results in a decrease of Gibbs energy upon increasing temperature. Where the decrease in G is more significant in systems with higher entropy. In other words, G is most sensitive to temperature in the gas state and least in the solid state.[16]

The molecules studied in the scope of this thesis belong to the class of organic dye molecules. A common structural feature of this molecule class is an extended aromatic system. As a result, this molecule class is found in a solid state at room temperature, which is the state that will be discussed more in this thesis. The solid state can be distinguished into two main categories, crystalline solids and non-crystalline solids, also referred to as amorphous. The differentiation between these two categories lies within the arrangement of the constituents. In a crystalline solid the constituents are arranged in a regular three-dimensional crystal lattice, having both long-range and short-range order. As opposed to this, the constituents can aggregate with no long-range order. The solid is then called shapeless and therefore amorphous. A typical example for an amorphous solid is a glass. A solid showing features of both crystallinity and amorphousness is referred to as semicrystalline.

The process of forming a crystalline solid is called crystallisation. The first step in this process is the nucleation of the crystal followed by crystal growth. Nucleation describes the formation of a crystal nucleus in the liquid state of the compound. To form such a nucleus an energy barrier has to be overcome since the free energy of the liquid state is greater than the free energy of the final state.[29] Once the nucleus has reached a critical size by enough molecules conglomerating, so the nucleus is stable, the growth of the crystal begins. Here, molecules will, upon collision with the crystal nucleus either attach to it or not. This depends on the conformation of the molecule at the time of impact. Crystallisation is hence dependent on three major factors.[30] The free energy, which determines the probability of a crystal nucleus to form, or in other words the probability of the molecules not returning into the liquid phase. A kinetic part, the diffusion rate, which describes the mobility of the molecules in the liquid state, in other words it

describes the probability of the molecule to reach the nucleus. The third term is the conformational entropy of the molecules. It determines if the molecules can be fitted to the nucleus, which requires the molecules to be in the correct conformation at the point of impact. Here molecules having fewer possible conformations when in the liquid state are more likely to partake in the crystal growth. As opposed to that, molecules displaying a rich variety of possible conformations, due to their molecular structure, should have a lower rate of crystallisation.[30]

Crystalline materials of pure compounds commonly exhibit a very narrow melting temperature range, in other words a very precise T_m. The reason for this is the highly ordered crystal lattice, which is formed in the crystallisation process. The bonds are all equal and break at the same time upon heating. In heterogeneous samples which are usually less crystalline than pure compounds the melting temperature range is wider, due to different bond energies in the crystal lattice. A liquid composed of different molecules can upon cooling either form a structured crystal or aggregate randomly to form an amorphous solid. Those two processes happen at different temperatures. The crystallisation temperature is the same as T_m, and the glass transition temperature (T_g) refers to the temperature upon which motion freezes and a sample forms a glass. The conversion of a material into an amorphous solid state is called vitrification. Vitrification is usually achieved by first heating the sample until it reaches its liquid form and subsequently cooling the sample rapidly below its T_g so the sample solidifies into a glass.

Experimental analysis of the thermal behaviour of molecules

Differential Scanning Calorimetry: To obtain information on the thermal transitions of solid materials differential scanning calorimetry (DSC) can be used. In DSC the energy that is transferred to or from a sample when it is undergoing a physical or chemical change is measured. To obtain this, the sample and a reference, which has a well-known heat capacity, are measured at the same time. They are both placed together in a chamber, so that they are kept at nearly the same temperature, throughout the measurement, while the temperature is increased linearly over time. The difference in amount of heat required by the sample and the reference for increasing their temperature is measured. When the sample undergoes a specific phase transition, such as glass transition, melting or crystallisation, the amount of heat required to maintain the same temperature as the reference will vary. This shows as either a change in baseline, a positive peak, or a negative peak in the obtained thermogram. Such a thermogram is schematically shown in **Figure 8**. From such a thermogram, a claim can be made about the nanostructure of the solid. It can be judged if the solid is amorphous or semicrystalline.

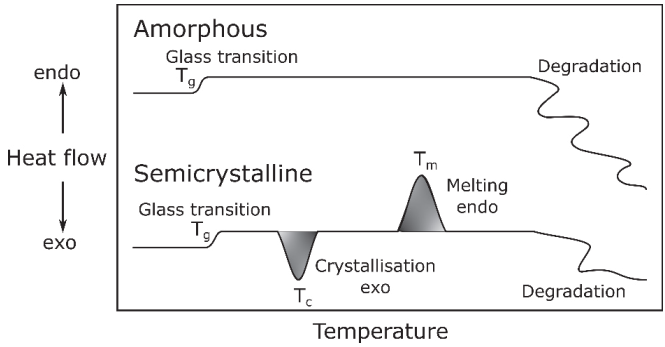

Figure 8. Schematic representation of a DSC scan showing glass transition, crystallisation, and melting. Exo refers to exotherm and endo to endotherm.

Fast scanning calorimetry: A method similar to DSC is fast scanning calorimetry (FSC). The principle of the measurement is the same, but here instead of the sample and reference being in a chamber, both probes are on a microchip. The chip already contains a reference sensor, and the sample is applied onto a second sensor on the same chip by either drop casting the dissolved sample or adding the solid. This instrument performs the same type of measurement but at much faster heating or cooling rates. In the measurements performed in project III the cooling speeds were varied from −0.1 to −1000 K s^{-1}. The resulting curves, one example of which is shown in **Figure 9**, were analysed to give the kinetic fragility values (*m*) of the measured compounds. The kinetic fragility describes how the viscosity of a material increases upon cooling and is used to classify glass-forming materials into fragile and strong glass-formers.[31-33]

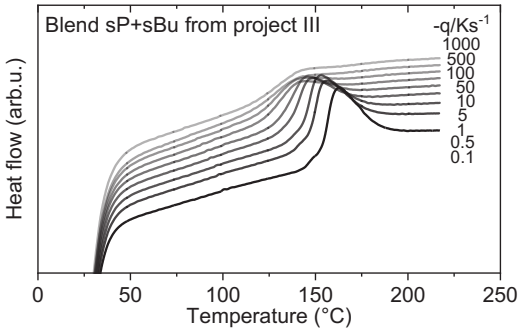

Figure 9. FSC thermogram of a blended film in project III showing a glass transition curve recorded with different cooling rates from -0.1 Ks^{-1} to -1000 Ks^{-1}.

Sample preparation of organic dye films

Spin coating: A simple process to prepare even and thin films on a substrate is spin coating. Prior to spin coating, the sample is dissolved in a solvent. The resulting solution is dropped onto the substrate. The substrate is subsequently rotated with an accelerating speed until the desired rotational speed is reached. During the rotation the sample is first spread out over the substrate due to centrifugal forces, while most of the solution is lost. After the sample has spread out, the film, which gets more viscose due to the loss of

solvent, gets thinner. The remaining solvent evaporates in the air flow and the result is a uniform solid thin film of the sample. The quality and thickness of the film can be controlled by changing the concentration of the sample, used solvent and rotating speed.

Drop casting: To prepare thicker films on a substrate one method that can be used is drop casting. Here a solution of the sample in a low boiling solvent, like dichloromethane, is prepared. The sample solution is dropped on the substrate and then the solvent is left to evaporate on its own. This process can be repeated several times to obtain a film with the desired thickness. The films obtained *via* drop casting are usually not entirely smooth due to uneven evaporation of the solvent over the surface of the film.

BODIPY dyes

Nowadays commercially available dyes reach over the UV-Vis to the near infrared (NIR) region and the number is growing steadily. Yet, the quest to find new fluorophores having an improved photostability or properties more specialised in a certain direction is ongoing. Among them the chromophore class of the boron-dipyrrins or boron-dipyrromethenes (BODIPYs), also referred to as "porphyrin's little sister", is held in high regards in various fields.[34]

This chapter will discuss the BODIPY dye class in various aspects. Firstly, the general structure and a short history is provided, followed by general synthetic strategies and functionalisation methods. Here the content will mainly focus on synthetic strategies used in projects I-IV which contribute to this thesis. In the consecutive section, the photophysical properties of the BODIPY dye class will be described. Additionally, a general overview on the influence of structural changes onto those properties will be highlighted. The findings of project II and project IV will be discussed in this section.

Structure and History

BODIPY, the core structure of which is shown in **Figure 10a**, consist of a dipyrromethene/dipyrrin framework complexed with a disubstituted boron, commonly difluoro-substituted. The dipyrromethene is built up from two pyrrole units fused together *via* an interpyrrolic methine (=CH−) bridge. The boron complexation hinders the *cis*/*trans*-isomerisation of the dipyrromethene and therefore increases the rigidity of the tricyclic compound class. This overall structure provides a planar molecule with a conjugated π-system, with π-electron delocalisation along the C-N-backbone.[35-36] Since the species involving the boron and nitrogen is of zwitterionic nature, BODIPYs have a net-neutral charge, with seven possible delocalised resonance structures, four of which are shown in **Figure 10b**.

BODIPY dyes were first reported in 1968 by Treibs and Kreuzer.[37] They discovered the BF_2-complex, consisting of two pyrrole units fused together by a carbon bridging atom, and described it as a stable and heavily fluorescing class of molecules, that could find application as laser dyes. In the 1980s, a water soluble BODIPY derivative was reported which created awareness of further potential of these compounds as fluorescent probes in medical and biological research.[38] Since then, the research interest in this chromophore class has grown, resulting in several thousand publications. The secret of their success lies within the chemical, photochemical and thermal stability of the boron-dipyrrin core. Additional to this stability, the molecule also exhibits strong and sharp absorption and emission with high molar absorptivity coefficients and fluorescence quantum yields close to unity.[39-40] Nevertheless, likely the most intriguing feature of this dye class is the outstanding chemical versatility of the boron-dipyrrin core, which allows

for selective functionalisation of every position of the chromophore core, either pre- or post-assembly.[34, 41-42] Additional to the 'ease' of structural modification, already small structural changes enable tuning of the photophysical properties. Consequently, BODIPY derivatives are widely used and find application in for example biological imaging,[43-47] photodynamic[48-49] and photothermal[50] therapy, sensing,[45, 51-52] organic electronics,[52-53] organic photovoltaics[54-56] and photocatalysis,[57] just to name a few.

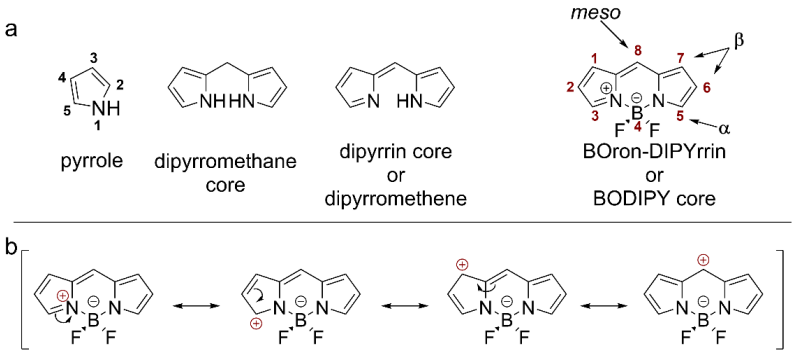

Figure 10. a: From left to right, core structure of pyrrole, dipyrromethane, dipyrromethene, and the BODIPY (IUPAC: 4,4-difluoro-4-bora-3a,4a-diaza-s-indacene) with the appropriate IUPAC numbering. The 3,5-positions of BODIPY are commonly specified as α-, whereas the 1,7- and 2,6-positions are referred to as the β-positions. The 8-position is often called the *meso*-position. Common boron dipyrrins, as shown here, have two fluorine atoms bound to the boron atom (4-position) . b: There are seven possible delocalised resonance structures of the BODIPY core, four of which are presented here, whereas the formal negative charge always remains on the boron.

Synthesis of BODIPY dyes

Before elaborating on the photophysical properties of the 'chameleon' BODIPY, as it was previously entitled in the literature, due to the property-tunability of the scaffold,[58] the synthesis of BODIPYs has to be addressed. The unsubstituted BODIPY core was first reported in 2009.[59] Synthesis of the unsubstituted core has proven to be rather difficult using previously established methods, due to the low stability of the unsubstituted dipyrromethene precursor, which decomposes at temperatures around -40 °C and above.[60] The focus in BODIPY synthesis has even before that been the modification and functionalisation of the dye. However, crediting the art of synthesising a wide range of functionalised BODIPYs one must take an excursion into pyrrole chemistry. Pyrrole chemistry is a field that could most certainly fill one or more likely several books.[61-65] The chemistry performed on these five membered heterocyclic moieties is decidedly highly versatile, which also explains the wide range of BODIPYs and why those are esteemed representatives of fluorophores. Although, since getting into the depth of pyrrole chemistry is undeniably beyond the scope of this work, this excursion will be limited to the chemistry utilised in the projects that built this thesis. Firstly, the different condensation reactions of pyrroles which lead to the dipyrromethane, or the dipyrromethene, and complexation to the BODIPY will be discussed. The pyrroles used in the scope of this work were alkylated in either α- or β-positions, therefore, it will be described how those alkylated pyrroles can be obtained in different ways. Lastly, the well-

known palladium-mediated Suzuki-Miyaura coupling reaction will be described, which was used to obtain arylated pyrroles.

From pyrrole to BODIPY: The first reported synthesis of BODIPYs, *via* acetylation of 2,4-dimethylpyrrole in boiling acetic anhydride in the presence of $BF_3{\cdot}OEt_2$ by Treibs and Kreuzer, would nowadays be considered to use rather harsh conditions. In the last years the methods to synthesise and modify BODIPYs have been extensively explored.[34, 39, 41, 66] Synthesis of functionalised BODIPYs can be achieved *via* condensation of pre-functionalised pyrroles, to the corresponding dipyrromethene unit. This is followed by an *in situ* boron complexation to the BODIPY, using triethylamine (NEt_3) and boron trifluoride diethyl etherate ($BF_3{\cdot}OEt_2$). Condensation of the pyrrole units, to either symmetric or asymmetric products, can be achieved in multiple fashions, a few of which are depicted in **Figure 11**. A one pot approach to yield symmetric BODIPYs, similar to the original route from Treibs and Kreuzer, is an acid-catalysed condensation between pyrrole and an acid chloride, or anhydride, yielding the dipyrromethene (**Figure 11a**).[67-69] A similar, and widely used approach is the acid-catalysed condensation of pyrrole with an aldehyde, typically aromatic aldehydes. This leads to the formation of the usually more stable precursor of the dipyrromethene, the dipyrromethane shown in **Figure 11b**. Due to the higher stability of the dipyrromethane the molecule can be isolated and further functionalised.[70] After the desired functionalisation of the dipyrromethane, treatment with an oxidant like 2,3-dichloro-5,6-dicyano-*p*-benzoquinone (DDQ), provides the dipyrromethene. Dipyrromethenes and therefore BODIPYs, carrying different aryl substituents in the *meso*-position, can be obtained using different arylated acid chlorides or aldehydes.

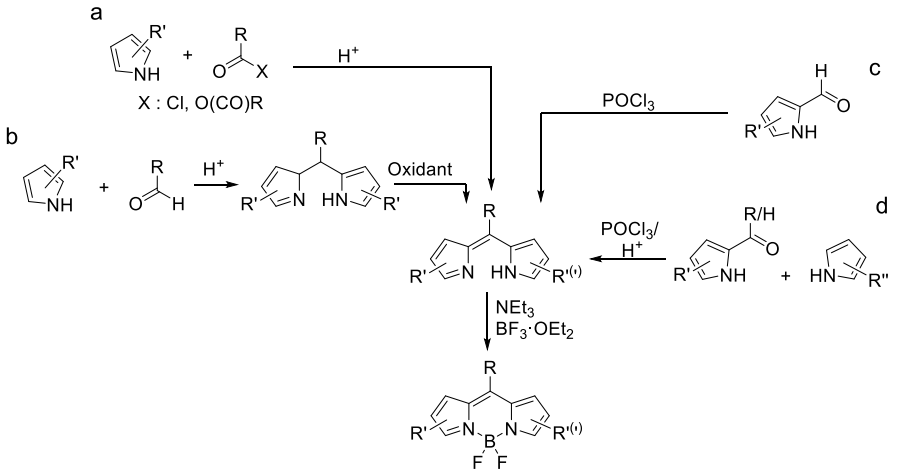

Figure 11. Representation of four different, commonly used syntheses paths a, b, c and d towards symmetric and unsymmetric BODIPYs using pre-functionalised pyrroles.

Alternatively, derivatives with a free *meso*-position can be generated by a self-condensation of pyrrole-2-carbaldehyde in the presence of phosphoryl chloride ($POCl_3$) that has been developed in 2008 by Burgess's group (**Figure 11c**).[71] The same

approach was utilised to synthesise asymmetric BODIPYs using two different pyrrole moieties (**Figure 11d**).[72] In the synthesis of symmetric dipyrromethenes the use of $POCl_3$ in this synthetic approach seems to be crucial to the suggested reaction mechanism shown in **Figure 12**. The use of other acid catalysts or Lewis-acids did not yield the symmetric product. Yet, in **project II** it was realised that the use of catalytic amounts of acetic acid with formylated pyrroles, followed by the addition of a second pyrrole, leads to the formation of the asymmetric product.[73] The use of those different condensation pathways leads to a great variety of BODIPY dyes, due to the wide range of pyrroles that can be used. In all the above-mentioned reactions, the highest yields are achieved using pyrroles with only one free α-position. Otherwise, the condensation can occur on both α-positions leading to the formation of a porphyrin instead of the desired product.[65]

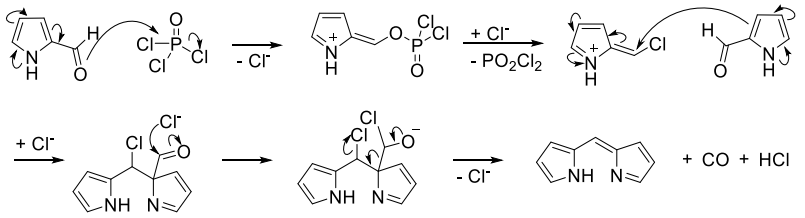

Figure 12. Proposed mechanism for the self-condensation of pyrrole-2-carbaldehyde in the presence of phosphoryl chloride, developed by Burgess's group.[71]

The 5-membered electron-rich heterocyclic pyrroles are quite resistant to nucleophilic addition or substitution, yet the range of electrophilic reactions is relatively large.[74] If not equipped with an electron withdrawing substituent, naked pyrrole, C-, or N-monoalkylated, and also C,C-dialkylated pyrrole is easily polymerised especially by strong acids. Here, the reactivity decreases in the order mentioned. This undesirable feature makes many electrophilic reagents unusable.[65] Another comment has to be made on the reactivity of pyrroles. In electrophilic reactions the position which is preferred for substitution is the C2/C5 or α-position. Accessing the C3/C4 or β-position of the naked pyrrole by means of electrophilic reactions has proven to be challenging to realise. One strategy to selectively substitute the β-position is by attaching either an electron withdrawing or bulky substituent to the nitrogen centre of the pyrrole, or a *meta*-directing electron withdrawing group to the α-position.[75-77]

Vielsmeier-Haack reaction: To synthesise pyrrole-2-carbaldehyde, which can be utilised for condensation to either symmetric or asymmetric BODIPY dyes, the Vilsmeier-Haack reaction can be performed. This formylation of electron rich aromatic and heterocyclic compounds with dimethylformamide (DMF) and $POCl_3$ is a widely used reaction, and the key steps are represented in **Figure 13**.[78] DMF and $POCl_3$ react to form an *N,N*-dimethyl chlormethyleneiminium cation *in situ*. This, so called Vilsmeier(-Haack) reagent, then acts as the electrophilic species and is attacked by the pyrrole to form an iminium ion intermediate. This intermediate is subsequently hydrolysed in an aqueous workup to yield the pyrrole-2-carbaldehyde.[79]

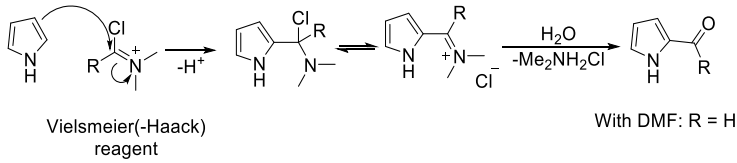

Figure 13. General mechanism of the Vilsmeier-Haack acylation reaction of pyrrole with the *in situ* produced Vilsmeier-Haack reagent.

Synthesis of alkylated pyrroles: Furthermore, as shown in **Scheme 1**, instead of DMF, different *N,N*-dialkyl amides can be used in a similar fashion in an acylation reaction to produce pyrryl-2-ketones. The carbonyl can then be reduced using common reducing agents like lithium aluminium hydride ($LiAlH_4$) or sodium borohydride ($NaBH_4$) This produces the corresponding α-alkylated pyrrole.[80-82] In **project I**, this strategy was used to synthesise 2-ethyl-pyrrole and 2-butyl-pyrrole. These pyrroles were subsequently subjected to a second Vielsmeier-Haack reaction, using DMF, to form the 2-alkyl-5-formyl-pyrroles. The formylated pyrroles were then used in a self-condensation as developed by Burgess, using $POCl_3$, followed by addition of first NEt_3 and then $BF_3{\cdot}OEt_2$. This resulted in the 3,5-alkylated BODIPYS **Et-BODIPY** and ***n*Bu-BODIPY**, shown in **Scheme 1**.[80]

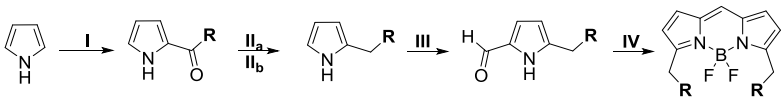

R = CH_3 **Et-BODIPY** 11 %[a]
R = C_3H_7 ***n*Bu-BODIPY** 10 %[a]

Scheme 1. Synthesis of α-alkylated BODIPYs carrying linear alkyl chains. Reaction conditions: **I**) 1. $POCl_3$, $(CH_3)_2NCOR$, DCE 2. NaOAc, H_2O **II$_a$**) $LiAlH_4$, THF **II$_b$**) $NaBH_4$, IPA **III**) 1. $POCl_3$, DMF, DCE 2. NaOAc, H_2O **IV**) 1. $POCl_3$, DCM 2. Et_3N, $BF_3{\cdot}OEt_2$. [a] the yields are given for step IV.

A different way to obtain alkylated pyrroles is *via* alkylation of pyrrylmagnesiumbromide.[83-84] This reaction yields α- and β-alkylated pyrroles, where the former is the major product. Unlike the Vielsmeier-Haack type reaction, this approach also gives access to pyrroles carrying branched alkyl chains in the α-position.

Alkylation of pyrrylmagnesiumbromide was used in **project I** to obtain pyrroles carrying branched alkyl chains in the α-position. Treatment with the designated alkyl bromide, in this case *tert*-butyl, *sec*-butyl and isopropyl-bromide, afforded a mixture of α- and β-substituted alkyl pyrroles. Sufficient separation of the two formed regioisomers was unsuccessful *via* distillation or column chromatography. Thus, the mixture was subjected to the next step, a Vielsmeier-Haack formylation. The obtained mixture of 2- and 3-alkyl-5-formylpyrroles could then be separated using column chromatography. The prepared 2-alkyl-5-formylpyrroles were afterwards subjected to the self-condensation and then complexation (**Scheme 2**). The condensation and complexation yielded ***t*Bu-BODIPY**, ***s*Bu-BODIPY** and **IP-BODIPY** in 15, 49 and 44 %. If the yields of these steps are compared to the yields of the 3,5-alkyl BODIPYs carrying linear alkyl chains, **Et-BODIPY** and ***n*Bu-BODIPY** 11 % and 10 %, a considerable increase can be seen, by having the

bulkier, branched isopropyl and *sec*-butyl substituents. However, the yield then drops again with the even bulkier *tert*-butyl substituents.[80] This indicates that the introduced steric bulk in the α-position either prevents side reactions or increases the stability of the dipyrromethene-intermediate. However, from the proposed mechanism of this reaction, shown in **Figure 12**, it is not obvious why steric bulk should affect the rate of the reaction. The addition of too bulky substituents though seems to create a steric hindrance, most probably in the complexation step, leading to a lower reaction yield.

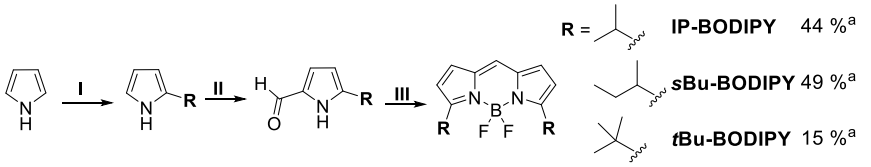

Scheme 2. Synthesis of the BODIPY derivatives, having different branched alkyl chain substituents in the 3,5-positions. Reaction conditions: **I**) 1. MgI, Et_2O 2. BrR, Et_2O 3. NH_4Cl_{aq} **II**) 1. $POCl_3$, DMF, DCE 2. NaOAc, H_2O **III**) 1. $POCl_3$, DCM 2. Et_3N, $BF_3{\cdot}OEt_2$. [a] the yields are given for step III.

Another strategy of obtaining a pyrrole with the desired substitution pattern is to synthesise the pyrrole itself. The Van Leusen reaction for example can be used to prepare 3,4-disubstituted-pyrroles. This reaction can also be used to prepare 3,4-diaryl-pyrroles, using electron deficient vinyl arenes, or 2,5-unsubstituted-3-nitropyrroles when using unsaturated nitro compounds as Michael acceptors.[85-86] In the reaction, tosylmethyl isocyanide (TosMIC), or more accurately the anion of TosMIC adds to a Michael acceptor, here an unsaturated ketone or ester. This step is followed by ring closure onto the isocyanide carbon. After the elimination of the tosylate anion the 3,4-disubstituted pyrrole is formed (**Figure 14**).

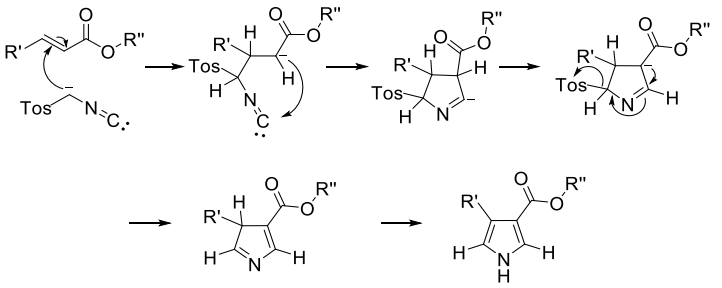

Figure 14. General mechanism of the Van Leusen reaction of TosMIC with an unsaturated ester to form 3,4-disubstituted pyrrole.

In a decarboxylation reaction using KOH and heat the ester substituent can be eliminated yielding the β-susbstituted pyrrole. In **project II** this synthetic route was developed to synthesise β-*sec*-butyl-pyrrole.[73] It was utilised again in **project III** to install different alkyl chains, giving products **1**-**4** in **Scheme 3**, using different unsaturated esters.[87] These can be synthesised *via* a Wittig-reaction using triethyl phosphonoacetate and different alkylaldehydes (step I in **Scheme 3**). The β-isobutyl-pyrrole **3** shows a lower overall yield than the other prepared pyrroles **1**, **2**, and **4**. This is mainly due to a significantly lower yield in the Van Leusen reaction (step II in **Scheme 3**) of 57 % compared to >90 % for

the three other compounds. The only difference here is the branching position of the alkyl chain, which only in the case of the isobutyl is not directly next to the double bond in the Michael acceptor used for the Van Leusen reaction. This indicates that having the branching position on the vicinal carbon to the double bond either stabilised the intermediate or facilitates the attack of the TosMic-anion.

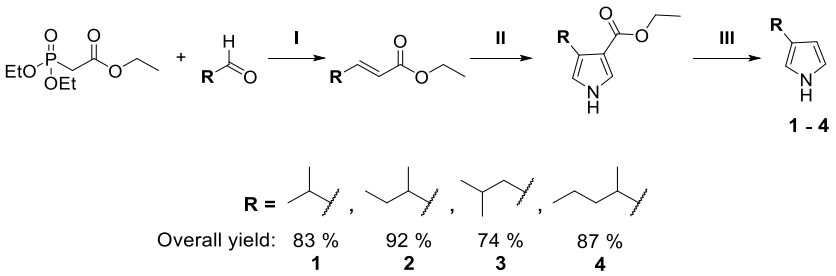

Scheme 3. Synthesis towards β-alkylated pyrroles. Reaction conditions: **I**) 1. NaH, THF, r.t., 14 h **II**) TosMIC, NaH, THF, r.t. o.n. **III**) KOH, $(CH_2OH)_2$, reflux, 5 h.

Suzuki-Miyaura cross coupling reaction: To obtain arylated pyrroles the palladium mediated Suzuki-Miyaura cross coupling can be used for the C-C bond formation between the pyrrole boronic acid, or ester, and an aryl halide. These reactions require an aqueous base and the active species Pd(0), which can be either added directly into the reaction, or formed *in situ* by reduction of Pd(II) usually partnered with a stabilising ligand that also facilitates the reaction.[88] Pyrrole boronic acid is known to undergo protodeboronation under basic conditions as well as elevated temperatures.[89-93] To circumvent this undesired side reaction the choice of catalyst is crucial. The reaction is reported to give rather poor yields or to not occur using conventional catalytic systems. Buchwald et al. developed precatalysts, XPhosPdG2 as an example, that can be used for this matter (**Figure 15**).[94] This precatalyst permits a rapid generation of the active species XPhosPd(0) at room temperature. Here, a mild base deprotonates the precatalyst which successively undergoes a reductive elimination to form XPhosPd(0). Using this catalyst allows the successful coupling reaction of these unstable boronic acids to occur under mild conditions. The protodeboronation of the pyrrole boronic acid can then be avoided almost completely. This strategy leads to excellent yields for the cross coupling reaction between different alkylated pyrrole boronic acids and arylhalides with both electron withdrawing and electron donating groups as shown in **Scheme 4**, performed at room temperature.[73] The Suzuki coupling with the same reaction conditions was used in both **project II**, using different arylbromides, and in **project III**, using differently alkylated pyrrole-boronic acids. The reactions were run for 4 h at room temperature with aqueous 0.5 M K_3PO_4 as a base, and a catalyst loading of 2 mol %, and led to yields between 72-93 %.

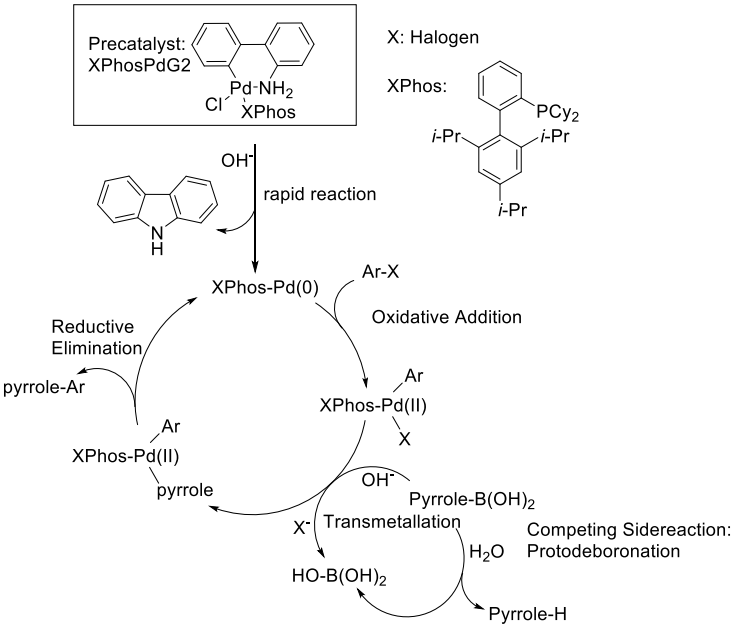

Figure 15. General mechanism of the Suzuki-Miyaura cross coupling reaction between an aryl halide and pyrrole boronic acid using XPhosPdG2 as precatalyst. The competing side reaction, protodeboronation, can be avoided almost completely using the precatalyst XPhosPdG2.[94]

The synthesised pyrroles shown in **Scheme 4** were subsequently used for preparation of BODIPYs used in **projects II** and **III**. The conditions for this are shown in **Scheme 5**.

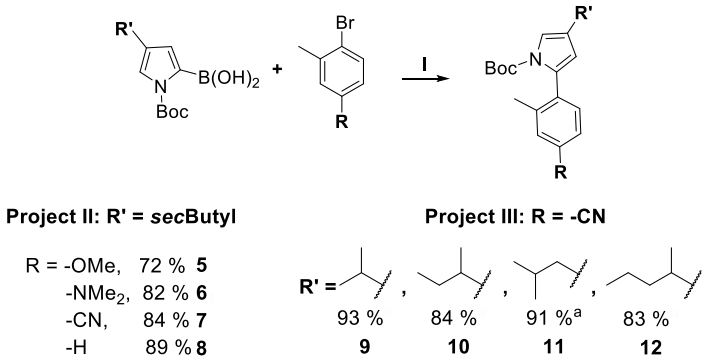

Scheme 4. Suzuki coupling between the alkylated pyrrole and different *para* substituted *ortho*-bromotoluene derivatives. Reaction conditions: **I**) XPhosPdG2, 0.5 M K_3PO_4, THF, r.t., 4 h.

In **project II** symmetric and asymmetric BODIPY derivatives carrying both electron-withdrawing (EWG) and electron-donating (EDG) groups were synthesised by using combinations of the Boc-deprotected versions of pyrroles **5**, **6**, **7**, and **8**.[73] To obtain the symmetrical BODIPYs **CN-CN-BDP** and **H-H-BDP** pyrroles **7** and **8** were subjected to a Vielsmeier-Haack formylation. The obtained α-formylated pyrroles were then used in a self-condensation to the dipyrromethene using $POCl_3$. This was followed by the

complexation to the BODIPY. Here the electron withdrawing effect of the cyano-group leads to a lower yield of 13 % for **CN-CN-BDP** as compared to **H-H-BDP**, which gave 38 % using the same conditions. The asymmetric BODIPYs **H-NMe$_2$-BDP**, **OMe-NMe$_2$-BDP** and **CN-NMe$_2$-BDP** were obtained by first subjecting one of the pyrrole partners to a Vielsmeier-Haack formylation. The formylated pyrroles were then mixed with their non-formylated partners and subjected to an acid catalysed condensation reaction using acetic acid (AcOH). The yields for the obtained BODIPY derivatives vary between 4 and 21 %. A trend towards the electronic character of the reacting pyrroles, according to the *para*-substituent, can be observed here as well. The non-formylated pyrrole in all the reactions used here was pyrrole **6**, which possesses the strongly electron donating *N,N*-dimethylamino (NMe_2) group. The reaction partners with the EDG and the EWG give the lowest and the highest yield respectively, whereas the yields of the reaction partner with neither lie in between. The condensation reaction towards asymmetric dipyrromethenes thus seems more efficient if one partner has an EDG and the other an EWG. It is also of importance which partner has which group. Condensation between the formylated version of pyrrole **6**, and pyrrole **7** was also attempted but didn't lead to the desired product. This leads to the conclusion, that the condensation reaction is not successful if the electron donating properties of the formylated reaction partner are too strong.

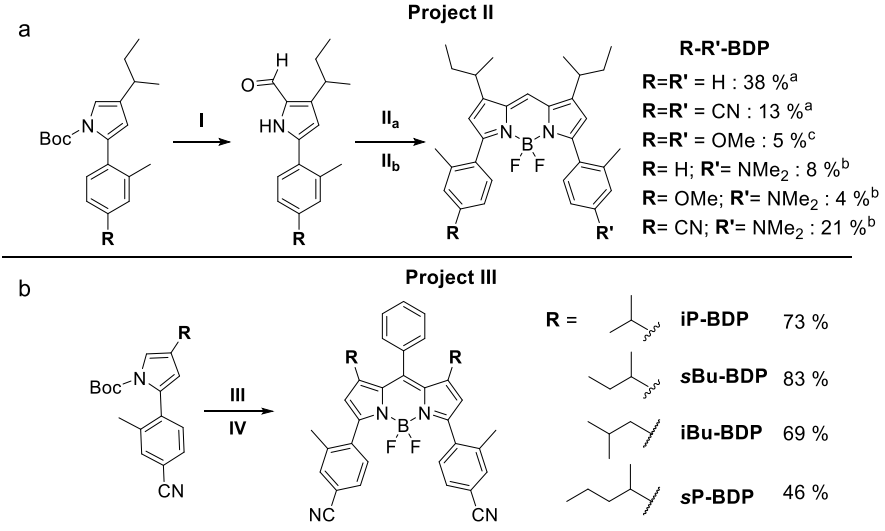

Scheme 5. a: Synthesis of the BODIPY derivatives from the respective Boc-protected pyrroles, used in project II. The names of the compounds are **R-R'-BDP** according to **R** and **R'**. Reaction conditions: **I**) 1. NaOMe (25w% in MeOH), THF 2. $POCl_3$, DMF, DCE 3. NaOAc, H_2O; **II$_a$**) **R=R'**: 1. $POCl_3$, DCM 2. Et_3N, $BF_3{\cdot}OEt_2$, DCM. **II$_b$**) **R≠R'**: 1. Deprotected pyrrole with R', AcOH, DCM; 2. Et_3N, $BF_3{\cdot}OEt_2$, DCM. [a] overall yields for I and II$_a$; [b] overall yields for I and II$_b$; [c] compound was obtained as a side product during the synthesis of OMe-NMe$_2$-BODIPY. b: Synthesis of the BODIPY derivatives of project III, carrying different alkyl chains in the 1,7-positions, from the according pyrroles. Reaction conditions: **III**) NaOMe 25w% in MeOH, THF, r.t., 2 h **IV**) 1. Benzaldehyde, TFA $_{cat}$, DCM, r.t. o.n. 2. DDQ, DCM, r.t. 1 h 3. Et_3N, $BF_3{\cdot}OEt_2$, r.t. o.n.

To obtain different alkylated BODIPY derivatives that were used in **project III**, different alkylated boronic acids, made from pyrroles **1**-**4**, were used in the Suzuki coupling.[87] The

coupling yielded pyrroles **9**, **10**, **11**, and **12** in high yields of 83 – 93 %. The deprotected pyrroles were subjected to an acid catalysed condensation reaction using benzaldehyde as the condensation partner, followed by DDQ as an oxidant. Complexation of the obtained dipyrromethene derivatives to the BODIPY was again carried out using NEt_3 and $BF_3{\cdot}OEt_2$. This yielded the symmetrical BODIPYs **iP-BDP**, ***s*Bu-BDP**, **iBu-BDP** and ***s*P-BDP** with a phenyl group in the *meso*-position in yields of 46-83 %.

Post-functionalisation: Once the core is assembled, BODIPYs are also highly susceptible to post-functionalisation. The different positions of the BODIPY core can be modified selectively. Another benefit except the site selective modification is that the synthesis of unstable pyrrole precursors can be avoided. Reactions reported for this purpose are numerous and expanding steadily. However, this section will only give a brief overview over the possibilities of post-functionalisation on the BODIPY core since it was not heavily applied in this work. Derivatisations on the BODIPY core can be categorised into reactions at the pyrrolic ring carbons (positions 1,2,3,5,6,7), the *meso*-carbon (position 8) and the boron atom (position 4).[41-42, 95] **Figure 16** shows an overview of the most common reaction types used for site-selective functionalisation of BODIPY dyes.[42] The resonance structures of the BODIPY core shown in **Figure 10b**, predict the reactivity of the different positions. The *meso*-position as well as the 1,3,5,7-positions have a higher positive charge as compared to the 2,6-positions. Therefore the 2,6-positions are more susceptible to electrophilic aromatic substitution reactions (S_EAr), whereas the 1,3,5,7- and *meso*-position will undergo nucleophilic aromatic substitution reactions (S_NAr) instead. The 2,6-position have also been found susceptible for oxidative C-C coupling reactions using either anhydrous iron trichloride ($FeCl_3$),[96] or the hypervalent iodine reagent phenyliodine(III)-bis(trifluoroacetate) (PIFA),[97] allowing the synthesis of oligomers by direct β-tethering of BODIPY units. Selective modifications on the 1,3,5,7-positions and the *meso*-position can also be done by the Knoevenagel condensation. In the recent years, transition metal catalysed coupling reactions as well as numerous C-H activation reactions have been developed to selectively functionalise all the pyrrolic carbon positions as well as the *meso*-position of the BODIPY.[66, 98] Replacement of the fluoride atoms on the borons is a less developed field, yet it can be achieved most efficiently by hard nucleophiles due to the boron atom being a hard Lewis acid.[42, 99]

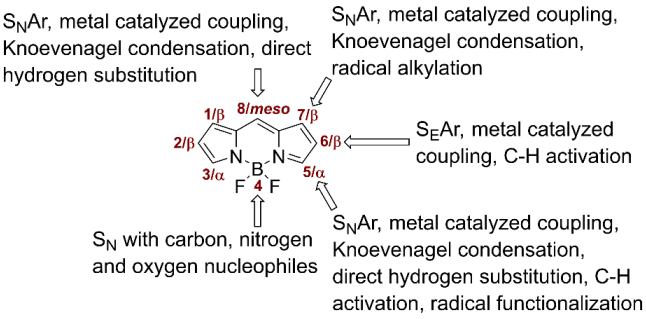

Figure 16. Overview of synthetic methods of post-functionalisation of BODIPY in different positions. The modifications possible on the pyrrolic carbons are only shown on the 5,6,7-positions but are equally valid for the 1,2,3-position and often disubstitution on both rings is possible.

β-Tethering of the previously reported **Ph-Antra-BDP**[100] was achieved in **project IV** using both PIFA, and anhydrous $FeCl_3$, to synthesise several small oligomers of the compound (**Scheme 6**). When using PIFA the **Dimer** of the compound could be obtained in 8 % yield and purified using three sequential purification steps, first and second were column chromatography on silica followed by preparative thin layer chromatography, as a third one. With anhydrous $FeCl_3$ the **Dimer**, two atropisomers of the **Trimer** and one isomer of the **Tetramer** were obtained, in 17 %, 2 %, 1 % and <1 % yield respectively. The compounds were separated using first column chromatography, where first a yellow shining fraction (unreacted **Ph-Antra-BDP**), then an orange shining fraction (**Dimer**) and finally a red shining fraction (mixture of higher oligomers) were collected. The fraction containing the **Dimer** was purified further using column chromatography. The red shining fraction was subjected to size exclusion chromatography. The obtained fractions were combined according to their absorption bands. A last preparative thin layer chromatography of the combined fractions yielded two different atropisomers of the **Trimer** and one isomer of the **Tetramer**. The structure and size of the oligomers could be verified by mass spectrometry and nuclear magnetic resonance (NMR) spectroscopy. In the ^{1}H-NMR spectra, the number of CH_3 peaks indicates the size of the oligomer. The two isolated atropisomers of the **Trimer** show different patterns regarding the separation of those peaks. The isolated **Tetramer** shows only one kind of peak pattern, indicating that only one isomer was isolated. However, the different atropisomers of the **Trimer** could not be further distinguished using NMR techniques, due to the too large distance of the anthracene units.

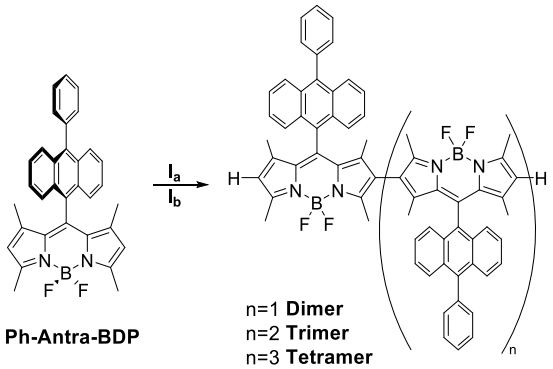

Scheme 6. Synthesis of the *meso*-10-phenylanthracene-BODIPY dimer (n = 1) and trimer (n = 2) and tetramer (n = 3) *via* two different routes. Reaction conditions: **I_a**) PIFA, $BF_3{\cdot}OEt_2$, DCM, -78°C - r.t, 1 h. **I_b**) anhydrous $FeCl_3$, DCM, r.t., 25 min.

Modification of the BODIPY core: Not just the periphery of the BODIPYs can be modified but also the core structure of the molecule. Next to the replacement of the fluorine atoms on the boron, another method for functionalisation of BODIPYs, used increasingly in the last years, is to change the bridging atom of the dipyrrin core. The bridging carbon atom between the pyrroles can be replaced with a nitrogen atom. This dye class with a N bridge is referred to as aza-BODIPYs (**Figure 17a**). The precursors of which, the tetra-aryl-aza-dipyrromethenes, shown in **Figure 17b**, were discovered in

1943.[101-102] Although they were discovered before the BODIPY class, they have not received a lot of attention at first. Just in the last couple of years this subclass of the BODIPYs has attracted an increasing amount of interest.[103-105] This aza-dipyrromethene can then be subjected to boron complexation using the same conditions as for the BODIPYs to give the aza-BODIPY.[101-102, 106]

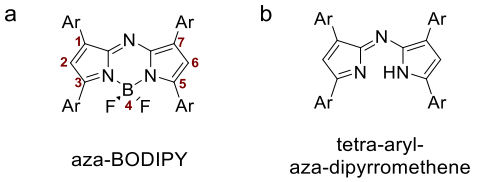

Figure 17. a: The generic tetra-arylated aza-BODIPY structure. b: The framework of the tetra-aryl-aza-dipyrromethene precursor.

Rogers and Davies, who reported these aza-dipyrromethenes first in 1943 presented the synthesis in two different ways shown in **Figure 18**. The first way (**Figure 18a**) was the transformation of a 2,4-diarylpyrrole into the 5-nitroso compound thereof, using nitrous acid (HNO_2). This compound then readily undergoes a condensation reaction with a second 2,4-diarylpyrrole to form the aza-dipyrromethene. The second way (**Figure 18b**) was the reaction of formamide or another ammonia source with two equivalents of a compound of the type diaryl-γ-nitro ketones or diaryl-γ-cyano ketones.[102]

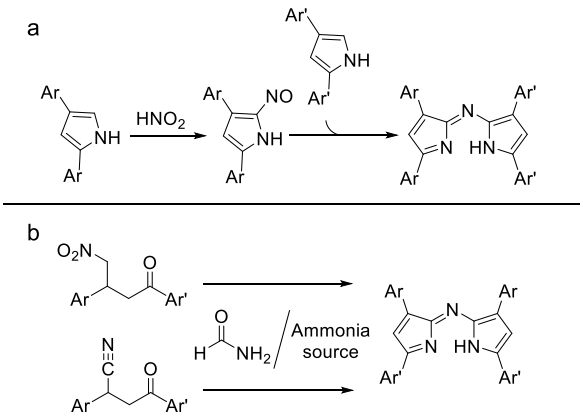

Figure 18. a and b: The synthetic pathways towards tetra-aryl-aza-dipyrromethines presented by Rogers and Davies.[102]

Until now, both pathways reported by Rogers and Davies are the basis for the commonly used methods to prepare aza-diyprromethenes. O'Shea's group developed the most popular routes for synthesising both symmetric and asymmetric aza-BODIPYs, based on those (**Figure 19a**).[107-108] To get symmetric aza-BODIPYs, diaryl-γ-nitro ketones can be synthesised in high yields *via* a Michael addition of nitromethane to α,β-unsaturated ketones in presence of diethylamine (Et_2NH) as a base. Subsequent treatment with ammonium acetate in either ethanol or butanol under reflux, forms the symmetric aza-dipyrromethene. The aza-dipyrromethene precipitates from the used solvent and can

later easily be purified by either filtration or chromatographic methods. The aza-BODIPY can then be synthesised by addition of $BF_3{\cdot}OEt_2$ in presence of a base like NEt_3.[107] To synthesise asymmetric aza-BODIPYs the same group introduced a strategy shortly after.[108] Here, a nitrosopyrrole, prepared by the reaction of pyrrole with sodium nitrite ($NaNO_2$) under acidic conditions at room temperature, reacts with another pyrrole in a condensation reaction in the presence of acetic anhydride and acetic acid. Aza-BODIPYs carrying up to four different aryl-substituents can be synthesised this way. The pyrroles can either be obtained using traditional pyrrole synthesis or by treatment of the previously used diaryl-γ-nitro ketones with NH_4OAc in acetic acid at 100 °C.

Carreira's group proposed around the same time that pyrroles treated with $NaNO_2$, AcOH and Ac_2O form the corresponding aza-dipyrromethene (**Figure 19b**).[109-110] This method can be used to synthesise both symmetric and asymmetric aza-BODIPYs. When adding 1 equivalent of $NaNO_2$ to a pyrrole and then adding a second pyrrole the asymmetric aza-dipyrromethene is formed. Adding 0.5 equivalents of $NaNO_2$ to a pyrrole the symmetric aza-dipyrromethene is formed.[73]

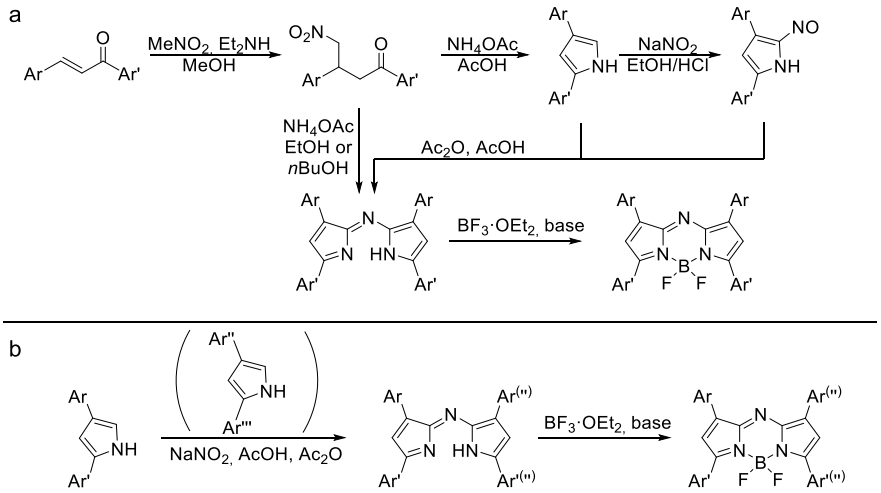

Figure 19. a: Synthetic strategies presented by O'Shea's group towards the symmetric and asymmetric aza-BODIPYs. b: Route developed by Carreira's group towards aza-BODIPYs.

Using the pathway depicted in **Figure 19b**, just as for BODIPYs, pyrrole chemistry can be utilised to synthesise differently substituted or fused pyrroles. These can subsequently be treated with $NaNO_2$, AcOH and Ac_2O to form the corresponding aza-dipyrromethene.[103, 110] These developed reactions allow access to a wide range of aza-BODIPYs. [111-116] However, these compounds have not yet been made without aryl rings. Synthesising either aza-dipyrromethene with aryl rings in the 3,5-position, where the 1,7-positions remain unsubstituted, or hexa-alkylated derivatives was so far unsuccessful. The aryl rings in the 1,7-positions though could be replaced by methyl substituents or other alkyl chains like the *sec*-butyl installed in the **Aza-R-R'** set shown in **Scheme 7**.[73, 116]

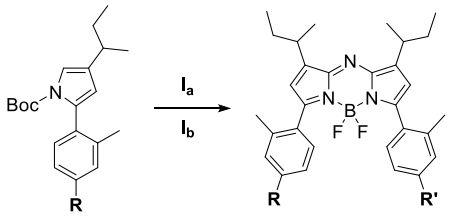

Aza-R-R'

R=R' : H : <5 %[a]
R=R' : CN : 6 %[a]
R= H; **R'**= NMe_2 : 16 %[b]
R= OMe; **R'**= NMe_2 : 9 %[b]
R= CN; **R'**= NMe_2 : 25 %[b]

Scheme 7. Synthesis of aza-BODIPY derivatives used in project II. The compounds are named **Aza-R-R'** according to their substituents. Reaction conditions: **I_a**) **R=R'**: 1. NaOMe (25w% in MeOH), THF 2. $NaNO_2$, AcOH, Ac_2O 3. Et_3N, $BF_3{\cdot}OEt_2$, DCM. **I_b**) **R≠R'**: 1. NaOMe (25w% in MeOH), THF 2. $NaNO_2$, AcOH 3. Deprotected pyrrole with R', Ac_2O; III) Et_3N, $BF_3{\cdot}OEt_2$, DCM. [a] overall yields for I_a; [b] overall yields for I_b

The **Aza-R-R'** set was synthesised in **project II**, next to the set of BODIPYs described earlier in this section.[73] This set of aza-BODIPYs is carrying the same substitution pattern as the BODIPY set and was likewise synthesised using the deprotected versions of pyrroles **5-8** (**Scheme 4**). Following the synthetic strategy developed by Carreira, one pyrrole partner was subjected to nitrosylation with $NaNO_2$ under acidic conditions. The resulting nitrosopyrrole then undergoes an acid catalysed condensation, with another pyrrole, to form the symmetric or asymmetric aza-dipyrromethene. These were isolated and without further purification directly used for the complexation reaction. In this reaction as for the BODIPYs the aza-dipyrromethene is treated with first NEt_3 and then $BF_3{\cdot}OEt_2$ to yield the corresponding aza-BODIPYs. To obtain the symmetrical aza-BODIPY derivatives **Aza-H-H** and **Aza-CN-CN**, 0.5 equivalents of $NaNO_2$ were added to 1 equivalent of the deprotected pyrrole. The symmetrical derivatives were obtained in very low yields of <5 % and 6 %. Given the prior mentioned difficulties of synthesising these compounds carrying no phenyl rings in the 1,7-positions, the lower yields compared to the symmetric BODIPY derivatives were not surprising. The asymmetric compounds **Aza-H-NMe_2**, **Aza-OMe-NMe_2**, and **Aza-CN-NMe_2** were obtained by treating the deprotected first pyrrole partner with an equimolar amount of $NaNO_2$ to form the aza-dipyrromethene. Here, similar as for the BODIPY derivatives, the nitroso-pyrrole was made from compounds **5**, **7**, and **8** and then subjected to the condensation reaction with deprotected pyrrole **6**. The complexation to the BODIPY was done in an identical fashion as for the symmetric aza-BODIPYs. The asymmetric derivatives were obtained in 16 %, 9 % and 25 % yield. The same trend regarding the electron donating/withdrawing character of the *para*-substituents that was observed for the BODIPY derivatives, was seen for the aza-BODIPYs but more pronounced.

The here described synthetic variety of the BODIPY dye class is only a small fraction of what has been done in this field. Yet I hope that this section conveys sufficiently what possibilities this scaffold holds for a synthetic chemist. The next section will hopefully spark the interest of the photo-physicist/chemist in this dye class as well.

Photophysical properties of the BODIPY dye class

It was already mentioned that BODIPY dyes have outstanding photophysical properties that make this dye class suitable for various fields. To successfully design dye molecules for specific applications, one must understand the structure-to-photophysical properties relationship of the dye in question. This section will give a general overview over the effect structural changes have on the photophysical properties of the BODIPY dye. Within this general overview the findings of projects II and IV will be presented more detailed.

The unsubstituted BODIPY core: The BODIPY molecule without substitution shows a sharp absorption band with a maximum at 504 nm, and a high molar absorptivity coefficient (ε_{max}: 76 000 $M^{-1}cm^{-1}$). The corresponding emission band is observed around 515 nm in cyclohexane.[117] The absorption varies only to a minor extent in different solvents. Only a slight blueshift of the λ_{abs} in more polar solvents is observed. Contrary to this, the emission band shows considerable variations in different solvents. The λ_{em} varies between 515 nm to 535 nm in different solvents, leading to an increase in the Stokes shift. However, in the tested solvents there was no clear trend observed regarding solvent polarity. High fluorescence quantum yields are observed in nonpolar and polar solvents. They increase with an increase in polarity. The molecule even shows moderate solubility in water with λ_{abs} of 498 nm, λ_{em} of 516 nm and Φ_F of 90 %.[59]

Modification at the boron: This field was underrated a long time before its value on the tunability of the BODIPY dye class was recognised. As already mentioned, the close to unity fluorescence quantum yield of the BODIPY dye are a result of the BF_2 complexation introducing rigidity into the molecular structure. The complexation successfully blocks the rotation and isomerisation of the flexible methine-bridge, which is the main non-radiative decay pathway in these dyes.[118-120] The fluorines, however, seem to have little effect on the absorbance and fluorescence properties. Upon substitution of the fluorine atoms with alcohols forming alkoxides almost no change in absorption and emission or Φ_F was seen. Yet, an increase in the water solubility was observed for several of the reported compounds, as compared to the BF_2 derivative.[39] Substitution of the fluorines with alkyl chains leads to a decrease in Φ_F which correlates with the size of the alkyl substituent. The more steric bulk the alkyl substituent introduces at the boron, the lower the observed fluorescence quantum yield.[121]

A far more interesting phenomenon was observed by substitution of the fluorine atoms with aryl and alkyne groups.[39] Substituents on the boron atom are not in the same plane as the BODIPY core. As a result of this, they are not in conjugation. The resulting compounds thus have the distinct features of both the BODIPY unit and of the boron-substituent in their absorption envelope. The emission envelope however shows only emission characteristic for the BODIPY. Even upon excitation of the boron substituent the emission envelope does not show an additional band, characteristic for the substituent, only the emission of the BODIPY is detected. This indicates a near quantitative energy transfer from the boron substituent to the BODIPY.[122] Previously reported BODIPY derivatives having pyrene[123] or anthracene[124] substituents at the

boron as shown in **Figure 20** can hence act as energy transfer cassettes.[125] Another effect of this fast energy transfer is an increase in the Stokes shift, since excitation at the wavelength of the pyrene or anthracene substituent leads to emission of the BODIPY unit. Due to the increased Stokes shift these compounds are suitable for applications like flow cytometry[34] or fluorescence microscopy,[122] where larger Stokes shifts are desirable.

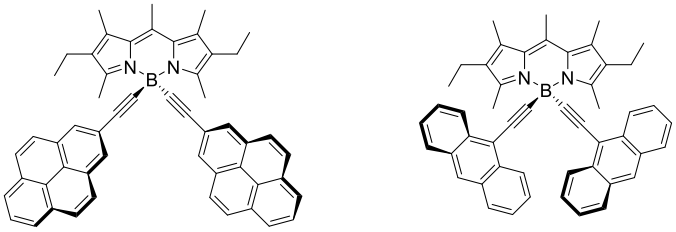

Figure 20. Examples of BODIPY having alkyne substituents on the boron. Pyrene-BODIPY (left) and anthracene-BODIPY (right) can act as energy transfer cassettes.[123-124]

Modification at the *meso*-position: The *meso*-position is described as very sensitive to substitution effects. Substitution at the *meso*-position with heteroatoms like oxygen and nitrogen, leads to a blue shift of both absorption and emission and an increase in the Stokes shift. Calculations of the HOMO and LUMO energies revealed that the energy of the HOMO remains mostly unchanged while the energy of the LUMO increases, resulting in an increase of the gap in between the two orbitals. This can be explained by the electron-donating nature of the group which, if attached in the *meso*-position of the BODIPY, leads to destabilisation of the LUMO, due to a high electron density at this position. The stronger the electron-donating character of the substituent the larger the hypsochromic shift. Thus, the amino substituents show a larger hypsochromic shift than alkyloxy-/aryloxy-substituents.[117, 126] As opposed to the electron-donating substituents, the *meso*-cyano BODIPYs are exhibiting a bathochromic shift in the absorption and emission bands.[127] This can be explained by the HOMO-LUMO gap as well. In this case the net stabilisation of the LUMO by the cyano group decreases the gap between the two states, thus, causing a red shift.[39, 127] Substitutions in the *meso*-position seem to have a special effect on the BODIPY, because cyano groups directly attached symmetrically in positions 2 and 6 show almost no effect on the transition energies. Nevertheless, an ester group in 2,6-position in combination with a *meso*-cyano-group reduces the red shift of the compound.[39]

Alkyl groups or a phenyl group in the *meso*-position do not show a large effect on either absorption or emission bands, but the *meso*-phenyl group presents itself with a drop in the fluorescence quantum yields. This drop is attributed to the free rotation of the phenyl group, which causes a loss of energy from the excited states *via* molecular motion. Already small 1,7-substituents, like methyl groups, restore the fluorescence quantum yields by means of blocking the free rotation of the *meso*-phenyl substituent.[39] More bulky alkyl substituents in the 1,7-positions although, as those attached in **project III**, cause the quantum yields to drop, most likely due to effects on the non-radiative decay pathways to different extents.[87]

Depending on the oxidation potential relative to that of the BODIPY core excited state, *meso*-substituents can act as either electron donors or acceptors in a photoinduced electron transfer.[39] As shown in **Figure 21**, this PeT can be either oxidative or reductive, depending on the alignment of the oxidation potentials with respect to the BODIPY core. In the reductive PeT electrons are transferred from the *meso*-substituent to the BODIPY core, and vice versa for the oxidative PeT. In the event of any PeT process the fluorescence of the BODIPY is quenched. This control over the fluorescence properties of the BODIPY class is achieved by using BODIPY electron-donor-acceptor dyads. Several sensors have been developed where the principle of turning the fluorescence on and off was used.[128-130] This can be done for example by the means of a chemical reaction between the probe and the analyte, which changes the chemical structure of the substituent unit. Before the probe reacts with the analyte PeT is active, from the substituent to the core, and the probe is non-emissive. After reacting with the analyte, the structure, and with that the oxidation potential of the substituent is changed which prohibits PeT. The probe then becomes fluorescent.[130]

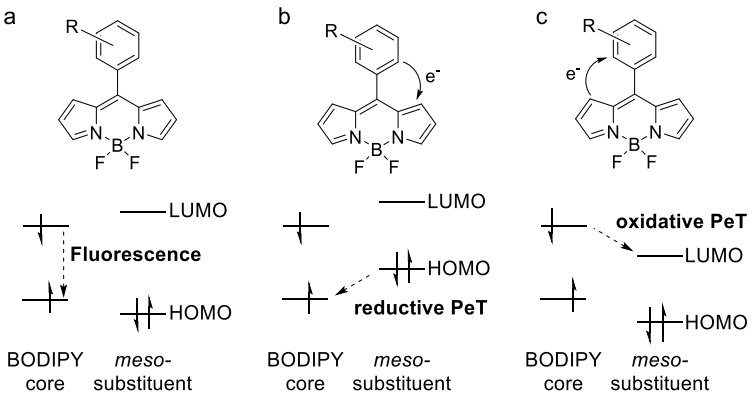

Figure 21. Representation of electron-donor-acceptor BODIPY dyads. a: a fluorescent dyad without any PeT-process happening. b: a BODIPY dyad undergoing reductive PeT. c: a BODIPY dyad undergoing oxidative PeT

The sensitivity of such systems to the solvent polarity can also be used for sensing.[131] Many substituents, for example pyrene, perylene or anthracene in the *meso*-position have been found to show a strong sensitivity towards solvent polarity.[100, 132-133] In the later presented example (**Ph-Antra-BDP**, **Figure 22a**) an electron donor unit is connected to the BODIPY, as an electron acceptor unit, in the *meso*-position. These dyads show a bright fluorescence. But for some of them, depending on the small structural changes, upon change in polarity of the solvent the fluorescence quantum yields drop drastically. Further investigation of such systems showed that the PeT from the donor to the acceptor unit forms a highly dipolar excited state, the CTS/CSS.[134] This CSS is stabilised or destabilised by the solvent, depending on its polarity. The energy of the CSS is therefore dependent on the solvent polarity.

Depending on its energy, the CSS can facilitate efficient ISC. Computational studies indicate that ISC is possible here because of the reduced energy-gap between the singlet

and triplet energy of the charge transfer state.[132] The separated charges can recombine and form the local triplet-excited state of either donor or acceptor *via* spin-orbit charge transfer intersystem crossing, given the right geometry of the structure.[135] If the donor and acceptor units are orthogonal to each other, the potential energy surfaces of the ^{1}CSS and ^{3}CSS states are closer together, making ISC possible.[133] More importantly, the orthogonal geometry of the donor and acceptor unit compensates for the change in electron spin angular momentum by the change in molecular orbital angular momentum.[100] Substituents that can rotate freely, or if there is a spacer unit in between the donor and acceptor show an only negligible amount of ISC. This is a result of the geometry of donor and acceptor being less likely to be orthogonal.[132]

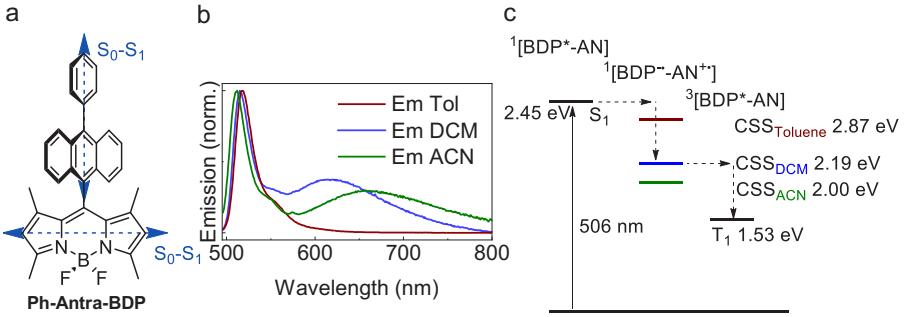

Figure 22. a: Structure of **Ph-Antra-BDP**, with the according S_0-S_1 transition dipole moments of the BODIPY and the anthracene moieties in blue. b: Normalised emission of Ph-Antra-BDP in toluene, DCM and ACN solution. c: Simplified illustration of the photophysical processes in **Ph-Antra-BDP**.[100]

The BODIPY-phenyl-anthracene dyad (**Ph-Antra-BDP**), used in **project IV**, is shown in **Figure 22a**.[100, 132] The dyad shows the absorption and emission features of both the BODIPY ($\lambda_{max\ abs}$ = 509 nm in toluene) and the corresponding electron donor unit, here the phenyl-anthracene ($\lambda_{max\ abs}$ = 375 nm in toluene). Upon excitation at either the BODIPY or the anthracene unit, the only spontaneous emission observed is that of the BODIPY unit with a maximum at 516 nm. The compound shows a fluorescence quantum yield of 80 % in toluene. By increasing the polarity of the solvent to DCM, the absorption is unchanged. However, a second, broader peak, attributed to the CSS emission, is visible in the emission envelope shown in **Figure 22b**, with a peak maximum at 622 nm. This is also accompanied with a drop in Φ_F from 80 % in toluene to 5 % in DCM. The same behaviour is observed in acetonitrile. The only difference being that the CS band is now shifted and has its maximum at 660 nm, and Φ_F drop to 2 %. This phenomenon of a solvent polarity depending, visible CS band has been observed for other, and also this BODIPY dyes previously.[136] The energies of the CS bands for **Ph-Antra-BDP** were calculated using electrochemically determined redox potentials of the acceptor unit and the donor unit in DCM. Just as in other reports of BODIPY dyads of this kind, it was determined that the population of the CSS is followed by charge recombination to the triplet state localised on the BODIPY.[100, 136] The energetics of the process is illustrated in a simplified way in **Figure 22c**. The triplet state quantum yields were determined to 90 % and 92 % in DCM and ACN respectively. Due to the efficient ISC event this dyad can be

used as a sensitiser, for example in triplet-triplet annihilation upconversion (TTA-UC).[100] The common way of introducing ISC into BODIPY dyes is *via* the heavy atom effect. Therefore, these dyads being able to undergo ISC without heavy atoms is a phenomenon that will inspire a great deal of research in fields, where applications depend on the formation of triplet states like for TTA-UC, photochemistry or photodynamic therapy.

Modification at the α/β-pyrrolic carbons: Much research has been devoted towards functionalising the pyrrolic positions of the BODIPY dye. Alkylation of the BODPIY core is relatively common. The first reported BODIPYs by Treibs and Kreuzer were alkylated derivatives. Upon symmetrical alkylation in the α- and β-positions the influence on the photophysical properties is only minor. 3,5-Alkylation with several different alkyl chains, branched or linear alike, as performed in **project I** (**Figure 23**), has only a minor effect on the absorption and emission properties and the fluorescence quantum yields remain close to unity, although, a small drop is seen when using linear chains instead of branched alkyl chains.[80] In **project III** (**iP-BDP**, ***s*Bu-BDP**, **iBu-BDP** and ***s*P-BDP)** it was observed that different alkylation in the 1,7-positions only leads to minor changes in absorption and emission properties, when compared to one another. However, the quantum yields differ, but this was discussed earlier, in regards to the additional *meso*-substituent.[87] It was furthermore reported that with an increase in the number of alkyl substituents, the absorption and emission becomes more red-shifted.[39] Unsymmetrical alkylation of the pyrrolic positions does not show a major change in transition energies either. Having alkyl substituents in the 2,6-positions, however, showed a drop in fluorescence quantum yields, which was attributed to electronic effects.[137]

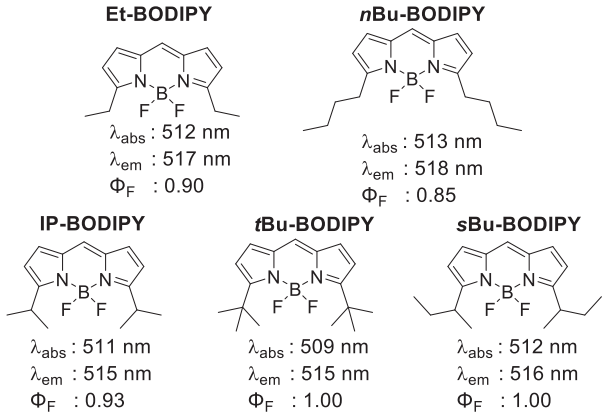

Figure 23. Different symmetric 3,5-alkylated BODIPY derivatives (used in project I) with their photophysical properties in DCM solution.

Extension of the aromatic system of the core and thereby an increase in the π-conjugation, results in a decrease of the HOMO-LUMO gap and thus a bathochromic shift of the absorption and emission properties. This extension can be achieved by either adding conjugated aromatic substituents or fusing benzene rings directly to the pyrrolic units.[72] The addition of conjugated aromatic systems can be done in the 1,3,5,7-positions resulting in mono- to tetra-substituted systems. The decrease in the HOMO-LUMO gap

is largest for the change from the non-substituted to the mono-substituted compound, and gets progressively smaller towards the tetra-substituted compound. Therefore, the ensuing red shift in the absorption and emission bands gradually gets smaller with the number of substituents. Following the energy gap law, which states that the rate of non-radiative decay increases exponentially with a lower transition energy, the fluorescence quantum yields are decreasing the more red-shifted the compound gets.[22]

Halogenation of the pyrrolic positions also introduces a bathochromic shift to the absorption and emission of the BODIPY.[138] Yet, the effect of halogenation on the fluorescence quantum yield is more interesting. An increase in the size of the halogen atom leads to a decrease in the fluorescence quantum yield. At the same time, due to an enhanced heavy atom effect the singlet-to-triplet ISC rate increases, leading to an increase in triplet state formation.[139-140] Due to this property halogenated BODIPYs can be used as triplet photosensitisers.[139, 141]

Electron donating groups (push) and electron withdrawing groups (pull) are both known to have an immense effect on the optical properties of BODIPYs. Either of them as a substituent in the pyrrolic 1-3 or 5-7 positions results in bathochromic shifts in absorption and emission. The explanation for this is that the electron donor unit increases both the HOMO and LUMO energies whilst having a larger effect on the HOMO energy. Vice versa the electron withdrawing fragment lowers the HOMO and LUMO energies having a larger effect on the LUMO energy. Therefore, both an electron donating as well as an electron donating group lower the HOMO-LUMO gap. How large this effect is depends on factors like strength of the EDG/EWG, distance to the core, as well as substitution position and pattern. Here, a special focus should be put on the push-pull principle. This principle describes attachment of an EDG on one end and an EWG on the other end of the same π-system. Push-pull or donor-π-acceptor (D-π-A) systems are well known to decrease the HOMO-LUMO gap.[142] This strategy is regularly applied to chromophores to induce a bathochromic shift, or in other words, to push absorption and emission towards the NIR-part of the spectrum.[143] The most frequently used electron donating groups for this purpose are functional groups such as alkoxy (typically methoxy/-OMe) or *N*,*N*-dialkylamino (mostly *N*,*N*-dimethylamino/-NMe_2). Also, auxiliary electron donors, such as electron rich heteroaromates (typically five membered rings like thiophene) or organometallic compounds like ferrocene have been used. Commonly used electron withdrawing groups are carbonyl-, nitro(NO_2) or cyano(-CN) groups as well as combinations thereof.[144] Another factor in these systems is their conjugation. A conjugated system acts as a π-linker unit promoting intramolecular charge transfer which highly contributes to the resulting decrease of the HOMO-LUMO gap.[145]

The push-pull principle naturally has been applied to BODIPYs previously.[146-148] Phenyl groups have been attached with an alkyne-bridge to the 2 and 6 positions of the BODIPY, carrying an EDG group on one side and an EWG group on the other side, both in the *para*-position of the phenyl ring. This causes, as predicted, a significant red shift as compared to alkylated or unsubstituted BODIPY dyes.[146] A similar system was examined, this time carrying electron donating, ethylene bridged *para*-alkoxy phenyl substituents in either the 3 or 5 position or in both positions. The S_0-S_1 transition of the

BODIPY is red-shifted in all these systems as well. However, the red shift was least significant in the case of the electron donating styryl group being only on the side of the EWG as show in **Figure 24** to the right. This concludes that the intramolecular charge transfer character is greater in the system that shows a larger distance between the EWG and the electron donating styryl group. Several more push-pull BODIPY systems have been investigated previously but will not be discussed further in the scope of this thesis.[147-148]

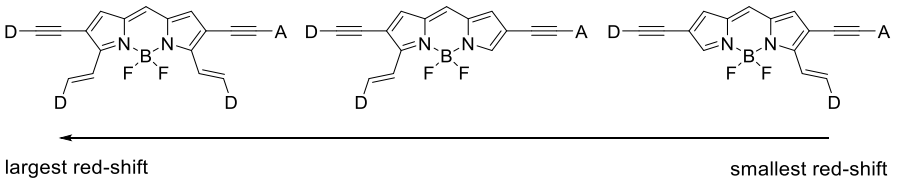

Figure 24. Graphical illustration of the push-pull BODIPY described above. The arrow indicates an increase in the red shift with regards to the substituents in the 3 and 5 position of the BODIPY.

In **project II** a series of BODIPY derivatives was prepared, carrying different EDG and EWG as *para*-substituents on a phenyl ring, attached in positions 3 and 5.[73] The *ortho*-methyl group of the phenyl substituent prevents the structure from planarising and therefore minimises an extension of the π-conjugation in the ground state. The absorption properties are therefore not affected to a large extent as can be seen in the negligible shift from $\lambda_{max\ abs}$(***s*Bu-BODIPY**) = 512 nm to $\lambda_{max\ abs}$(**H-H-BDP**) = 517 nm, and a broadening of the absorption envelope. The shift could also be attributed to the spectra being recorded in different solvents and can therefore be disregarded. However, the emission is shifted from $\lambda_{max\ em}$(***s*Bu-BODIPY**) = 517 nm to $\lambda_{max\ em}$(**H-H-BDP**) = 563 nm increasing the Stokes shift of the compound immensely. Moreover, BODIPY derivatives were decorated with EDG and EWG, resulting in either symmetrical or asymmetrical systems that can be differentiated in pull-pull, push-push, push-pull and no substituents. The results of the photophysical evaluation are summarised in **Table 1** and **Figure 25**. Adding only EWGs (pull-pull) as in **CN-CN-BDP**, shows almost indistinguishable optical properties as compared to **H-H-BDP**. **OMe-OMe-BDP**, having weak EDG (push-push), shows a red shift in both absorption maximum ($\lambda_{max\ abs}$ = 527 nm) and emission maximum ($\lambda_{max\ em}$ = 591 nm) as well as a broadening of the absorption envelope. Adding the stronger electron donating *N,N*-dimethylamino substituent leads to a red shift of about 20-40 nm depending on the other substituent. **H-NMe$_2$-BDP** has the smallest effect followed by **OMe-NMe$_2$-BDP**. The push-pull system **CN-NMe$_2$-BDP** shows, as expected, the largest effect on both absorption and emission ($\lambda_{max\ abs}$ = 569 nm/$\lambda_{max\ em}$ = 674 nm). When looking at the absorption envelope, however, all the BODIPY derivatives show the same onset of absorption on the high energy side. Thus, the red shift in absorption maximum can only be attributed to a broadening of the peak. This effect cannot be seen in the same way for the emission envelope. The emission of the compounds shows broadening as well but is very similar to each other, unlike the absorption envelope. The substitution pattern hence has a strong effect on the emission maximum and the

absorption envelope following the same trend. The quantum yields drop with the red shift of absorption and emission, according to the energy gap law.

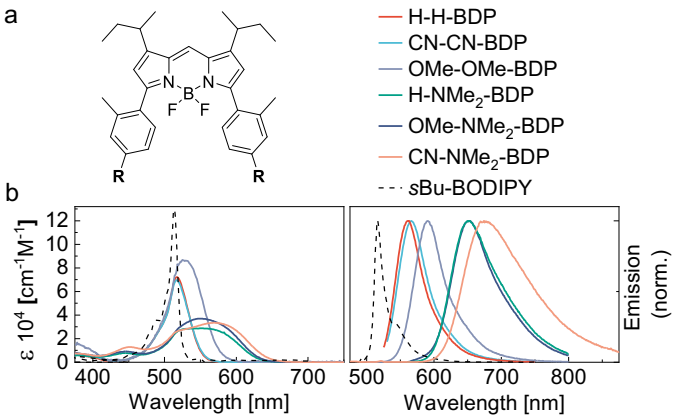

Figure 25. a: Structural representation of R-R'-BDP. b: Absorption and emission spectra of the BODIPY derivatives from project II.

Table 1. Photo physical characterisation of synthesised BODIPY derivatives R-R'-BDP according to the substituents. All experiments were done in toluene solution at 22 °C (refractive index for Φ_f determination: 1.497).

R-R'-BDP	$\lambda_{max\ abs}$ [nm]	$\lambda_{max\ em}$ [nm]	Stokes shift (cm^{-1})	Φ_f	τ [ns]	ε [$M^{-1}cm^{-1}$]
H-H BDP	517	563	1580	1.0[a]	4.53	90 000
CN-CN BDP	517	566	1675	1.0[a]	4.49	70 000
OMe-OMe BDP	527	591	2055	0.94[a]	4.69	86 000
H-NMe_2 BDP	530-553	653	3136	0.46[b]	4.00	29 000
OMe-NMe_2 BDP	546	652	2978	0.58[b]	4.59	37 000
CN-NMe_2 BDP	569	674	2738	0.12[b]	1.59	34 000

[a]: Fluorescein in 0.1 M NaOH (Φ_f = 0.91) was used as a reference compound for Φ_f determination.[149] (Excitation at 491 nm, Refractive index: 1.33)[b]: Cresyl violet in MeOH at 22 °C (Φ_f = 0.54) was used as a reference compound for Φ_f determination.[149] (Excitation at 560 nm, Refractive index: 1.33)

From BODIPY to aza-BODIPY: The replacement of the bridging atom in between the pyrrolic units from a carbon to a nitrogen leads to the class of BODIPYs known as aza-BODIPYs. This small structural change usually leads to a remarkable bathochromic shift of about 80 nm, leading to some compounds absorbing in the red or NIR region. Another general observation is that these compounds typically have lower fluorescence quantum yields as compared to BODIPYs. Nevertheless, where BODIPYs need to rely on the heavy atom effect or other means, aza-BODIPYs show a higher potential of undergoing singlet-to-triplet intersystem crossing.[150]

The origin of the red shifted transition seen for the aza-BODIPYs has been previously investigated using a structurally similar, yet different BODIPY.[150] The electronegative aza-N-bridge lowers the energy of the LUMO without having a big effect on the energy of the HOMO. The resulting smaller HOMO-LUMO gap is responsible for the red shift.

Due to the difference in the structure, the effect of the aza-N-bridge, however, might have been slightly exaggerated. In **project II** we confirmed the previous experimental findings comparing BODIPY (**H-H-BDP**) and aza-BODIPY (**Aza-H-H**) structural homologues. However, the observed red shift of 65 nm is slightly smaller than the 100 nm red shift, previously reported.

As for the BODIPYs, the push-pull strategy also finds a lot of application for aza-BODIPYs. Here, there are several studies evaluating the effect of push-pull systems from the 1,7-position to the 3,5-positions. EDG or EWG groups are attached in the *para*-position of the phenyl rings in those position. The symmetrical combinations of aza-BODIPYs have been prepared previously, with varying EDG groups in the 3,5-position[50] as well as varying EWG-groups in the 1,7-positions[151], both while the other group is fixed. The EDG and EWG showing the strongest effect is the *N,N*-dimethylamino group and the cyano group respectively. The combination of both the CN-NMe_2 derivative shows $\lambda_{max\ abs}$ = 857 nm and $\lambda_{max\ em}$ = 967 nm in chloroform. The fluorescence quantum yield is too low to determine. This was attributed to the NMe_2-group assisting an intramolecular photo-induced electron transfer reaction that results in a rapid non-radiative, thermal decay.[50, 152] Due to the potential for ISC and the significant bathochromic shift that brings absorption and emission maxima in the NIR regime the prepared push-pull aza-BODIPYs show great potential for bio applications like bioimaging or photothermal therapy.[46]

The aza-BODIPY derivatives synthesised in **project II** carry different EDG and EWG in the *para*-position of non-conjugated *ortho*-methyl-phenyl rings attached in the positions 3 and 5.[73] Here, just as for the BODIPY derivatives, different systems were synthesised, pull-pull, push-push, push-pull and no substituents (**Figure 26**, **Table 2**). **Aza-H-H** having no pronounced electron withdrawing or donating effect, already shows a red shift of about 65 nm for the absorption maximum and roughly 105 nm for the emission maximum as compared to ***s*Bu-BODIPY** ($\lambda_{max\ abs}$ = 512 nm and $\lambda_{max\ em}$ = 517 nm in DCM). Adding strong EWGs in both positions 3 and 5 (**Aza-CN-CN**) shows no distinct change in the absorption and emission features, except a small red shift of 5 nm of the emission maximum. Contrary to this the combination of a strong electron donator like a NMe_2-group in combination with either no substituent (**Aza-H-NMe_2**) or a weaker EDG (**Aza-OMe-NMe_2**) leads to a large red shift of another 85 nm to $\lambda_{max\ abs}$ = 663 nm in both cases. The emission is affected slightly differently for those two compounds. The emission envelope of **Aza-H-NMe_2** is slightly broader with a slightly less shifted peak maximum, as compared to the push-push system **Aza-OMe-NMe_2**. The push-pull system **Aza-CN-NMe_2**, as already seen for both BODIPYs (**CN-NMe_2-BDP**) and aza-BODIPYs, showed the largest substituent effect pushing the absorption and emission maxima to 671 nm and 750 nm respectively. The emission quantum yields of the compounds are 18 % and 19 % for **Aza-H-H** and **Aza-CN-CN** respectively and drop to <5 % for the three other derivatives. This result follows the expectations of the energy gap law and previous reports, describing lower quantum yields in aza-BODIPYs as compared to BODIPYs.

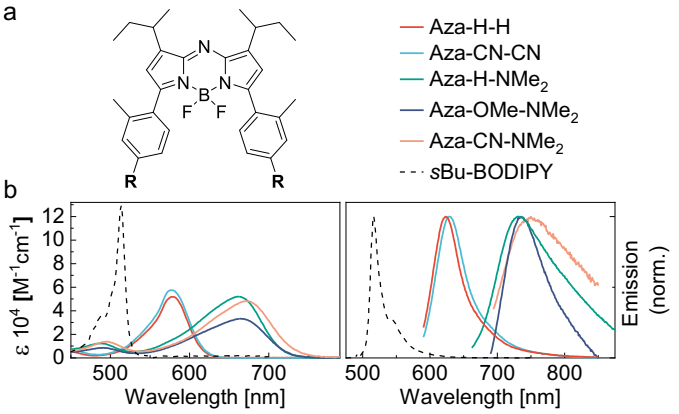

Figure 26. a: structural representation of **Aza-R-R'**. b: Absorption and emission spectra of the aza-BODIPY dyes from project II.

Table 2. Photo physical characterisation of aza-BODIPY derivatives Aza-R-R' according to the substituents. Experiments were done in toluene solution at 22 °C (refractive index for Φ_f determination: 1.497).

Aza R-R'	$\lambda_{max\ abs}$ [nm]	$\lambda_{max\ em}$ [nm]	Stokes shift (cm^{-1})	Φ_f	τ [ns]	ε [$M^{-1}cm^{-1}$]
Aza H-H	578	623	1250	0.18[a]	1.33	52 000
Aza CN-CN	577	628	1407	0.19[a]	1.23	68 000
Aza H-NMe$_2$	663	730	1384	0.01[b]	< n[c]	52 000
Aza OMe-NMe$_2$	663	736	1496	0.04[b]	< n[c]	33 000
Aza CN-NMe$_2$	671	750	1570	<0.01[b]	< n[c]	48 000

[a]: Cresyl violet in MeOH at 22 °C (Φ_f = 0.54) was used as a reference compound for Φ_f determination.[149] (Excitation at 560 nm, Refractive index: 1.33) [b]: Oxazine 1 in EtOH (Φ_f = 0.11) was used as a reference compound for Φ_f determination.[149](Excitation at 646 nm, Refractive index: 1.36) [c]: n describes the lowest detectable lifetime of the instrument

Comparison of BODIPY and aza-BODIPY: Both dye classes, the BODIPYs as well as the aza-BODIPYs are well researched areas. The effects of different substituents and the influence of EDG and EWG have been investigated extensively on each of these groups. In **project II** not only the effects of different electronic substituents on each of the classes were investigated, but the classes were also compared. The sets of molecules are structural homologues with only one difference, the bridging atom. The effects of the different EWG and EDG combinations were already described for each class in previous sections. In summary, the effects on the red shift of absorption and emission follow a similar trend regarding the substitution pattern. However, the effects seen on the different classes are interestingly highly different. The absorption of the BODIPY derivatives shows a distinct broadening, having the same onset on the high energy side, while the emission envelope shifts in its entirety. This results in a smaller red shift of the absorption maximum. The aza-BODIPYs contrarily show a larger shift in absorption and emission, whilst both features shift in their entirety. This leads to a growing Stokes-shift in the set of BODIPYs whereas the Stokes-shift of the aza-BODIPYs stays the same throughout the whole set (**Figure 27a**).

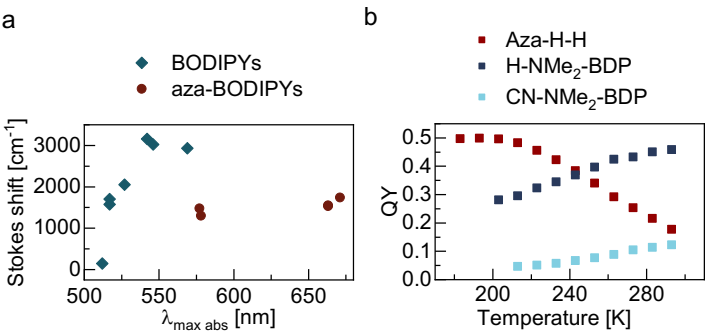

Figure 27. a: Stokes shift of BODIPY derivatives (blue squares) and aza-BODIPY derivatives (red dots) plotted against the maximum absorption of the corresponding compound. b: Temperature dependent quantum yield measurements of **Aza-H-H** (red), **H-NMe$_2$-BDP** (dark blue) and **CN-NMe$_2$-BDP** (light blue).

The fluorescence quantum yield within the sets follows the expected behaviour. Nonetheless, when comparing the quantum yields of **H-NMe$_2$-BDP** and **Aza-H-H**, which have similar transition energies, an interesting difference is noticeable. Φ_F of **Aza-H-H** (Φ_F = 19 %) is much smaller than the one of **H-NMe$_2$-BDP** (Φ_F = 46 %). **Aza-H-H** showed an increased non-radiative rate which could be a result of either IC or ISC. The rate of IC is sensitive to temperature and can therefore be lowered or even removed by decreasing the temperature, and Φ_F should increase up to 100 %, when lowering the temperature. Whereas the rate of ISC is less sensitive to temperature. The temperature dependence of the fluorescence quantum yields was measured to get more insight on the excited state decay pathway(s) (**Figure 27b**). Where **Aza-H-H** showed an increase of Φ_F to a plateau of around 50 %, when decreasing the temperature to 180-200 K, Φ_F of both **H-NMe$_2$-BDP** and **CN-NMe$_2$-BDP** decreased when decreasing the temperature. For **Aza-H-H** this indicates that the low fluorescence quantum yields do not only originate from a single non-radiative pathway. However, the BODIPY derivatives **H-NMe$_2$-BDP** and **CN-NMe$_2$-BDP** have considerably different excited-state relaxation pathways.

Dimerisation and oligomerisation: The previous sections describe how structural changes to the BODIPY dye, by the means of substitution or exchange of core atoms, can influence the photophysical properties. This section will describe some of the findings that have resulted from dimerising and oligomerising the BODIPY monomer. Oligomerisation of the BODIPY dye can be achieved by either direct linkage to each other or by using linkers in between the monomeric units. Of the BODIPY dyes of the latter nature only those, linked together by an α-α-ethylene linkage will be mentioned here. This linkage can be repeated several times, leading also to higher oligomers like hexamers or octamers.[153-154]The result is BODIPY oligomers with very narrow and red-shifted absorption and emission bands, very high molar absorption coefficients and fluorescence quantum yields close to unity. These compounds were found to have an intramolecular arrangement leading to a head-to-tail orientation of the transition dipole moments of the single units. This results in a J-type excitonic-coupling.

Direct coupling of BODIPY units has been shown in different fashions. Coupling of BODIPYs in the *meso*-position has been done to either obtain the *meso-meso*-linked or

meso-β-linked dimer.[155] The monomers used here have methyl substituents in the 1,3,5,7-position, leading to a dihedral angle of almost 90° in between the BODIPY units. Due to the orthogonality of the dimers, the mixing of the π-systems of the single units can be averted, leading to two virtually isolated chromophores, which are equally likely to be excited. Both the prepared *meso*-*meso*-dimers and the *meso*-β-dimer show similar transition energy to the monomer. The goal of the orthogonal design of the here prepared dimers was to facilitate ISC in these molecules. The targeted triplet state formation was observed in the prepared derivatives, with the highest efficiency of 51 % for the *meso*-β-dimer.

Direct α-α-coupling has been shown by Bröring et al. leading to BODIPY dimers.[156] These dimers a large dihedral angle (> 90°) in between the monomeric units. The absorption observed for the α-α-dimer shows two major bands with maxima at at 490 and 559 nm. In comparison, the monomer has one absorption band with a maximum at 529 nm. This is indicative for an excitonic splitting, which was explained by the spatial relationship, as well as the orientation of the transition dipole moments of the monomeric units. The emission shows one about 80 nm red-shifted emission band, which results in a largely increased Stokes shift. The observed features were indicative for either an excimeric character in the excited state or a large geometric displacement in the excited state.

β-Tethering of unsubstituted BODIPY units, to obtain dimers and trimers with a continuous π-conjugation has been reported by Shinokubo et al.[157] The dimer and trimer show bathochromic shifts of around 100 nm and 170 nm respectively with a maximum emission of the trimer at 731 nm. The bathochromic shift is accompanied by a decrease in both fluorescence quantum yields and molar absorptivity. Ziessel et al. and Bard et al. reported two different methods of preparing β-tethered BODIPY dimers and trimers carrying methyl substituents in the 1,3,5,7-positions.[96-97] The resulting compounds show no effective π-conjugation, due to a large dihedral angle in between the BODIPY units. Absorption and emission of these compounds still show a bathochromic shift. This indicates some communication in between the BODIPY units. Yet, the dimer and trimer show an increased molar absorptivity coefficient and the decrease in fluorescence quantum yield is less significant.

In **project IV** a series of β-tethered BODIPY oligomers, based on **Ph-Antra-BDP** (**Figure 22**) was synthesised. The **Dimer**, two conformers of the **Trimer** and **Tetramer** were obtained. Since the two conformers of the **Trimer** show indistinguishable photophysical properties, their properties will be summarised in the discussion as the **Trimer**. The BODIPY oligomers are non-conjugated, due to methyl substituents in the 1,3,5,7-positions. The absorption and emission spectra of the BODIPY series obtained in **project IV** are shown in **Figure 28**. A similar absorption and emission behaviour is observed as compared to previous non-conjugated β-tethered BODIPYs.[96-97] **Ph-Antra-BDP** shows absorption and emission at 506 nm and 516 nm, respectively. The **Dimer**, **Trimer** and **Tetramer** absorption is shifted to 542 nm, 569 nm, and 582 nm, respectively. Emission is shifted to 584 nm, 607 nm, and 617 nm, respectively. The molar

absorptivity coefficients increase with the number of BODIPY units in the oligomer. They follow the trend of an enhanced transition dipole moment.

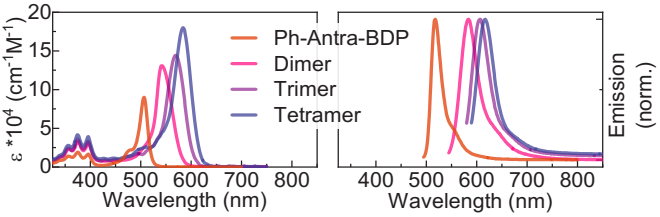

Figure 28. Absorbance (in DCM) and emission (in toluene) of the BODIPY-anthracene dyad oligomer series synthesised in project IV. The emission is recorded upon excitation at 490 nm (**Ph-Antra-BDP**), 540 nm (**Dimer**), 570 nm (**Trimer**) and 585 nm (**Tetramer**).

This behaviour indicates that the staggered oligomeric units show a highly different communication pathway as conjugated BODIPYs. The transition dipole moments of the BODIPY units are aligned in a head-to-tail fashion in the oligomeric molecules. This is a phenomenon seen in J-aggregates leading to a lowering of the S_1 energy. This is seen as a red shift of the absorption and emission.[158] The observed behaviour of the oligomer absorbance and emission corroborates the hypothesis of excitonic-coupling being the main interaction pathway. **Ph-Antra-BDP** has been described to efficiently populate the locally excited triplet state of the BODIPY through SOCT-ISC. Exciton-coupling has a large effect on the singlet energy. However, the triplet energy as well as the energy of the CSS, observed in **Ph-Antra-BDP**, should be less affected. This is because their transition dipole moments are small, giving a negligible exciton coupling. Therefore, the S_1-T_1 energy gap can be lowered significantly.

To gain information on the energy of the CSS, the electrochemical behaviour of **Ph-Antra-BDP** and the **Dimer** were analysed. **Ph-Antra-BDP** shows clear one-electron reduction and oxidation waves, that correlate very well with previously reported values.[100] The **Dimer** shows two one-electron reduction waves. Where the value of the first waves is highly similar to that of **Ph-Antra-BDP**. The reduction waves are related to the BODIPY units. Due to coupling of two units together a second reduction wave is expected. This behaviour was also observed previously in non-conjugated BODIPYs. The first BODIPY reduction occurs at an almost identical potential as the single BODIPY unit. Electrochemical behaviour of the second unit, however, is influenced by the first one leading to a slightly shifted reduction potential.[96] On the oxidation side only one clear one-electron wave can be seen for the **Dimer**. In **Ph-Antra-BDP** the oxidation is attributed to the anthracene unit of the dyad. The anthracene units in the **Dimer** have a too large distance to each other to efficiently interact. Therefore, only one peak is expected on the oxidation side. The oxidation potential shows a small shift of 80 meV. Nevertheless, the shift in the energy of the CSS is less significant as the shift in the S_1 energy, when going from **Ph-Antra-BDP** to **Dimer**.

The population of the T_1 state in **Ph-Antra-BDP** is, apart from transient absorption measurements, also indicated by a drop in Φ_F in more polar solvents, like DCM and ACN as compared to toluene. **Dimer**, **Trimer** and **Tetramer** show a less significant drop in Φ_F

in DCM. However, the fluorescence is significantly quenched in ACN, indicating an efficient SOCT-ISC mechanism. Transient absorption shows both stimulated emission bands for all oligomers in both ACN and DCM. However, the oligomers give a much smaller signal as compared to **Ph-Antra-BDP**. The lifetime of the observed ground state bleach was determined to be >100 μs for all oligomers. Also, in aerated solvent no signals could be observed. This indicates that the oligomers still populate the triplet state. Thus, the principle of exciton coupling can form an important design strategy for low energy absorbing sensitisers in the future.

The in this section described photophysical properties of the BODIPY dye class, as well as their tuneability upon structural changes paint a colourful picture of a highly versatile fluorophore.

Towards a dye glass

The photophysical properties of the BODIPY dye class, as well as most other dye classes, are primarily investigated in dilute solutions. To gather insight in the photophysical processes happening within the system, that is the common and appropriate approach. Higher concentrations disturb the photophysical processes happening upon interaction of the molecule with light. However, many applications require dyes to be used in solid state. Dyes tend to form highly aggregated or crystalline solid states, due to their extended aromatic core structures. Attractive π-π interactions favour aggregation and crystallisation of dye molecules upon solidification. The monomeric optical properties, exhibited by the single molecule in dilute solution, can be heavily distorted or even disappear in the solid state. Aggregation is well known to cause broadening of the absorption and emission envelope, quenching of fluorescence, and scattering of light to a large degree. These phenomena, displayed in films of dyes, even if they show sharp absorption and emission bands, with unity fluorescence quantum yields in a dilute solution, render a lot of dyes inappropriate for solid state applications. To be able to utilise the monomeric properties of dyes in the solid state, like thin films, new methods as well as new dye materials need to be developed. In this chapter, a strategy to make a new dye material, a room temperature dye glass, is described. Within that, the results of project I and project III are discussed.

The importance of film structure and morphology

Many characteristic properties of a thin film are directly influenced by its structure and its morphology. The film structure influences conductivity, porosity, and optical reflectivity of the film, and therefore directly relates to the performance of the film.[159-160] The solid-state structure and morphology therefore play an important role in the development of new materials and methodologies.[161] Controlling the aggregation and crystallisation behaviour of the molecule can be done in several ways. An important factor to consider is the processing method used to prepare the film. Different processing methods and conditions govern the structure and morphology of a film. Finding the optimal processing conditions is therefore crucial for the final properties of the film.[162] Unrelated to the processing method, the structure of the film is equally dependent on the structure of the film components.

Established strategies

Alkyl chain engineering: One strategy that should be highlighted here is often referred to as alkyl chain or side chain engineering/tuning, which is a common strategy for softening of optically active materials or polymeric materials.[163] Alkyl chains are attached either to the π-core of the molecule or in the periphery of the π-core. The working principle of

this technique is the modification and manipulation of intermolecular interactions. Many molecules used in the fields of optics, optoelectronics or organic electronics have extended π-conjugated structures. As a result of these structures, the intermolecular interaction most seen in these systems are π-π interactions. This can lead to low solubilities and a mixture of crystalline and randomly aggregated domains in the solid state. Attaching alkyl chains to the molecule can now increase their solubility, prevent or control aggregation in films, and govern crystallisation in bulk. This is possible due to the balance between attractive and repulsive interactions in between the molecules. This principle mainly targets the π-π interactions, originating from the extended π-core, and the van der Waals interactions, exhibited by the alkyl chain substituents. Those factors highly contribute to the physical state of materials at room temperature. Often linear alkyl chains of varying length have been used in this field.[164] Branched alkyl chains have nonetheless, shown a more prominent effect in creating disorder in a system.[165] This can subsequently lead to a more amorphous solid state. Here both the flexibility and the bulkiness of the branched alkyl chains have an impact on successful manipulation of the π-π interactions.[166] Not only the type of alkyl chains, linear or branched, or their length play an important role in this strategy, also the placement within the molecule or polymeric chain is of importance.[167-170]

This strategy has been highly successful in the fields of functional molecular liquids[165-166] and organic electronics.[163-164, 171] In the case of the π-core being a chromophore the alkyl chains can exhibit a small effect on the photophysical properties often through positioning, which can for example lead to blocking of a rotational bond. Given an appropriate length, the alkyl chains can enclose the π-core. This results in unperturbed photophysical properties, when going from solution to the solid state. However, another effect observed in alkyl chain engineering is phase separation. This can lead to the formation of nano particles or monolayers.[172-173] Therefore this strategy can be seen as problematic if the smoothness and continuity of a film is targeted. Furthermore, alkyl chains can often be a considerably larger portion of the molecule, making this strategy mainly applicable in fields independent of concentration.

Multi component mixtures / Entropic mixing: Controlling the morphology of solids is also often done by the means of entropic mixing, resulting in multicomponent mixtures of solid materials. Mixing causes an increase in entropy of the liquid state.[174] This changes the rate of both crystal nucleation and growth. Thus, the thermodynamic and kinetic driving force for crystallisation is reduced.

The driving force of crystallisation in a mixed system can be described by the change in Gibbs free energy of the mixed state (ΔG_{mix}). This change depends on both, the enthalpy of the mixed state (ΔH_{mix}), and the entropy of the mixed state (ΔS_{mix}), which is influenced by the temperature. Their relationship is described in **Equation 15**.[30]

$$\Delta G_{mix} = \Delta H_{mix} - T\Delta S_{mix} \quad (15)$$

All these factors must be considered in order to control the driving force of crystallisation. The change in enthalpy in highly influenced by the interactions between the single components. An ideal system would have $\Delta H_{mix} = 0$. However, intermolecular

interactions, like hydrogen bonding or π-π interactions are attractive forces, and therefore result in $\Delta H_{mix} < 0$. This results in a lower free energy of the mixed state, and thus a higher rate of crystallisation. However, intermolecular interactions too repulsive in nature can cause $\Delta H_{mix} > T\Delta S_{mix}$. This would result in a separation of the single components and mixing would not occur. Therefore, the intermolecular interactions in between the single components must be balanced very well. The choice of the components themselves plays thus a big role in multicomponent mixtures.[30] The number of components has to be likewise considered. The influence on the change in entropy upon mixing has already been stated. However, it has been shown that the kinetic factors of mixing can be influenced by the number of components.[33] The latter statement is however still not explained sufficiently. More research thus needs to be devoted to the relation between the number of components and the kinetic factors of mixing, specifically.

The strategy of entropic mixing is applied in, for example, organic solar cells, which have been shown to improve upon mixing of different components.[175-176] In many multicomponent mixtures different compounds are blended together, which can also affect their optical properties. Blends containing two or more different optically active molecules, will exhibit the combined absorption and emission properties of all components of the blend. This limits application of these blends to applications where monomeric absorption or emission properties are not required. One way to circumvent this effect is to mix an optically active compound with optically inactive additives. Compounds used here are usually polymers with no optical activity, or sugars.[177-178] However, this leads to a reduction of the amount of optically active component in the blend. This limits this strategy, just like alkyl chain engineering, to concentration independent applications.

The importance of molecular design

Using the principle of entropic mixing, the crystallisation behaviour of the system could be influenced to such extent that the material forms an amorphous glass instead of a crystalline solid state. Upon mixing of the different derivatives, the entropy is increased resulting in a reduced rate of crystallisation. Practically, this can be observed by a lower melting point which, upon the right number of derivatives should become lower than the glass transition point. This has been shown before, however the T_g of the blended material was below zero degree resulting in a liquid at room temperature.[179] The same principle being applied to a system with a T_g above room temperature consequently leads to the formation of a glassy material at room temperature. This is here combined with the principle of balancing the attractive π-π interactions of the BODIPY core by attaching alkyl chains, exhibiting repulsive van der Waals interactions, inspired by alkyl chain engineering.

The sets of molecules used in **project I** and **project III** were both designed to have highly similar molecular structures.[80, 87] The point of that being, that upon mixing the system will resemble an ideal system, where the ΔH_{mix} can be considered close to zero. The consequence of this is that the change of Gibbs free energy in the system depends now on the change of entropy upon mixing. To avoid too large repulsive interactions, the alkyl

chains attached to the core were kept relatively short. Linear alkyl chains as well as branched alkyl chains were used in **project I**, to see how the different alkyl chains influence the packing behaviour, which is practically correlated to T_m and T_g.

An equally important reason for designing molecules having highly similar structures, relates to the optical properties of the material. The optical properties of BODIPY dyes, as well as other dyes, are highly dependent on the molecular structure, as previously described. The molecules, used for blending, must therefore exhibit indistinguishable absorption and emission features in the solution state, to qualify for blending. Only then a material can be obtained, which exhibits monomeric optical properties, while having an extreme dye concentration.

In **project I** different short alkyl chains were attached directly to the 3,5-positions of the BODIPY core. To obtain an extreme dye concentration in the final material, the molecules were kept as small as possible. The molecules used here, **Et-BODIPY**, ***n*Bu-BODIPY**, **IP-BODIPY**, ***s*Bu-BODIPY** and ***t*Bu-BODIPY** are shown in **Figure 23** (**page 41**). The optical properties in solution are indistinguishable (black lines in **Figure 29**), making the five derivatives optimal candidates for entropic mixing.

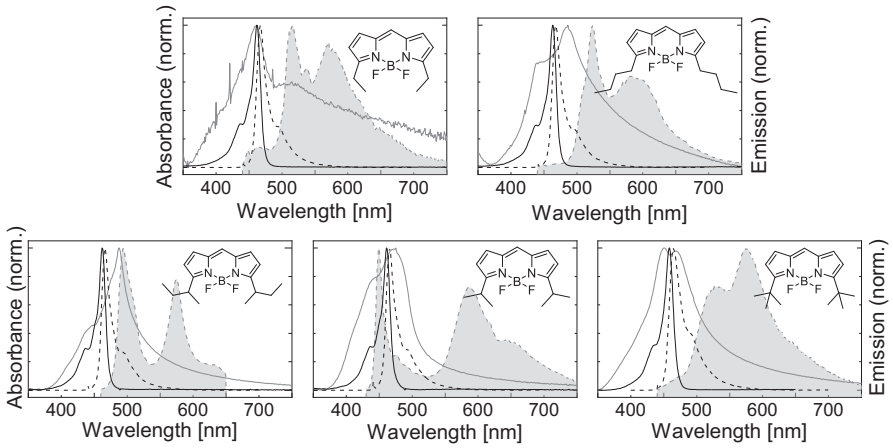

Figure 29. Absorption (solid line) and emission (dotted line) spectra of all five BODIPY derivatives used in project I, where the molecular structure is shown in the corner of the according plot. The black lines show the spectra of the dye in solution and the grey lines those in thin films, of which the emission is filled.

To study the optical properties of the derivatives in solid state, thin films of the single dyes were spin coated onto a glass substrate. The thin films were then analysed using polarised optical microscopy as well as optical spectroscopy. The films of all five derivatives show a significant degree of aggregation. Both branched and linear alkyl chains showed large, aggregated, or crystalline domains in polarised spectroscopy. Mentionable here is that the largest aggregated domains were observed for ***n*Bu-BODIPY**, and the aggregated domains of **IP-BODIPY** present themselves in a rod like structure. Optical spectroscopy of the films, spectra of which are presented in **Figure 29**, gave further, affirmative information. Unlike the sharp transition bands seen in solution, the films show broad absorption bands and scattering of light to a large degree, implying an

inhomogeneous environment. The emission bands of all five derivatives are broad and both the ***s*Bu-BODIPY** and the **IP-BODIPY** films show even two distinct emission bands. The two emission bands, and the shift thereof indicate the formation of at least two different aggregated species.

To analyse if entropic mixing can disrupt the efficient packing behaviour of the single derivatives, the compounds were blended. The blends were subsequently spin coated on glass substrates, in the same manner as the single derivatives, and analysed using the same methods. Binary blends of the BODIPY derivatives carrying branched alkyl chains – **IP-BODIPY**, ***s*Bu-BODIPY** and ***t*Bu-BODIPY** – show no signs of large, aggregated domains anymore. However, the other blended films do. Blends involving linear alkyl chains show large rod like aggregate structures. The spectra of four of the prepared films, obtained from optical spectroscopy, are shown in **Figure 30**.

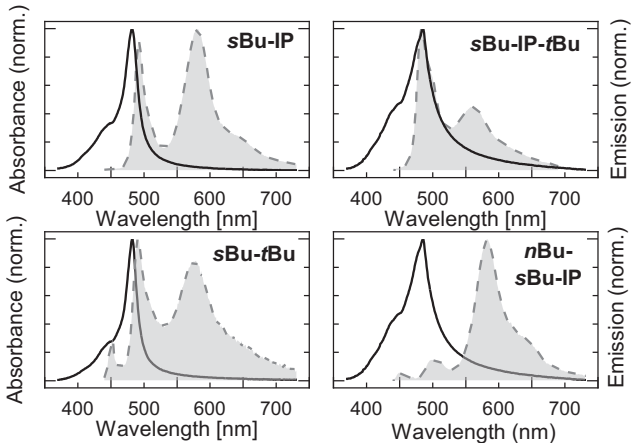

Figure 30. Absorption (black solid line) and emission (grey filled area) spectra of four representative blends.

Most of the blended films still show broad absorption and emission bands. However, the ***s*Bu-IP** blend shows a considerably narrower linewidth of the main absorption peak as compared to the pristine films, as well as less scattering. The absorption maximum is red-shifted about 20 nm as compared to the solution value of 512 nm, nonetheless, shows almost monomeric character. The blend shows a sharp emission band with very small Stokes shift, resembling the monomeric emission observed in solution. A second, broader emission band at a lower energy is observed as well, resembling the one in the pristine films. Other blends containing ***s*Bu-BODIPY** follow a similar trend in emission, yet the distribution of the two bands varies. The varying distribution of the emission bands could indicate different degrees of aggregation in the films. The fluorescence of the ***s*Bu-IP** blend (film) is 15 %, which compares to earlier reports of BODIPYs doped 15 w/w% in polymers.[180] Compared to the pristine films of ***s*Bu-BODIPY** and **IP-BODIPY**, with fluorescence of 8 and 2 % respectively, the blended film outperforms the single component films.

Exited state lifetimes of the two distinct emission bands were performed to get a better understanding of the system. Where the low-energy transition has a substantially longer excited state lifetime. In the ***s*Bu-*t*Bu** blend, the average lifetime of the higher energy emission band is 1.0 ns, and the low energy emission band shows an average lifetime of 3.3 ns. Further analysis reveals a build-up of the low energy emission with the same time constant as the high energy emission decay. This indicates that the low energy emission acts as a relaxation route of the high energy monomeric excited state. The absence of an absorption band corresponding to the low energy emission can indicate two things. Either the concentration of the aggregated species is low, or its transition dipole moment is small. Absorbance of the low energy transition is also absent in excitation spectra. A relative long lifetime of the low energy transition could indicate excimer formation, however, the relatively narrow bandwidth of the second emission band rather supports the hypothesis of J-aggregates being formed. J-aggregated dimers have previously been observed in BODIPY-polymer mixtures, which further backs this hypothesis.[180] Other blended films, however, show broader absorption features, indicating different types of aggregates in various blends.

Blending of two or more BODIPY derivatives of this design resulted in a considerable improvement of the thin film properties. Not only did some films exhibit almost monomeric absorption features and increased fluorescence but also the aggregation behaviour could be notably influenced. This can be ascribed to the higher entropy in the system upon mixing and results in lower scattering of the film and absence of large, aggregated domains. For this purpose, branched alkyl chains performed considerably better than linear ones, where the *sec*-butyl-chain was the best. Most likely this is a result of the *sec*-butyl chain forming stereoisomers, resulting in a racemic mixture of the compounds. A racemic mixture of a compound by itself resembles a multicomponent mixture, which is simply, a system containing of more than one compound. The ***s*Bu-IP** blend was also placed in an optical cavity, where it reached the strong coupling regime, to demonstrate the importance of dye films with sharp absorption bands, low scattering, and extreme dye concentration.

The blended material however proved to be rather resilient to handle for further analysis, like DSC. The stability of the by spin coating prepared films was rather poor. The film would sublimate over time, indicating an insufficient molecular weight of the components. The aggregation also caused reproducibility issues. While the absorption could be reproduced, the ratio of the emission bands varied depending on the film. To succeed in converting a material into an amorphous solid, the dye molecule design required extensive improvement.

Some of the compounds used in **project II** were studied using DSC and FSC, to see if a glass transition above room temperature could be seen. The examined aza-BODIPYs, however, showed no T_g and suffered degradation near their melting points. They were therefore rendered inappropriate for a further study of entropic mixing. The **H-H-BDP** and **CN-CN-BDP** showed no degradation around their T_m. FSC was attempted to get a T_g of the materials, however, **H-H-BDP** could not be measured successfully. The chip used in the measurement showed only a circle of the compound around the sensor, but

no compound remained on the sensor itself. The **CN-CN-BDP** was measured successfully and showed a glass transition above room temperature. Due to the low yields obtained in the synthesis of these compounds the molecular structure and with that the synthesis was refined.

In **project III** the design of the molecule was addressed more strategically, as the molecular structure itself has a large influence on the crystallisation behaviour. The molecules utilised here are based on the design of **CN-CN-BDP**. The compounds **iP-BDP**, **iBu-BDP**, ***s*Bu-BDP**, and ***s*P-BDP** are shown in **Figure 31**. Compared to the compounds used in **project I**, these molecules are larger. The molecular weight of the molecules must be still small enough, so the dye concentration does not decrease too much, yet has to be sufficiently large, to be useable in thermal analysis. The *para*-cyanophenyl substituents in positions 3 and 5 of the BODIPY core, kept from the design of **CN-CN-BDP**, are adding molecular weight. Planarisation of the rings would lead to a larger conjugated π-system. This would have a large impact on the optical properties but, more importantly, would contribute to π-π interactions, to a large extent. However, distortion in molecular structure, such as rotation about a single bond increases the disorder of the system. Therefore, to block the rotation partially but with that effectively avoid planarisation of the phenyl rings, a methyl group was attached in the *ortho*-position of the ring. The phenyl substituent in the *meso*-position of the BODIPY core adds more molecular weight, and additionally drastically improves the yields of the BODIPY condensation reaction. To prevent planarisation of this phenyl substituent, alkyl chains were attached in the 1,7-positions of the BODIPY. By attaching different alkyl chains the four derivatives were obtained. The different alkyl chains chosen were all branched due to them giving better results in previous studies. Also, two alkyl chains were chosen, *sec*-butyl and *sec*-pentyl, which result in racemic mixtures and therefore already resemble a multicomponent mixture. The compounds were first analysed independently to assess the molecular design.

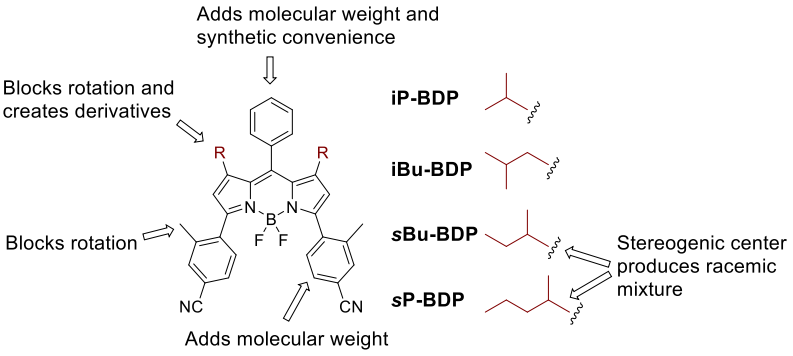

Figure 31. Molecular design of the molecules used in project III.

The optical properties of the molecules in solution are described in the previous chapter. With the alkyl chains being the only structural difference, the molecules in solution exhibit highly similar absorption and emission features and are therefore ideal for entropic mixing. To analyse the solid-state properties, thin films of the single derivatives were spin

coated onto glass substrates and analysed using polarised optical microscopy and optical spectroscopy. The films show no sign of aggregated or crystallised domains and are homogeneous. In **Figure 32** absorption and emission properties of the derivatives in solution and in a thin film are presented. Almost identical optical properties were observed for the pristine thin films of the dyes as compared to the dilute solutions. Except for the **iP-BDP**, which shows a shoulder in the emission spectrum, which is not present in the solution spectrum, and could indicate a small degree of aggregation in the film. Otherwise, only a small red shift of the absorption (7-8 nm) and emission (10-14 nm) as compared to the dyes in toluene solution was observed. However, this shift can be attributed to the drastic and rapid change in environment. The absorption envelope of the films is also slightly broadened, which could be a result of the rapid solvent removal in the spin coating process, trapping the molecules in a fixed conformation. The glassy state of the thin films could be a result of either the processing method or the films being very thin (~ 10 nm).

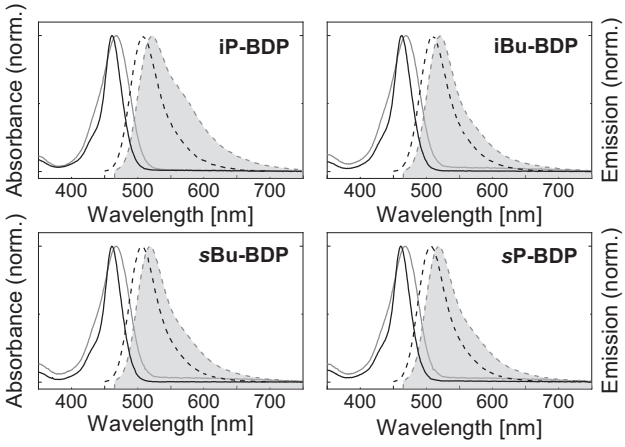

Figure 32. Absorption (solid line) and emission (dotted line) spectra of the BODIPY derivatives used in project III, where the name is shown in the corner of the according plot. The black lines show the spectra of the dye in solution and the grey lines those in thin films, of which the emission is filled.

To observe how the compounds behave in neither of these situations, the derivatives were drop casted onto a glass substrate resulting in thicker films (3 – 4 μm). The slow solvent evaporation here should give a more realistic picture of the crystallisation and aggregation behaviour of the dyes. The drop casted films were subsequently investigated using polarised optical microscopy and the **iP-BDP** drop casted film was also subjected to grazing-incidence wide-angle x-ray scattering (GIWAXS) analysis. The micrographs of the drop casted films of **iP-BDP** and **iBu-BDP** show aggregated or crystalline domains and a high degree of cracking. GIWAXS analysis of the **iP-BDP** film verified multi-crystallinity. The drop casted films of ***s*Bu-BDP** and ***s*P-BDP** on the other hand, show no distinct features of aggregation or crystallinity, and are more homogeneous. This however does not prove the absence of aggregation or crystallinity. It could also be a result of very small, ordered domains that are not detectable by the human eye.

To get a better understanding of the compound's crystallisation behaviour, DSC and FSC were performed. **iP-BDP** was not appropriate for this analysis. Thermogravimetric analysis showed a weight loss of the material in very close proximity to T_m. In other words, a loss of material can't be avoided during melting of the material and therefore the results would not be reliable. The other three compounds, however, were suitable for DSC and FSC. The DSC thermograms are shown in **Figure 34a**. For ***s*Bu-BDP** and **iBu-BDP** relatively high T_m peaks were observed with maxima at 266 °C and 279 °C, respectively. Melting peaks were also observed in the second heating cycles which leads to the conclusion that the compounds solidify with a certain degree of order after the first melting. The ***s*P-BDP**, however, showed first, a considerably lower T_m in the first heating cycle with a maximum of 132 °C. Additionally a T_g in the second heating cycle around 110 °C was observed, and lastly no melting peak in the second heating cycle. Considering the two latter observations, the assumption can be made that the compound does not crystallise or aggregate after the first melting but instead solidifies into an amorphous solid state. FSC was attempted to gather further insight and information about the kinetic fragility of the compounds. However, several processes were observed in the same cooling process, including glass transition and crystallisation, preventing a reliable analysis of the recorded data.

Having a compound that solidifies into an amorphous state already shows the benefits of the molecular design. Nonetheless, to see if the material would form a glass state at room temperature, with a measurable kinetic fragility and even improved properties, blends of the different derivatives were fashioned. Blending further increases the entropy of the system and should therefore lower the crystallisation rate even more. As no thermal analysis of **iP-BDP** was possible the compound was excluded from blending. The other three compounds were used to prepare binary blends, made of two compounds – ***s*P+*s*Bu**, ***s*P+iBu**, and ***s*Bu+iBu** -, and one ternary blend containing all three compounds - ***s*P+*s*Bu+iBu** -. The ***s*Bu+iBu** was excluded from further studies, since a first recording of a DSC-thermogram showed several processes happening during the heating, making analysis of the material unreliable. The three other blends were found appropriate for further studies and were first made into thin films by spin coating and analysed using optical spectroscopy. The absorption and emission of the thin films, shown in **Figure 33** is of monomeric nature. Polarised optical microscopy featured no aggregation or crystallisation features, only showed the homogeneity of the films.

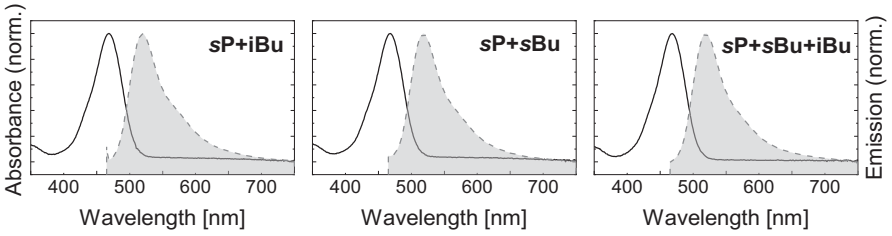

Figure 33. Absorption (black solid line) and emission (grey filled area) spectra of the two binary blends, *s*P+iBu and *s*P+*s*Bu, and the ternary blend, *s*P+*s*Bu+iBu.

The monomeric absorption and emission as well as the homogeneous features could be a result of the thinness of the films or the processing method, as for the single component thin films. Thus, thicker, drop casted films of the blended materials were fabricated. Polarised optical microscopy still shows no distinct features of aggregation or crystallisation for either of the blended materials. The ternary blend was further investigated using GIWAXS, where the absence of crystallinity peaks was observed. DSC and FSC analysis were performed subsequently to obtain more information. DSC of all three studied, blended materials showed no T_m in either of the two heating curves. A clear T_g around 110 °C was instead observed for all three blends in both heating thermograms, which are shown in **Figure 34b**. This indicates that the blended materials are in an amorphous solid state. More importantly no melting is required for the materials to reach this amorphous state, opposite of the results of the ***s*P-BDP**. FSC analysis of the three materials showed clean heating curves that were analysed to receive the kinetic fragility of the compounds. The kinetic fragility gives a lower value for the ternary blend as for the binary, ***s*P+*s*Bu** and ***s*P+iBu**, with 85, compared to 120 and 128, respectively. This indicates that the ternary blend shows a higher glass forming ability then the binary blends.

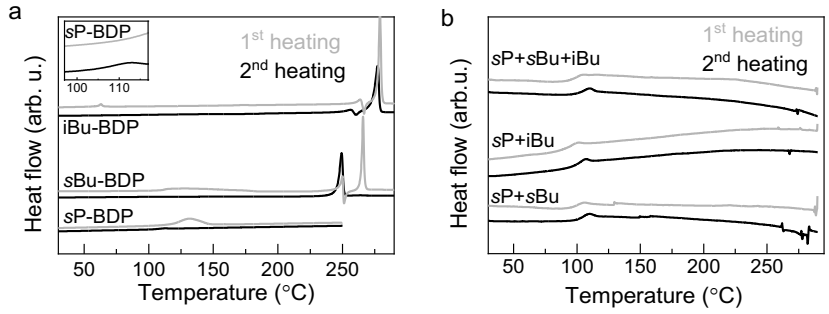

Figure 34. a: DSC thermograms of the single BODIPY derivatives iBu-BDP, *s*Bu-BDP, *s*P-BDP. b: DSC thermograms of the binary blends, *s*P+*s*Bu and *s*P+iBu, and the ternary blend *s*P+*s*Bu+iBu.

The optical stability of a thin film of the ternary blend was also observed over a period of two weeks, and compared to the **iP-BDP** thin film. The absorption envelope of the ternary blend shows no change, where the absorption of **iP-BDP** undergoes a rapid significant broadening of the absorption peak. Emission scans of the **iP-BDP** revealed the emergence of a distinct second emission band at 620 nm. The ternary blend shows development of a small shoulder around 620 nm after several days. This indicates that aggregation occurs over time in the thin films. It, however, occurs more accelerated in the **iP-BDP** film as compared to the ternary blend, where after two weeks only very weak features indicating aggregation were visible.

The design of the BODIPY molecules used in this study has proven to show higher abilities to form a dye glass at room temperature than the ones used in **project I**. The blended materials and even the single dye derivatives contain the monomeric absorption and emission features, displayed in dilute solution, in a thin film, apart from a minor red

shift. The thin film of the ternary blend even showed a decent optical stability over the course of several days. Even using drop casting as an alternate processing method, the blended material showed no sign of aggregation and crystallisation in either polarised optical microscopy or thermal analysis. The drop casted film of the ternary blend also showed no crystallinity peaks using GIWAXS, as opposed to the equally processed **IP-BDP** film. The kinetic fragility of the blended materials shows that the ternary blend has a higher ability to form a glass than the binary blends. However, the most outstanding result is that the blended material forms a dye glass at room temperature without the necessity of previous melting, and regardless of the processing method This yet again highlights the importance of strategic molecular design.

It has been shown that a material's ability to crystallise and aggregate is lowered by entropic mixing. Liquid dye materials and now also a dye glass at room temperature can be prepared using this strategy.[33, 179] By changing the component ratios of a blend the crystallisation and aggregation properties of the material could be further controlled. Furthermore, the kinetic fragility has been seen to decrease with the number of components in a blend.[33, 87] However, this relationship is not yet theoretically explained. Further investigations into this relationship would increase the understanding of entropic mixing. With that, new prospects in the development of dye materials could evolve.

Concluding remarks

The objective of the research presented here was to increase the fundamental knowledge of the correlation of molecular design and intrinsic molecular properties of organic dyes. A better understanding of this relationship could enable fabrication of tailor-made dyes and new dye materials. The research presented here was performed using members of the BODIPY dye class. Structural design was used to both investigate a system as well as manipulate a system methodically.

Although, the BODIPY and aza-BODIPY class are two well researched dye classes, their structure to optical properties relationship is still not fully understood. The influence of the molecular design on the optical properties was investigated in **project II**. Therefore, two sets of molecules were designed, one BODIPYs, the other one aza-BODIPYs. By using combinatoric chemistry four pyrroles carrying different EWG and EDG were used to synthesise in total eleven different compounds (five aza-BODIPYs and six BODIPYs). The different combinations of EWG and EDG create compounds of the push-push, pull-pull, push-pull categories. The molecules are symmetrical and asymmetrical, with regards to the long axis of the BODIPY. A substitution dependent red shift was observed for both sets of molecules. However, the absorption shift observed for the aza-BODIPYs differs noticeably from the one of the BODIPYs. Also, an increase in the Stokes shift was observed for the BODIPYs but not for the aza-BODIPYs. Additionally, a temperature-activated excited state deactivation pathway was observed for aza-BODIPYs. The BODIPY dyes having relatively similar transition energies however do not show the same deactivation pathway. These findings provide further insight in the photophysics of the BODIPY dyes depending on their structures.

Decreasing the energy gap in between the S_1 state and the T_1 state can minimise the energy loss while still promoting ISC. In **project IV** the BODIPY-anthracene-dyad Ph-Antra-BDP was strategically oligomerised, in a non-conjugated fashion, by β-tethering of the monomer. The dimer, trimer, and tetramer of the Ph-Antra-BDP were obtained and isolated successfully. Photophysical evaluation of the system showed that the S_0-S_1 transition energy is indeed lowered. This is observed by a red shift of the BODIPY absorption and emission bands. This phenomenon is caused by exciton-coupling and hence, the effect of the coupling is large for the singlet energy. However, the effect on the energy of the CSS, and the triplet energy is negligible in comparison. The oligomers all populate the triplet state. Nevertheless, experimental determination of the triplet energy would be highly beneficial to get a full picture of the prepared system.

Structural changes do not only affect the optical properties of a compound, but also the physical properties. This can be utilised, not only to design application-oriented dyes, but also to manufacture a new dye material, such as a room temperature dye glass. In **project I** and **project III** a strategy to obtain said new material was developed and

improved. To realise this, the principles of alkyl chain engineering and entropic mixing were combined. By attaching small alkyl chains to the core structure of the molecule a balance of the π-π interactions and van der Waals forces is targeted. This can lower the aggregation and crystallisation potential of the dye molecule. Blending of two or more derivatives of a dye molecule, that exhibit the same photophysical properties, increases the entropy of the system. The derivatives used in **project I** have, as only modification, short alkyl chains attached in positions 1 and 7 of the BODIPY core. The compounds show indistinguishable, sharp absorption and emission bands in dilute solution. In a thin pristine film of the dyes the absorption and emission envelopes are highly distorted, due to aggregation or crystallisation in the film. Upon mixing of two or more dyes together and fabrication of thin films of the blended material however, some blends especially the *s*P-IP blend shows almost monomeric absorption properties. All blended films still show signs of aggregation, most likely of the J-type in the film, leading to a second emission band.

The design of the dyes for **project III** was improved accordingly. The BODIPYs have a higher molecular weight and an overall bulkier structure. Different alkyl chains were attached in positions 3 and 5 of the BODIPY core to, again, give access to different derivatives. As the smaller dyes the bigger ones, again only differentiating in their alkylation, show highly similar absorption and emission properties in dilute solution. In thin pristine films the absorption and emission features remain of monomeric nature. Thin films also show no sign of aggregation, most likely caused by the processing method. Nonetheless, thicker films and the bulk material, reveal that the pristine material aggregates or crystallises. The *s*P-BDP however shows a glass transition after initial melting of the material. Thermal analysis shows, that the blended materials form a glass even without previous melting. Thin blended films show monomeric absorption and emission features, and thicker films and the bulk material show no sign of aggregation of crystallisation anymore. The fragility of the ternary blend is lower than of the binary blends, indicating a better glass forming ability. The structural architecture of the dyes evolved from project I to project III. This led to the successful preparation of a new dye material. This emphasises the importance of strategic molecular design and how it can be used in the future, to prepare new materials. Additionally, the developed strategy relies on fundamental thermodynamic principles. It could therefore be utilised to produce a room temperature glass of other molecular scaffolds, than BODIPYs, given the right T_g.

References

[1] H. Skelton, *Review of Progress in Coloration and Related Topics* **1999**, *29*, 43-64.

[2] A. Abel, in *Colour Design (Second Edition)* (Ed.: J. Best), Woodhead Publishing, **2012**, pp. 557-587.

[3] H. Berke, *Chem. Soc. Rev.* **2007**, *36*, 15-30.

[4] K. Hübner, *Chem. unserer Zeit* **2006**, *40*, 274-275.

[5] M. M. Sousa, M. J. Melo, A. J. Parola, P. J. T. Morris, H. S. Rzepa, J. S. S. de Melo, *Chem. Eur. J.* **2008**, *14*, 8507-8513.

[6] C. Cooksey, A. Dronsfield, *Biotech. Histochem.* **2009**, *84*, 179-183.

[7] L. F. Fieser, *J. Chem. Educ.* **1930**, *7*, 2609.

[8] E. D. Głowacki, G. Voss, L. Leonat, M. Irimia-Vladu, S. Bauer, N. S. Sariciftci, *Isr. J. Chem.* **2012**, *52*, 540-551.

[9] R. H. Howland, *J. Psychosoc. Nurs. Ment. Health Serv.* **2016**, *54*, 21-24.

[10] R. H. Schirmer, B. Coulibaly, A. Stich, M. Scheiwein, H. Merkle, J. Eubel, K. Becker, H. Becher, O. Müller, T. Zich, *Redox report* **2003**, *8*, 272-275.

[11] M. J. Ohlow, B. Moosmann, *Drug Discov. Today* **2011**, *16*, 119-131.

[12] G. Accorsi, G. Verri, M. Bolognesi, N. Armaroli, C. Clementi, C. Miliani, A. Romani, *ChemComm* **2009**, 3392-3394.

[13] J. C. Maxwell, *Philos. Trans. Royal Soc.* **1865**, *155*, 459-512.

[14] N. J. Turro, V. Ramamurthy, V. Ramamurthy, J. C. Scaiano, *Principles of molecular photochemistry: an introduction*, University science books, **2009**.

[15] A. Einstein, *Ann. Phys.* **1905**, *322*, 132-148.

[16] P. Atkins, P. W. Atkins, J. de Paula, *Atkins' physical chemistry*, Oxford university press, **2014**.

[17] V. Balzani, P. Ceroni, A. Juris, *Photochemistry and photophysics: concepts, research, applications*, John Wiley & Sons, **2014**.

[18] P. Klán, J. Wirz, *Photochemistry of organic compounds: from concepts to practice*, John Wiley & Sons, **2009**.

[19] N. J. Turro, V. Ramamurthy, J. C. Scaiano, *Modern molecular photochemistry of organic molecules, Vol. 188*, University Science Books Sausalito, CA, **2010**.

[20] A. D. McNaught, A. Wilkinson, *Compendium of chemical terminology, Vol. 1669*, Blackwell Science Oxford, **1997**.

[21] M. Kasha, *Discuss. Faraday Soc.* **1950**, *9*, 14-19.

[22] R. Englman, J. Jortner, *J. Lumin.* **1970**, *1-2*, 134-142.

[23] M. T. Colvin, A. B. Ricks, A. M. Scott, D. T. Co, M. R. Wasielewski, *J. Phys. Chem. A* **2012**, *116*, 1923-1930.

[24] M. Hussain, A. M. El-Zohry, Y. Hou, A. Toffoletti, J. Zhao, A. Barbon, O. F. Mohammed, *J. Phys. Chem. B* . **2021**, *125*, 10813-10831.

[25] Z. E. X. Dance, S. M. Mickley, T. M. Wilson, A. B. Ricks, A. M. Scott, M. A. Ratner, M. R. Wasielewski, *J. Phys. Chem. A* **2008**, *112*, 4194-4201.

[26] P. Muller, *Pure Appl. Chem.* **1994**, *66*, 1077-1184.

[27] L. Pauling, *Proc. Natl. Acad. Sci. U.S.A.* **1928**, *14*, 359-362.

[28] E. V. Anslyn, D. A. Dougherty, *Modern physical organic chemistry*, University science books, **2006**.

[29] J. J. De Yoreo, P. G. Vekilov, *Rev. Mineral. Geochem.* **2003**, *54*, 57-93.

[30] A. D. de Zerio, C. Müller, *Adv. Energy Mater.* **2018**, *8*, 1702741.
[31] N. A. Mauro, M. Blodgett, M. L. Johnson, A. J. Vogt, K. F. Kelton, *Nat. Commun.* **2014**, *5*, 4616.
[32] K. F. Kelton, *J. Phys.: Condens. Matter* **2016**, *29*, 023002.
[33] S. Hultmark, A. Cravcenco, K. Kushwaha, S. Mallick, P. Erhart, K. Börjesson, C. Müller, *Sci. Adv.* **2021**, *7*, eabi4659.
[34] R. Ziessel, G. Ulrich, A. Harriman, *New J. Chem.* **2007**, *31*, 496-501.
[35] Y.-W. Wang, A. B. Descalzo, Z. Shen, X.-Z. You, K. Rurack, *Chem. Eur. J.* **2010**, *16*, 2887-2903.
[36] A. B. Descalzo, H.-J. Xu, Z. Shen, K. Rurack, *Ann. N.Y. Acad. Sci.* **2008**, *1130*, 164-171.
[37] A. Treibs, F.-H. Kreuzer, *Liebigs Ann.* **1968**, *718*, 208-223.
[38] H. J. Wories, J. H. Koek, G. Lodder, J. Lugtenburg, R. Fokkens, O. Driessen, G. R. Mohn, *Recueil des Travaux Chimiques des Pays-Bas* **1985**, *104*, 288-291.
[39] A. Loudet, K. Burgess, *Chem Rev* **2007**, *107*, 4891-4932.
[40] J. Bañuelos, *Chem. Rec.* **2016**, *16*, 335-348.
[41] G. Ulrich, R. Ziessel, A. Harriman, *Angew. Chem.* **2008**, *120*, 1202-1219.
[42] N. Boens, B. Verbelen, M. J. Ortiz, L. Jiao, W. Dehaen, *Coord. Chem. Rev.* **2019**, *399*, 213024.
[43] I. López-Duarte, T. T. Vu, M. A. Izquierdo, J. A. Bull, M. K. Kuimova, *ChemComm* **2014**, *50*, 5282-5284.
[44] P. L. Zhang, Z. K. Wang, Q. Y. Chen, X. Du, J. Gao, *Bioorg Med Chem Lett* **2019**, *29*, 1943-1947.
[45] E. Ozcan, H. H. Kazan, B. Çoşut, *Luminescence* **2020**, *35*, 168-177.
[46] Z. Shi, X. Han, W. Hu, H. Bai, B. Peng, L. Ji, Q. Fan, L. Li, W. Huang, *Chem. Soc. Rev.* **2020**, *49*, 7533-7567.
[47] W. Zhao, F. Xiao, G. Jin, B. Li, *Spectrochim. Acta A Mol. Biomol. Spectrosc.* **2021**, *262*, 120118.
[48] A. Kamkaew, S. H. Lim, H. B. Lee, L. V. Kiew, L. Y. Chung, K. Burgess, *Chem. Soc. Rev.* **2013**, *42*, 77-88.
[49] D. Chen, Z. Wang, H. Dai, X. Lv, Q. Ma, D.-P. Yang, J. Shao, Z. Xu, X. Dong, *Small Methods* **2020**, *4*, 2000013.
[50] S. Rattanopas, K. Chansaenpak, K. Siwawannapong, K. Ngamchuea, S. Wet-osot, J. Treekoon, T. Pewklang, T. Jinaphon, K. Sagarik, R.-Y. Lai, L. Cheng, A. Kamkaew, *ChemPhotoChem* **2020**, *4*, 5304-5311.
[51] C. Thivierge, J. Han, R. M. Jenkins, K. Burgess, *J. Org. Chem.* **2011**, *76*, 5219-5228.
[52] B. M. Squeo, V. G. Gregoriou, A. Avgeropoulos, S. Baysec, S. Allard, U. Scherf, C. L. Chochos, *Prog. Polym. Sci.* **2017**, *71*, 26-52.
[53] M. Poddar, R. Misra, *Coord. Chem. Rev.* **2020**, *421*, 213462.
[54] J. J. Chen, S. M. Conron, P. Erwin, M. Dimitriou, K. McAlahney, M. E. Thompson, *ACS Appl. Mater. Interfaces.* **2015**, *7*, 662-669.
[55] R. Srinivasa Rao, A. Bagui, G. Hanumantha Rao, V. Gupta, S. P. Singh, *ChemComm* **2017**, *53*, 6953-6956.
[56] K. Gkini, A. Verykios, N. Balis, A. Kaltzoglou, M. Papadakis, K. S. Adamis, K.-K. Armadorou, A. Soultati, C. Drivas, S. Gardelis, I. D. Petsalakis, L. C. Palilis, A. Fakharuddin, M. I. Haider, X. Bao, S. Kennou, P. Argitis, L. Schmidt-Mende, A. G. Coutsolelos, P. Falaras, M. Vasilopoulou, *ACS Appl. Mater. Interfaces.* **2020**, *12*, 1120-1131.
[57] P. De Bonfils, L. Péault, P. Nun, V. Coeffard, *Eur. J. Org. Chem.* **2021**, *2021*, 1809-1824.
[58] S.-L. Rebeca, B. Jorge, in *BODIPY Dyes* (Eds.: B.-P. Jorge, L. Rebeca Sola), IntechOpen, Rijeka, **2018**, p. Ch. 1.
[59] I. J. Arroyo, R. Hu, G. Merino, B. Z. Tang, E. Pena-Cabrera, *J. Org. Chem.* **2009**, *74*, 5719-5722.
[60] J. Van Koeveringe, J. Lugtenburg, *Recl. Trav. Chim. Pays-Bas* **1977**, *96*, 55-57.

[61] R. A. Jones, *Pyrroles, Volume 48, Part 1*, John Wiley & Sons, **2009**.
[62] A. Gossauer, *Die Chemie der Pyrrole, Vol. 15*, Springer-Verlag, **2013**.
[63] R. A. Jones, G. P. Bean, *The Chemistry of Pyrroles: Organic Chemistry: A Series of Monographs, Vol. 34, Vol. 34*, Academic Press, **2013**.
[64] B. A. Trofimov, I. M. Al'bina, E. Y. Schmidt, L. N. Sobenina, *Chemistry of pyrroles*, CRC press, **2014**.
[65] J. A. J. K. Mills, *HETEROCYCLIC CHEMISTRY, 4TH ED*, Wiley India Pvt. Limited, **2008**.
[66] W. Sheng, F. Lv, B. Tang, E. Hao, L. Jiao, *Chin. Chem. Lett.* **2019**, *30*, 1825-1833.
[67] Z. Li, E. Mintzer, R. Bittman, *J. Org. Chem.* **2006**, *71*, 1718-1721.
[68] M. Zhang, E. Hao, Y. Xu, S. Zhang, H. Zhu, Q. Wang, C. Yu, L. Jiao, *RSC Adv.* **2012**, *2*, 11215-11218.
[69] D. Wang, J. Fan, X. Gao, B. Wang, S. Sun, X. Peng, *J. Org. Chem.* **2009**, *74*, 7675-7683.
[70] C. Yu, L. Jiao, H. Yin, J. Zhou, W. Pang, Y. Wu, Z. Wang, G. Yang, E. Hao, *Eur. J. Org. Chem.* **2011**, *2011*, 5460-5468.
[71] L. Wu, K. Burgess, *Chem Commun (Camb)* **2008**, 4933-4935.
[72] L. Jiao, C. Yu, M. Liu, Y. Wu, K. Cong, T. Meng, Y. Wang, E. Hao, *J. Org. Chem.* **2010**, *75*, 6035-6038.
[73] C. Schäfer, J. Mony, T. Olsson, K. Börjesson, *J. Org. Chem.* **2022**, *87*, 2569-2579.
[74] A. H. Jackson, A. H. Jackson, M. Artico, H. J. Anderson, C. E. Loader, A. Gossauer, P. Nesvadba, N. Dennis, in *Chem. Heterocycl. Compd.*, **1990**, pp. 295-548.
[75] T. Tsuchimoto, *Chem. Eur. J.* **2011**, *17*, 4064-4075.
[76] A. R. Katritzky, K. Suzuki, S. K. Singh, H.-Y. He, *J. Org. Chem.* **2003**, *68*, 5720-5723.
[77] P. Bélanger, *Tetrahedron Lett.* **1979**, *20*, 2505-2508.
[78] in *Comprehensive Organic Name Reactions and Reagents*, pp. 2872-2879.
[79] G. Jones, S. P. Stanforth, in *Organic Reactions*, pp. 1-330.
[80] C. Schäfer, J. Mony, T. Olsson, K. Börjesson, *Chem. Eur. J.* **2020**, *26*, 14295-14299.
[81] W. Herz, C. F. Courtney, *J. Am. Chem. Soc.* **1954**, *76*, 576-578.
[82] in *Organic Chemistry: A Series of Monographs, Vol. 34* (Eds.: R. A. Jones, G. P. Bean), Academic Press, **1977**, pp. 209-247.
[83] A. J. Castro, J. F. Deck, N. C. Ling, J. P. Marsh, G. E. Means, *J. Org. Chem.* **1965**, *30*, 344-350.
[84] P. Skell, G. Bean, *J. Am. Chem. Soc.* **1962**, *84*, 4660-4661.
[85] N. D. Smith, D. Huang, N. D. P. Cosford, *Org. Lett.* **2002**, *4*, 3537-3539.
[86] N. Ono, E. Muratani, T. Ogawa, *J. Heterocycl. Chem.* **1991**, *28*, 2053-2055.
[87] C. Schäfer, S. Hultmark, Y. Yang, C. Müller, K. Börjesson, *Chem. Mater.* **2022**, *34*, 9294-9302.
[88] D. Blakemore, in *Synthetic Methods in Drug Discovery: Volume 1, Vol. 1*, The Royal Society of Chemistry, **2016**, pp. 1-69.
[89] P. A. Cox, A. G. Leach, A. D. Campbell, G. C. Lloyd-Jones, *J. Am. Chem. Soc.* **2016**, *138*, 9145-9157.
[90] K. Billingsley, S. L. Buchwald, *J. Am. Chem. Soc.* **2007**, *129*, 3358-3366.
[91] H. G. Kuivila, J. F. Reuwer Jr, J. A. Mangravite, *Can. J. Chem.* **1963**, *41*, 3081-3090.
[92] K. L. Billingsley, K. W. Anderson, S. L. Buchwald, *Angew. Chem. Int. Ed. Engl.* **2006**, *45*, 3484-3488.
[93] D. M. Knapp, E. P. Gillis, M. D. Burke, *J. Am. Chem. Soc.* **2009**, *131*, 6961-6963.
[94] T. Kinzel, Y. Zhang, S. L. Buchwald, *J. Am. Chem. Soc.* **2010**, *132*, 14073-14075.
[95] N. Boens, B. Verbelen, W. Dehaen, *Eur. J. Org. Chem.* **2015**, *2015*, 6577-6595.
[96] A. B. Nepomnyashchii, M. Bröring, J. Ahrens, A. J. Bard, *J. Am. Chem. Soc.* **2011**, *133*, 8633-8645.
[97] S. Rihn, M. Erdem, A. De Nicola, P. Retailleau, R. Ziessel, *Org. Lett.* **2011**, *13*, 1916-1919.

[98] S. Wang, Z. Wang, H. Gao, L. Jiang, H. Liu, F. Wu, Y. Zhao, K. S. Chan, Z. Shen, *ChemComm* **2021**, *57*, 1758-1761.
[99] A. L. Nguyen, *Boron Functionalization of BODIPY Dyes, and Their Evaluation as Bioimaging Agents*, Louisiana State University and Agricultural & Mechanical College, **2015**.
[100] Z. Wang, J. Zhao, *Org. Lett.* **2017**, *19*, 4492-4495.
[101] M. A. T. Rogers, *J. Chem. Soc. (Resumed)* **1943**, 590-596.
[102] M. A. T. Rogers, *Nature* **1943**, *151*, 504-504.
[103] Y. Ge, D. F. O'Shea, *Chem. Soc. Rev.* **2016**, *45*, 3846-3864.
[104] L. I. Shamova, Y. V. Zatsikha, V. N. Nemykin, *Dalton Trans.* **2021**, *50*, 1569-1593.
[105] J. Wang, C. Yu, E. Hao, L. Jiao, *Coord. Chem. Rev.* **2022**, *470*, 214709.
[106] W. Davies, M. A. Rogers, *J. Chem. Soc. (Resumed)* **1944**, 126-131.
[107] A. Gorman, J. Killoran, C. O'Shea, T. Kenna, W. M. Gallagher, D. F. O'Shea, *J. Am. Chem. Soc.* **2004**, *126*, 10619-10631.
[108] M. J. Hall, S. O. McDonnell, J. Killoran, D. F. O'Shea, *J. Org. Chem.* **2005**, *70*, 5571-5578.
[109] W. Zhao, E. M. Carreira, *Angew. Chem.* **2005**, *117*, 1705-1707.
[110] W. Zhao, E. M. Carreira, *Chem. Eur. J.* **2006**, *12*, 7254-7263.
[111] Y.-W. Wang, A. B. Descalzo, Z. Shen, X.-Z. You, K. Rurack, *Chem. Eur. J.* **2012**, *18*, 7306-7309.
[112] M. Liras, J. Bañuelos Prieto, M. Pintado-Sierra, F. L. Arbeloa, I. García-Moreno, A. Costela, L. Infantes, R. Sastre, F. Amat-Guerri, *Org. Lett.* **2007**, *9*, 4183-4186.
[113] C. W. Bird, J. Lu, *Tetrahedron Lett.* **1992**, *33*, 7253-7254.
[114] G. Sathyamoorthi, M.-L. Soong, T. W. Ross, J. H. Boyer, *Heteroat. Chem* **1993**, *4*, 603-608.
[115] E. B. Knott, *J. Chem. Soc. (Resumed)* **1947**, 1196-1201.
[116] D. Wu, D. F. O'Shea, *Org. Lett.* **2013**, *15*, 3392-3395.
[117] J. O. Flores-Rizo, I. Esnal, C. A. Osorio-Martínez, C. F. A. Gómez-Durán, J. Bañuelos, I. López Arbeloa, K. H. Pannell, A. J. Metta-Magaña, E. Peña-Cabrera, *J. Org. Chem.* **2013**, *78*, 5867-5877.
[118] S. Murphy, G. B. Schuster, *J. Phys. Chem.* **1995**, *99*, 8516-8518.
[119] V. Khimenko, A. K. Chibisov, H. Görner, *J. Phys. Chem. A* **1997**, *101*, 7304-7310.
[120] S. A. Soper, Q. L. Mattingly, *J. Am. Chem. Soc.* **1994**, *116*, 3744-3752.
[121] H. L. Kee, C. Kirmaier, L. Yu, P. Thamyongkit, W. J. Youngblood, M. E. Calder, L. Ramos, B. C. Noll, D. F. Bocian, W. R. Scheidt, R. R. Birge, J. S. Lindsey, D. Holten, *J. Phys. Chem. B* . **2005**, *109*, 20433-20443.
[122] A. Harriman, G. Izzet, R. Ziessel, *J. Am. Chem. Soc.* **2006**, *128*, 10868-10875.
[123] G. Ulrich, C. Goze, M. Guardigli, A. Roda, R. Ziessel, *Angew. Chem. Int. Ed.* **2005**, *44*, 3694-3698.
[124] C. Goze, G. Ulrich, R. Ziessel, *Org. Lett.* **2006**, *8*, 4445-4448.
[125] R. Ziessel, C. Goze, G. Ulrich, *Synth* **2007**, *2007*, 936-949.
[126] J. Bañuelos, V. Martín, C. F. A. Gómez-Durán, I. J. A. Córdoba, E. Peña-Cabrera, I. García-Moreno, Á. Costela, M. E. Pérez-Ojeda, T. Arbeloa, Í. L. Arbeloa, *Chem. Eur. J.* **2011**, *17*, 7261-7270.
[127] G. Sathyamoorthi, J. H. Boyer, T. H. Allik, S. Chandra, *Heteroat. Chem* **1994**, *5*, 403-407.
[128] T. Ueno, Y. Urano, K.-i. Setsukinai, H. Takakusa, H. Kojima, K. Kikuchi, K. Ohkubo, S. Fukuzumi, T. Nagano, *J. Am. Chem. Soc.* **2004**, *126*, 14079-14085.
[129] T. Ueno, Y. Urano, H. Kojima, T. Nagano, *J. Am. Chem. Soc.* **2006**, *128*, 10640-10641.
[130] Y. Gabe, Y. Urano, K. Kikuchi, H. Kojima, T. Nagano, *J. Am. Chem. Soc.* **2004**, *126*, 3357-3367.
[131] M. Kollmannsberger, K. Rurack, U. Resch-Genger, W. Rettig, J. Daub, *Chem. Phys. Lett.* **2000**, *329*, 363-369.

[132] M. A. Filatov, S. Karuthedath, P. M. Polestshuk, S. Callaghan, K. J. Flanagan, M. Telitchko, T. Wiesner, F. Laquai, M. O. Senge, *Phys. Chem. Chem. Phys.* **2018**, *20*, 8016-8031.
[133] N. Kiseleva, M. A. Filatov, J. C. Fischer, M. Kaiser, M. Jakoby, D. Busko, I. A. Howard, B. S. Richards, A. Turshatov, *Phys. Chem. Chem. Phys.* **2022**, *24*, 3568-3578.
[134] M. A. Filatov, S. Karuthedath, P. M. Polestshuk, S. Callaghan, K. J. Flanagan, T. Wiesner, F. Laquai, M. O. Senge, *ChemPhotoChem* **2018**, *2*, 606-615.
[135] K. Chen, W. Yang, Z. Wang, A. Iagatti, L. Bussotti, P. Foggi, W. Ji, J. Zhao, M. Di Donato, *J. Phys. Chem. A* **2017**, *121*, 7550-7564.
[136] K. Rurack, M. Kollmannsberger, U. Resch-Genger, J. Daub, *J. Am. Chem. Soc.* **2000**, *122*, 968-969.
[137] E. V. de Wael, J. A. Pardoen, J. A. van Koeveringe, J. Lugtenburg, *Recueil des Travaux Chimiques des Pays-Bas* **1977**, *96*, 306-309.
[138] V. Lakshmi, M. Rajeswara Rao, M. Ravikanth, *Org. Biomol. Chem.* **2015**, *13*, 2501-2517.
[139] W. Hu, R. Zhang, X.-F. Zhang, J. Liu, L. Luo, *Spectrochim. Acta A Mol. Biomol. Spectrosc.* **2022**, *272*, 120965.
[140] R. P. Sabatini, T. M. McCormick, T. Lazarides, K. C. Wilson, R. Eisenberg, D. W. McCamant, *J. Phys. Chem. Lett.* **2011**, *2*, 223-227.
[141] K. Chen, Y. Dong, X. Zhao, M. Imran, G. Tang, J. Zhao, Q. Liu, *Front. Chem.* **2019**, *7*.
[142] D. F. Perepichka, M. R. Bryce, *Angew. Chem.* **2005**, *117*, 5504-5507.
[143] S. Achelle, A. Barsella, C. Baudequin, B. Caro, F. Robin-le Guen, *J. Org. Chem.* **2012**, *77*, 4087-4096.
[144] F. Bureš, *RSC Adv.* **2014**, *4*, 58826-58851.
[145] C. Chen, C. Fang, *Chem. Asian J.* **2020**, *15*, 1514-1523.
[146] S. Niu, G. Ulrich, P. Retailleau, R. Ziessel, *Tetrahedron Lett.* **2011**, *52*, 4848-4853.
[147] C. Bonnier, D. D. Machin, O. Abdi, B. D. Koivisto, *Org. Biomol. Chem.* **2013**, *11*, 3756-3760.
[148] S. Xuan, N. Zhao, X. Ke, Z. Zhou, F. R. Fronczek, K. M. Kadish, K. M. Smith, M. G. H. Vicente, *J. Org. Chem.* **2017**, *82*, 2545-2557.
[149] A. M. Brouwer, *Pure Appl. Chem.* **2011**, *83*, 2213-2228.
[150] J. K. Karlsson, A. Harriman, *J. Phys. Chem. A* **2016**, *120*, 2537-2546.
[151] L. Jiao, Y. Wu, S. Wang, X. Hu, P. Zhang, C. Yu, K. Cong, Q. Meng, E. Hao, M. G. H. Vicente, *J. Org. Chem.* **2014**, *79*, 1830-1835.
[152] Y. Xu, T. Feng, T. Yang, H. Wei, H. Yang, G. Li, M. Zhao, S. Liu, W. Huang, Q. Zhao, *ACS Appl. Mater. Interfaces.* **2018**, *10*, 16299-16307.
[153] L. J. Patalag, J. Hoche, R. Mitric, D. B. Werz, B. L. Feringa, *Angew. Chem. Int. Edit.* **2022**.
[154] L. J. Patalag, L. P. Ho, P. G. Jones, D. B. Werz, *J. Am. Chem. Soc.* **2017**, *139*, 15104-15113.
[155] Y. Cakmak, S. Kolemen, S. Duman, Y. Dede, Y. Dolen, B. Kilic, Z. Kostereli, L. T. Yildirim, A. L. Dogan, D. Guc, E. U. Akkaya, *Angew. Chem. Int. Ed.* **2011**, *50*, 11937-11941.
[156] M. Bröring, R. Krüger, S. Link, C. Kleeberg, S. Köhler, X. Xie, B. Ventura, L. Flamigni, *Chem. Eur. J.* **2008**, *14*, 2976-2983.
[157] Y. Hayashi, S. Yamaguchi, W. Y. Cha, D. Kim, H. Shinokubo, *Org. Lett.* **2011**, *13*, 2992-2995.
[158] N. J. Hestand, F. C. Spano, *Chem. Rev.* **2018**, *118*, 7069-7163.
[159] F. L. Forgerini, R. Marchiori, *Biomatter* **2014**, *4*, e28871.
[160] H. Wang, Y. Xu, X. Yu, R. Xing, J. Liu, Y. Han, *Polymers* **2013**, *5*, 1272-1324.
[161] C. L. Radford, T. L. Kelly, *Can. J. Chem.* **2021**, *99*, 921-932.
[162] Y. Liu, A. Yangui, R. Zhang, A. Kiligaridis, E. Moons, F. Gao, O. Inganäs, I. G. Scheblykin, F. Zhang, *Small Methods* **2021**, *5*, 2100585.
[163] F. Lu, T. Nakanishi, *Sci. Technol. Adv. Mater.* **2015**, *16*, 014805.
[164] J. Min, Y. N. Luponosov, A. Gerl, M. S. Polinskaya, S. M. Peregudova, P. V. Dmitryakov, A. V. Bakirov, M. A. Shcherbina, S. N. Chvalun, S. Grigorian, N. Kaush-Busies, S. A. Ponomarenko, T. Ameri, C. J. Brabec, *Adv. Energy Mater.* **2014**, *4*, 1301234.

[165] M. J. Hollamby, T. Nakanishi, *J. Mater. Chem. C* **2013**, *1*, 6178-6183.
[166] A. Ghosh, T. Nakanishi, *ChemComm* **2017**, *53*, 10344-10357.
[167] F. Lu, T. Takaya, K. Iwata, I. Kawamura, A. Saeki, M. Ishii, K. Nagura, T. Nakanishi, *Sci. Rep.* **2017**, *7*, 3416.
[168] X. Yao, W. Shao, X. Xiang, W.-J. Xiao, L. Liang, F.-G. Zhao, J. Ling, Z. Lu, J. Li, W.-S. Li, *Org. Electron.* **2018**, *61*, 56-64.
[169] T. Lei, J.-H. Dou, J. Pei, *Adv. Mater.* **2012**, *24*, 6457-6461.
[170] D. Adamczak, A. Perinot, H. Komber, A. Illy, S. Hultmark, B. Passarella, W. L. Tan, S. Hutsch, D. Becker-Koch, C. Rapley, A. D. Scaccabarozzi, M. Heeney, Y. Vaynzof, F. Ortmann, C. R. McNeill, C. Müller, M. Caironi, M. Sommer, *J. Mater. Chem. C* **2021**, *9*, 4597-4606.
[171] K. Jiang, Q. Wei, J. Y. L. Lai, Z. Peng, H. K. Kim, J. Yuan, L. Ye, H. Ade, Y. Zou, H. Yan, *Joule* **2019**, *3*, 3020-3033.
[172] K. Fukuda, H. Nakahara, T. Kato, *J. Colloid Interface Sci.* **1976**, *54*, 430-438.
[173] J. Yoon, J. Kwag, T. J. Shin, J. Park, Y. M. Lee, Y. Lee, J. Park, J. Heo, C. Joo, T. J. Park, P. J. Yoo, S. Kim, J. Park, *Adv. Mater.* **2014**, *26*, 4559-4564.
[174] A. Ben-Naim, *Entropy* **2007**, *9*, 133-136.
[175] X. Liu, Z. Liang, S. Du, J. Tong, J. Li, R. Zhang, X. Shi, L. Yan, X. Bao, Y. Xia, *ACS Appl. Energy Mater.* **2021**, *4*, 1774-1783.
[176] L. Yu, M. Zhang, J. Tang, R. Li, X. Xu, Q. Peng, *Chem. Mater.* **2021**, *33*, 7396-7407.
[177] M. T. Cicerone, J. F. Douglas, *Soft Matter* **2012**, *8*, 2983-2991.
[178] C. Müller, *Chem. Mater.* **2015**, *27*, 2740-2754.
[179] K. Kushwaha, L. Yu, K. Stranius, S. K. Singh, S. Hultmark, M. N. Iqbal, L. Eriksson, E. Johnston, P. Erhart, C. Muller, K. Borjesson, *Adv. Sci.* **2019**, *6*, 1801650.
[180] A. J. Musser, S. K. Rajendran, K. Georgiou, L. Gai, R. T. Grant, Z. Shen, M. Cavazzini, A. Ruseckas, G. A. Turnbull, I. D. W. Samuel, J. Clark, D. G. Lidzey, *J. Mater. Chem. C* **2017**, *5*, 8380-8389.